REPUBLIC OF TÜRKİYE
YILDIZ TECHNICAL UNIVERSITY
GRADUATE SCHOOL OF SCIENCE AND ENGINEERING

REDUCING FOSSIL FUEL CONSUMPTION IN CEMENT INDUSTRY: MODELING OF GAS EMISSIONS AND INNOVATIVE SOLAR CALCINER APPROACH

Havva Hande CEBECİ

DOCTOR OF PHILOSOPHY THESIS

Department of Chemical Engineering

Program of Chemical Engineering

Supervisor

Prof. Dr. Hasan SADIKOĞLU

Co-Supervisor

Assist. Prof. Dr. Özgün YÜCEL

December, 2024

REPUBLIC OF TÜRKİYE

YILDIZ TECHNICAL UNIVERSITY

GRADUATE SCHOOL OF SCIENCE AND ENGINEERING

REDUCING FOSSIL FUEL CONSUMPTION IN CEMENT INDUSTRY: MODELING OF GAS EMISSIONS AND INNOVATIVE SOLAR CALCINER APPROACH

A thesis submitted by Havva Hande CEBECİ in partial fulfillment of the requirements for the degree of **DOCTOR OF PHILOSOPHY** is approved by the committee on 06.12.2024 in Department of Chemical Engineering, Program of Chemical Engineering.

Prof. Dr. Hasan SADIKOĞLU Yildiz Technical University Supervisor	Assist. Prof. Dr. Özgün YÜCEL Yildiz Technical University Co- supervisor

Approved By the Examining Committee

Prof. Dr. Hasan SADIKOĞLU, Supervisor
Yildiz Technical University _____

Prof. Dr. Nil ACARALI, Member
Yildiz Technical University _____

Prof. Dr. Mustafa ÖZİLGEN, Member
Yeditepe University _____

Prof. Dr. Fatma Jale GÜLEN, Member
Yildiz Technical University _____

Assist. Prof. Dr. Meral YILDIRIM YALÇIN, Member
Istanbul Aydin University _____

I hereby declare that I have obtained the required legal permissions during data collection and exploitation procedures, that I have made the in-text citations and cited the references properly, that I haven't falsified and/or fabricated research data and results of the study and that I have abided by the principles of the scientific research and ethics during my Thesis Study under the title of "Reducing Fossil Fuel Consumption in Cement Industry: Modeling of Gas Emissions and Innovative Solar Calciner Approach" Thesis Title supervised by my supervisor, Prof. Dr. Hasan SADIKOĞLU. In the case of a discovery of false statement, I am to acknowledge any legal consequence.

Havva Hande CEBECİ

Signature

Dedicated to my family

ACKNOWLEDGEMENTS

I wish to express my deepest gratitude to my thesis advisor, Prof. Dr. Hasan SADIKOĞLU, and my co-advisor, Assist. Prof. Dr. Özgün YÜCEL**,** for their invaluable guidance, insightful advice, and unwavering support throughout my doctoral studies. Their mentorship has been instrumental in shaping this work and my academic journey. I am especially thankful to them for their encouragement and support during my application and acceptance process for a postdoctoral position in the United States, which marked a significant milestone in my career.

My heartfelt appreciation and affection go to my esteemed mother, Gülten CEBECİ, my father, Faruk CEBECİ**,** and my brother, İlker CEBECİ, along with his family. Their consistent trust, unconditional love, and unwavering support have been the cornerstone of my personal and educational achievements.

I would also like to extend my sincere gratitude to the scientific community**,** whose collective knowledge and advancements have inspired and informed my research.

Furthermore, I am thankful to Dal Engineering Group for their collaboration and assistance in facilitating access to vital information from the cement plant, which significantly contributed to the success of this thesis.

Finally, I am deeply indebted to my friends, colleagues, and everyone who has supported and encouraged me throughout this journey.

Havva Hande CEBECİ

TABLE OF CONTENTS

LIST OF SYMBOLS vii

LIST OF ABBREVIATIONS ix

LIST OF FIGURES x

LIST OF TABLES xi

ABSTRACT xii

ÖZET xiv

1 INTRODUCTION 1

1.1 Background 1

1.2 The Objective of Thesis 5

1.3 The Hypothesis of Thesis 6

2 PROCESS OVERVIEW AND EMISSION MODELLING USING COMPUTATIONAL TOOLS IN CEMENT PRODUCTION 8

2.1 The Conventional Cement Production Process 8

2.1.1 Preparing of Raw Material 8

2.1.2 Pyro-Process Unit 9

2.1.3 Pre-Heater and Pre-Calciner 9

2.1.4 Rotary Kiln 11

2.1.5 Clinker Cooling 15

2.1.6 Alkali Bypass 16

2.2 The Fuels in Cement Production Plant 16

2.2.3 Refuse Derived Fuel (RDF) 21

2.2.4 Tire Derived Fuel (TDF) 23

2.2.5 Waste Oil (WO) 24

2.3 Literature Survey of Modelling Calciner 25

2.4 Material and Methods 28

2.4. Geometrical Model 29

2.4.2 Boundary Conditions 29

2.4.3 Fuel Properties and Characterization 30

2.4.4 Combustion Gas Compositions 31

2.4.5Raw Meal Properties....32
2.4.6Temperature and Gas Species Measurements....33
2.4.7Adiabatic Flame Temperature of Fuels....33
2.5 Numerical Calculations....35
2.5.1NASA CEA Reaction Modelling....37
2.5.2Chemkin-Pro Reaction Modelling....38
2.6 Result and Discussion....39
2.6.1Validation of the Accuracy of the Model....40
2.6.2Comparison of NASA CEA and Chemkin-Pro....41
3 INTEGRATING SOLAR CALCINER TECHNOLOGY FOR REDUCTION EMISSION IN CEMENT PRODUCTION 47
3.1 Literature Survey of Implementing Solar Calciner in Cement Plant....47
3.2 Modelling of the Hybrid Solar Cement Process....49
3.2.1CO_2 Emission Reduction Potential....50
3.2.2Heliostat field layout....51
3.2.3Heliostat system....52
3.2.4System for central receiving....52
3.2.5DNI and investigated plant location....53
3.3 Result and Discussion....54
3.3.1Comparison CO_2 Emission Reductions in Conventional and Solar Calciner Systems....54
3.3.2The Operational Efficiency of Conventional Calciner Utilizing Solarization....56
4 CONCLUSION 61
REFERENCES 63
A APPENDIX PROCESS OVERVIEW AND EMISSION MODELLING USING COMPUTATIONAL TOOLS IN CEMENT PRODUCTION 71
B APPENDIX INTEGRATING SOLAR CALCINER TECHNOLOGY FOR REDUCTION EMISSION IN CEMENT PRODUCTION 96
PUBLICATIONS FROM THE THESIS 100

LIST OF SYMBOLS

$T_{ambient}$	Ambient temperature, [K]
A_{hel}	Area of a heliostat, [m^2]
$\dot{m}_{clinker}$	Clinker mass flow rate, [kg/s]
$\dot{m}_{CO_{2,conv}}$	CO_2 reduction for convectional calciner, [kg/s]
$q_{conv.loss}$	Convection loss, [kW]
ϵ	Emissivity
η_{hel}	Heliostat Efficiency [%]
θ	Incident angle, [^{o}]
$LHV_{mixture,\ calciner}$	Lower heating value of mixture of fuels into calciner, [kJ/kg]
$LHV_{mixture,\ kiln}$	Lower heating value of mixture of fuels into kiln, [kJ/kg]
$\dot{m}_{HTF}$	Mass flow rate of heat transfer fluid, [kg h^{-1}]
Y_{rm,CO_2}	Mass fraction of CO_2 in the raw meal, [%]
A_r	Lateral surface of the receiver, [m^2]
$\dot{m}_{CO_{2,red,max}}$	Maximum reduction of CO_2 , [kg/s]
$\dot{m}_{CO_{2,sol,min}}$	Minimum CO_2 reduction for solar calciner, [kg/s]
f_{mix}	Mixed convection coefficient
$\dot{m}_{mixture,\ calciner}$	Mixture of fuels mass flow into calciner, [kg/s]
$\dot{m}_{mixture,\ kiln}$	Mixture of fuels mass flow into kiln, [kg/s]
$q_{ref.loss}$	Power loss reflected from the receiver, [kW]
$q_{rad.loss}$	Radiation loss, [kW]
$\dot{m}_{rm}$	Raw meal mass flow rate, [kg/s]
$\dot{m}_{rm}/\dot{m}_{clinker}$	Raw meal to clinker factor
δ	Solar absorptance of the receiver surface
q_{rec}	Solar energy transferred, [kW]
q_{inc}	Solar power incident on a mirror, [kW]
q_{ref}	Solar thermal power reflected towards the central receiver, [kW]

q_{trans}	Solar thermal power to heat transfer fluid, [kW]
$C_{CO_{2,calciner}}$	Specific CO_2 emissions of fuel mixtures into calciner, [kg/kJ]
$C_{CO_{2,kiln}}$	Specific CO_2 emissions of fuel mixtures into kiln, [kg/kJ]
Cp_{HTF}	Specific heat capacity of heat transfer fluid, [kJ kg^{-1} K^{-1}]
σ_0	Stefan-Boltzmann coefficient, [$Wm^{-2}K^{-4}$]
$q_{rec.loss}$	Thermal power loss of solar energy in the receiver, [kW]
$q_{trans.loss}$	Thermal power loss of solar energy via transportation, [kW]
T_{wall}	Wall temperature, [K]

LIST OF ABBREVIATIONS

AF	Alternative Fuels
BD	Beam Down
CSP	Concentrated Solar Power
DNI	Direct Normal Irradiation
LHV	Lower Heating Value
RDF	Refuse Derived Fuel
TDF	Tire Derived Fuel
TSS	Thermal Storage System
TT	Top of Tower
PH/PC	Pre-heater/Pre-calciner
WO	Waste Oil

LIST OF FIGURES

Figure 1.1 Flowchart summarizing the thesis process and methodology 5

Figure 2.1 The flow diagram outlining gas and material flows of the pyro-process of a convectional cement production plant 8

Figure 2.2 Typical schematic representation of a modern large kiln system of FLS design a)ILC single preheater, b)SLC with dual-string preheater 11

Figure 2.3 The illustration of the species present at various temperatures during the clinker production process in ILC cement plant with reaction times . 14

Figure 2.4 The Jetflex® burner from FLSmidth 15

Figure 2.5 Typical Grate Clinker Cooler 16

Figure 2.6 Geometry and boundary conditions of the existing calciners 29

Figure 2.7 Adiabatic flame temperature of fuels 35

Figure 2.8 Flow chart of reaction mechanism modeling through NASA CEA and Chemkin-Pro Solver 37

Figure 2.9 Diagram of calciner and main burner for calculation combustion gas composition with chemkin-pro 39

Figure 2.10 Combustion Gas Products of Prediction NASA CEA(a,b) and Chemkin-Pro (c,d) Software respectively. a;c) Comparison of combustion for existing model in different temperature b;d) Comparison of gas products for existing and alternative models 46

Figure 3.1 Solar cement plant schematic diagram 49

Figure 3.2 The annual DNI resource of the province in Turkey 54

Figure 3.3 Comparison kg CO_2 /ton clinker of existing and alternative scenarios in the convectional calciner and solar calciner 56

Figure 3.4 Impact of DNI on CSP performance for existing and alternative scenarios in Turkey's provinces: a) Scenario 1, Scenario 13; b) Scenario 2, Scenario 5, Scenario 12; c) Scenario 15 59

Figure 3.5 Impact of heliostat number of the solar receiver on CSP performance for existing and alternative scenarios in Turkey's provinces 60

Figure 3.6 Impact of thermal efficiency of the solar receiver on CSP performance for existing and alternative scenarios in Turkey's provinces 60

LIST OF TABLES

Table 2.1 The amounts of fossil and alternative fuels fed from existing calciner and main burner 30

Table 2.2 Kiln and calciner combustion gas composition 32

Table 3.1 Climate data of Turkey province 53

Table 3.2 Requirement heat source value of convectional calciner 57

ABSTRACT

Reducing Fossil Fuel Consumption In Cement Industry: Modeling Of Gas Emissions And Innovative Solar Calciner Approach

Havva Hande CEBECİ

Department of Chemical Engineering

Doctor of Philosophy Thesis

Supervisor: Prof. Dr. Hasan SADIKOĞLU

Co- supervisor: Assist. Prof. Dr. Özgün YÜCEL

Chapter 1 proposes NASA CEA and Chemkin-Pro simulations to evaluate emissions from alternative and fossil fuels in the cement calciner. In the existing system, we measured emissions from the cement calciner and verified these data using NASA-CEA and Chemkin-Pro simulations. We developed 15 scenarios in addition to the existing system by varying the ratios of alternative fuels and fossil fuels (petcoke, lignite) fed by the calciner and main burner. Based on the ultimate and proximate analysis results, we calculated the adiabatic flame temperatures of the fuels and the combustion gas composition as a volume percentage. Alternative models with the closest calorific value to the existing system selected (Scenario 1, Scenario 2, Scenario 5, Scenario 12, and Scenario 13) and emissions such as CO_2, NO_x, SO_x, and H_2O (moisture) compared, injection points determined according to fuel types and verified with literature.

Chapter 2 proposes operating the conventional cement production process in a hybrid mode. The proposed system preserved the preheating, calcination, and rotary kiln processes from conventional production but integrated a solar calciner with a

solar power plant to carry out the calcination process. We calculated CO_2 emissions in various scenarios, considering the annual direct normal radiation (DNI) distribution in different provinces of Turkey, to assess the potential for CO_2 reduction. Using a 100% solar-powered calciner reduced CO_2 emissions by up to 20%, while increasing the use of alternative fuels results in CO_2 reductions ranging from 16% to 24%. Mersin and Şanlıurfa offer the most effective results for solar calciners, achieving higher CO_2 reductions (up to 24%). We have proven that optimizing heliostat numbers enhances system performance and reduces CO_2 emissions in cement production.

Keywords: Alternative fuel, cement production process, CO_2 reduction, combustion gas emission, solar calciner

ÖZET

Çimento Endüstrisinde Fosil Yakıt Tüketiminin Azaltılması: Gaz Emisyonlarının Modellenmesi Ve Yenilikçi Solar Kalsinatör Yaklaşımı

Havva Hande CEBECİ

Kimya Mühendisliği Anabilim Dalı
Doktora Tezi

Danışman: Prof. Dr. Hasan SADIKOĞLU

Eş-Danışman: Dr. Öğretim Üyesi Özgün YÜCEL

Bölüm 1, çimento kalsinatöründeki alternatif ve fosil yakıtların emisyonlarını değerlendirmek için NASA-CEA ve Chemkin-Pro simülasyonlarını önermektedir. Mevcut sistemde, çimento fabrikasının kalsinatöründen ölçümler alındı ve bu veriler NASA-CEA ve Chemkin-Pro simülasyonları kullanılarak doğrulandı. Mevcut sisteme ek olarak, kalsinatör ve ana brülöre beslenen alternatif yakıtlar(atıktan türetilmiş yakıt, lastikten türetilmiş yakıt, atık yağ) ve fosil yakıtların (petkok, linyit) oranlarını değiştirerek 15 senaryo geliştirdik.Nihai ve yakın analiz sonuçlarına dayanarak, yakıtların adyabatik alev sıcaklıklarını ve yanma gazı bileşimini hacim yüzdesi olarak hesaplandı. Mevcut sisteme en yakın kalorifik değere sahip alternatif modeller seçildi (Senaryo 1, Senaryo 2, Senaryo 5, Senaryo 12 ve Senaryo 13) ve CO_2, NO_x, SO_x ve H_2O (nem) gibi emisyonlar karşılaştırıldı, yakıt türlerine göre enjeksiyon noktaları belirlendi ve literatürle doğrulandı.

Bölüm 2, geleneksel çimento üretim sürecinin hibrit bir modda işletilmesini önerilmektedir. Önerilen sistem, konvansiyonel üretimden ön ısıtma, kalsinasyon ve döner fırın süreçlerini korudu ancak kalsinasyon sürecini gerçekleştirmek için

bir güneş kalsinatörünü bir güneş enerjisi santrali ile entegre edildi. Farklı senaryolar altında, Türkiye'nin farklı illerindeki yıllık doğrudan normal radyasyon (DNI) dağılımını dikkate alarak CO_2 emisyonları hesaplandı ve CO_2 azaltma potansiyelini değerlendirildi. %100 güneş enerjili bir kalsinatör kullanılması, CO_2 emisyonlarını %20'ye kadar azaltırken, alternatif yakıtların kullanımının artırılması CO_2 azaltımlarını %16'dan %24'e kadar çıkarmaktadır. Mersin ve Şanlıurfa, solar kalsinatörler için en etkili sonuçları sunarak daha yüksek CO_2 azaltımları (yüzde 24'e kadar) elde etti. Heliostat sayılarını optimize etmenin sistem performansını artırdığını ve çimento üretiminde CO_2 emisyonlarını azalttığı kanıtlanmıştır.

Anahtar Kelimeler: Alternatif yakıt, çimento üretim prosesi, CO_2 azaltma, yanma gazı emisyonu, solar kalsinasyon

1
INTRODUCTION

1.1 Background

Cement production is the major carbon dioxide (CO_2) emissions (Cansiz et al., 2023), accounting for 26% of total industrial emissions (Luo et al., 2024). Multifaceted efforts are underway to prevent global warming (Clark et al., 2024) and eliminate emissions from cement production, with more than 20 countries aiming to achieve net zero emissions by 2050 as part of the United Nations sustainability goals (Nehdi et al., 2024). To achieve carbon neutrality in the cement sector include improving reducing clinker and cement ratios (Martignon, 2020), thermal and electrical energy efficiency (Barbhuiya et al., 2024), implementing carbon capture and storage technologies, and increasing the use of alternative fuels (AF) (Chai et al., 2022). Although fossil fuels such as coal, petroleum coke, oil, natural gas, and lignite are mostly used in cement factories, the use of various solid wastes as AF has increased in cement factories in recent years. The most important profits of using AF in cement production are cost savings, utilization of waste, reduction of storage areas, prevention of ash/fly ash emissions by incineration in cement kilns, savings in natural raw material resources, and reduction of CO_2 emissions resulting from fossil fuel use (Nehdi et al., 2024). CO_2 emissions from cement factories could be reduced by processing AF, but in some cases, non-CO_2 air pollutants could increase. Based on analyses of the impact of non-CO_2 emissions, it was observed that sulfur dioxide (SO_2) emissions from the US cement industry increased when replacing coal with scrap tires and solid waste, while a slight decrease was observed for biomass and waste oil. Collaboration with sewage sludge was found to decrease SO_2 emissions from the US cement industry. It was reported that the US cement industry could reduce nitrogen oxide (NOx) emissions when using AF instead of coal and that collaboration with waste oil represented the

greatest potential for NO_x reduction. In descending order, sewage sludge, solid waste, scrap tires, and biomass were reported to have the lowest potential for reducing NO_x emissions (Hasanbeigi & Bhadbhade, 2023) .

In the cement industry, the thermal substitution ratio (TSR) corresponds to the ratio of AF to fossil fuels in terms of thermal energy (Sharma et al., 2022). TSR can reach up to 80-100% in a calciner, while a kiln burner can only achieve a TSR of 50-60%. To overcome these challenges in the cement industry, to use of AF is significant, reducing the dependence on fossil fuels and increasing TSRs. However, AF have operational challenges in the calciner and kiln (Beguedou et al., 2023). The estimation of adiabatic flame temperature (AFT) plays a role in controlling various combustion parameters, exploring different combustion scenarios, and determining their effects on both the AFT and the chemical composition of the combustion products (Jamali et al., 2019). While the flame temperatures of the fuels can be determined depending on the moisture, volatility, and ash content; It is important in determining the feeding locations of fuels (Sharma, 2023) and emissions released as a result of combustion (Bhave et al., 2022). NASA CEA (Applied Chemical Equilibrium) and CHEMKIN-Pro, two widely used software tools in the field of chemical kinetics and thermodynamics, will be used to calculate both kinetic and equilibrium models of reactions. NASA CEA is specifically designed to determine the chemical equilibrium compositions and properties of complex mixtures and is widely used in applications such as rocket propulsion, combustion analysis, and other high-temperature chemical equilibrium problems. It provides calculations of equilibrium compositions, thermodynamic properties (such as enthalpy, entropy, and specific heats), and performance parameters (such as specific impulse and thrust) under specified conditions (Gordon &McBride, 1994) . CHEMKIN-Pro provides transient and steady-state solutions that include concentrations, temperature profiles, and reaction rates of chemical species in various reactor configurations. It solves time-dependent or steady-state conservation equations for mass, energy, and species concentrations using detailed reaction mechanisms and can simulate transient events and detailed reaction kinetics in time. CHEMKIN-Pro has a wide range of kinetic modeling applications in the automotive, aerospace, chemical processing, and environmental industries,

while NASA CEA is widely used in aviation, especially for the design and analysis of rocket engines and high-temperature propulsion systems. In summary, CHEMKIN-Pro provides a comprehensive platform for detailed kinetic modeling and dynamic simulations in a variety of chemical processes, while NASA CEA is specializes for equilibrium calculations in high-temperature systems (Kee et al., 1989). There are several studies in the literature conducted using different software programs to calculate gas emissions resulting from combustion. Hosseini et al. (2013) studied palm oil combustion properties with NASA CEA software, focusing on CO, CO_2, and NO emissions . Zajemska et al. (2014) used CHEMKIN-PRO to calculate the flue gas composition from natural gas combustion, with gas dynamics modeled in COMSOL. Kayadelen et al. (2017) examined natural gas and methane mixtures in a methane-air engine using the equilibrium constant method, comparing results with NASA and GASEQ software. Sieradzka et al. (2020) modeled refuse-derived fuel (RDF) pyrolysis with Ansys Chemkin-Pro, examining mole fractions of various gases at different temperatures and proposing reaction pathways. Ansys Chemkin-Pro software. Yılmaz et al. (2021) developed models to predict combustion products in a domestic boiler, validated against CHEMKIN software. Oxy-methane, oxy-hydrogen, air-methane, and air-hydrogen AFTs were determined under stoichiometric conditions, with a reaction temperature of 298.15 K and a pressure of 1 bar by modeling the reaction mechanisms at NASA CEA (Marzouk, 2023). Carotenuto et al. (2023) developed a numerical model using a restricted chemical equilibrium approach for the gasification of sewage sludge and implemented it in the Aspen Plus software. Sánchez et al. (2024) developed a model by OpenFOAM (Open source Field Operation And Manipulation) for modeling the combustion chamber of a Ward-Cimpa furnace to increase furnace efficiency and explore the possibility of using agricultural waste as fuel.

The manufacture of cement utilizes various fossil fuels to supply thermal energy demands. In addition to coal derivatives such petroleum coke and lignite, natural gas and biomass are the most prevalent fossil fuels. The combustion of fossil fuels generates greenhouse gas emissions (Sahoo et al., 2021). Researchers predict a 2–7% reduction in greenhouse gas emissions when solar calciners replace conventional fossil fuel calciners. Another study reported that the calcination

process consumes 80% of the energy in the cement industry and is responsible for 7% of global greenhouse gas emissions. Environmentally friendly solar calcination is used to make cement. They used life cycle assessment to compare three types of solar energy for calcination. A full solar thermal system; a hybrid system where solar thermal provides 14% of the thermal energy; and a hybrid system with a traditional fossil fuel-based calciner where solar thermal provides 33% of the thermal energy. Reports indicate that cement industries can integrate solar thermal systems up to 36%, reducing climate change impact by 15–40%, based on irradiances in different regions of the world. However, the disadvantages include increased land occupation, a higher risk of human toxicity and cancer (102%), and the depletion of metals and minerals (6%) due to the involvement of construction processes in the production of solar systems (Tomatis et al., 2020). The calcination process is responsible for roughly 66% of these emissions. The clinker fuel constitutes 13% of the residual 34% of emissions, whereas the traditional calciner fuel represents 21% (Gardarsdottir et al., 2019; Voldsund at al., 2019). Fuel substitution is important for heat substitution and reducing carbon emissions in cement production. In this context, we can utilize low-carbon fuels like solid waste, natural gas, biomass energy, and solar energy (Wang et al., 2024). Researchers have recently investigated the application of concentrated solar power (CSP) in the calcination process of cement manufacture. A traditional cement plant can utilize a solar tower system, which includes a solar reactor or a preheater tower at its top, to harness solar energy (Sahoo et al., 2023a). The research indicates two potential designs for the solarization of the calcination process (González & Flamant, 2014). The existing preheater tower supports the tower-top (TT) configuration of the solar reactor, while the ground anchors the beam-down (BD) design model. In the TT architecture, optical losses are minimal in comparison to a beam-down plant. The BD design facilitates the feeding and maintenance of raw materials in the solar reactor. Nonetheless, it incurs higher expenses due to the requirement for secondary reflectors and possesses a reduced power capacity. TT design possesses exceptional attributes (Meier et al., 2005).

In Chapter 1, we modeled these gas emissions and examined their impacts. In Chapter 2, we conducted an innovative study on solar calciner, which shows a

recent trend of reducing CO_2 emissions in cement plants. Thesis process and methodology overview is summarized in flow diagram is illustrated in Figure 1.1.

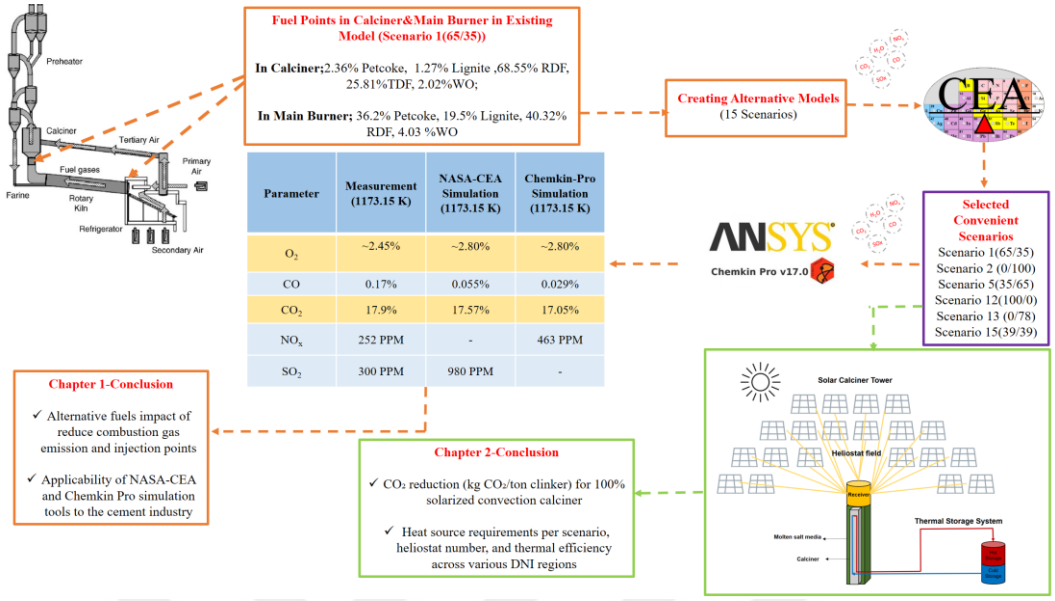


Figure 1.1 Flowchart summarizing the thesis process and methodology (The cement calciner image produced by Fidaros et al., (2006))

1.2 The Objective of Thesis

Chapter 1 (process overview and emission modelling using computational tools in cement production) aims to explore the use of NASA CEA and CHEMKIN-Pro software in cement production. The study will also examine the combustion processes of traditional fossil fuels such as petroleum coke and lignite, as well as alternative fuels such as RDF, TDF, and waste oil, and the resulting emissions such as CO_2, NO_x, and SO_x. The study verified and analyzed real measurement data from a cement plant in Central Anatolia using NASA CEA and Chemkin-Pro simulations. We evaluate the volumetric composition of combustion gases, adiabatic flame temperature (AFT), and emission rates based on various fuel types and mixture ratios. We developed alternative scenarios for the current system, creating 15 different model scenarios by varying the ratios of fossil and alternative fuels. We selected five distinct scenarios in CHEMKIN-Pro, namely scenario 2, scenario 5, scenario 12, scenario 13, and scenario 15, based on NASA CEA results, and evaluated the emission gases in each. The aim of these scenarios was to reduce environmental impacts and optimize fuel. The study's goal is to come up with a new

way to use sustainable energy and lower emissions in cement production. It will do this by looking at how well NASA CEA and Chemkin-Pro software can be used in the cement industry and how easy they are to use compared to other modeling tools.

Chapter 2 (integrating solar calciner technology for reduction emission in cement production) aims to investigate the potential of integrating solar energy into cement production processes and using alternative fuels to reduce CO_2 emissions. The study explores the potential emission reductions through the integration of a 100% solar-powered calciner system into conventional production processes, and assesses the system's performance in various fuel scenarios. Analyses conducted in different geographical regions with high DNI (direct normal irradiance) values in Turkey revealed the effects of solar energy use on thermal efficiency, and determined the contributions of alternative fuels to emission reduction. In this context, the aim of the study is to promote the use of sustainable energy sources by reducing the use of fossil fuels in cement production, to reveal the effectiveness of solar energy and alternative fuel combinations to reduce CO_2 emissions, and to present a comprehensive roadmap for transitioning to a sustainable production process in the cement industry.

1.3 The Hypothesis of Thesis

In Chapter 1, in which NASA CEA and CHEMKIN-PRO simulations are applied to evaluate the emissions from alternative and fossil fuels in the cement calciner, the following questions are sought to be answered.

- Can NASA CEA and CHEMKIN-PRO simulations provide reliable and consistent results for validation and benchmarking in the emission analysis of alternative and fossil fuels utilized in cement plant calciners?
- Can increasing alternative fuel ratios enhance environmental performance relative to the existing fossil fuel system in mitigating harmful emissions such as CO_2, NO_x, SO_2, and H_2O?
- Can the optimization of injection locations for AF yield the most effective scenarios for enhancing combustion efficiency and reducing emissions?

In Chapter 2, where the implementation of %100 solar calciner to convectional calciner in different DNI regions is evaluated, the following questions are sought to be answered.

- How much can a solar calciner reduce CO_2 emissions in the traditional cement production process?
- How much can the use of alternative fuels and solar energy reduce CO2 emissions in cement production?
- How can we determine whether regions of Turkey with high DNI (direct normal irradiance) values have more efficient solar calciners?
- To what extent is it important to optimize the number of heliostats to increase the efficiency of solar calciners?
- What is the impact of integrating solar energy in cement production on reducing the use of fossil fuels in regions with high DNI values?

2
PROCESS OVERVIEW AND EMISSION MODELLING USING COMPUTATIONAL TOOLS IN CEMENT PRODUCTION

2.1 he Conventional Cement Production Process

The main pathways for cement manufacture vary concerning equipment design, operational methods, and fuel consumption. The cement production process mainly involves three major steps. The first step is quarrying and raw material preparation. The second step, pyro-processing, involves preheating raw materials, kiln operation, and clinker cooling. The third step involves grinding, storage, and shipping (Rahman et al., 2013a).The other two processes (steps 1 and 3) mainly consume electricity. Pyroprocessing (step 2) typically uses 99% of the energy content of the fuels and about 20% of the electrical input (Khuruna et al., 2002). The flow diagram of convectional cement production plant is illustrated in Figure 2.1.

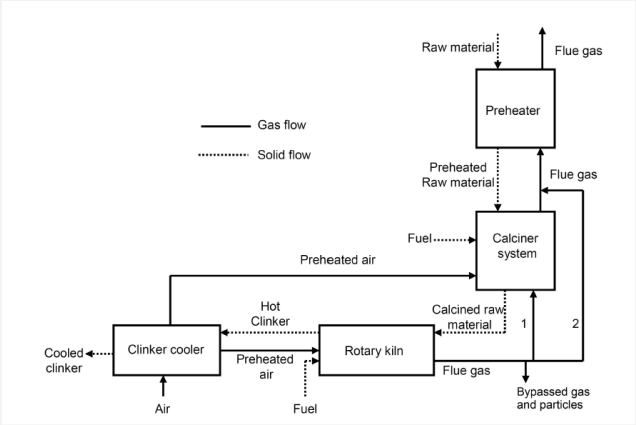


Figure 2.1 The flow diagram outlining gas and material flows of the pyro-process of a convectional cement production plant (Larsen, 2007)

2.1.1 Preparing of Raw Material

Cement manufacture occurs at the quarry with the extraction and transportation of raw materials to the facility. Quarrying could be conducted by either ripping or drilling and blasting methods. Regardless, the recovered material must have

uniform quality, and the necessary degree of mine planning is supported either by an underground survey throughout the mining region or by the analysis of cuttings obtained during blasthole drilling (Alsop, 2001). Raw material preparation involves the production of meal by grinding and mixing components such as limestone, clay, and sand. These materials provide the chemical components, such as $CaCO_3$, silicon dioxide (SiO_2), aluminum oxide (Al_2O_3), and hematite(Fe_2O_3). The first stage involves crushing limestone and drying components like clay and sand. The next stage involves grinding the desired meal composition with certain additives. This mixture is prepared for the clinker production process (Maldonado, 2021).

2.1.2 Pyro-Process Unit

The downstream cyclone utilizes gases from the calciner and rotary kiln to heat the feed material, transforming it into calcined meal. The fossil fuel sustains the reaction heat using the hot air from the cement cooler. The rotary kiln elevates the temperature of the calcined raw meals to 1550 K. At elevated temperatures, minerals transform into clinker. The cooler utilizes ambient air for cooling the clinker and then releases excess air. The exhaust from the clinker cooler generates electricity (Polat & Tari, 2023).

2.1.3 Pre-Heater and Pre-Calciner

Suspension preheaters and precalciners reduce fuel waste in conventional dry-process cement manufacturing. The main component of the preheater is the cyclone. The number of cyclones utilized in the preheater tower ranges from 1 to 6. Fan power is necessary for circulating the gases through the cyclone system. The hot air from the clinker cooling stage passes through to the preheater tower to dry and preheat the raw materials. The cyclone string of the preheater tower feeds the hot raw material to the calciner. The combustion air coming from the bottom section of the kiln flows to the calciner through the cooler, known as tertiary air(Rahman et al., 2013a). Suspension preheaters and precalciners reduce fuel wastage in conventional dry-process cement production. The main component of the preheater is the cyclone. The number of cyclones used in the preheater tower ranges from 1 to 6. Fan power is required to circulate the gases through the cyclone system. It uses an induced draft (ID) fan that draws countercurrent to the material flow from the kiln and preheater tower. The non-calcined meal is introduced into the gas stream

through the channel across the upper two cyclone units. The ID fan draws this raw material into the first cyclone and separates it from the gas. The gas conducts heat while the non-calcined meals stays trapped in the heated gas flow. The material enters the preheater tower through the channel between the second and third stage cyclones and flows by gravity through the first stage cyclone. The lower cyclones generally operate at 80% efficiency, separating 80% of the raw material from the gas and sending it to the lower cyclone. The remaining solid particles carried by the gas pass to the upper-stage cyclone. The efficiency of the upper cyclone stage reaches 95% due to the use of twin cyclones. Centrifugal force separates the material from the gas in the second-stage cyclone. The cyclone tower dried the raw meal, dehydrates and separates from clay minerals. The calcination $MgCO_3$ with oxidation of organic compounds in the raw material occur. The preheater's temperature is raised to approximately 800°C, while the temperature of the counterflow gas is reduced from 900°C to 350°C. The hot air from the clinker cooling stage passes into the preheater tower to dry and preheat the raw materials. The cyclone train of the preheater tower feeds the hot raw material to the calciner. Combustion air from the lower section of the kiln flows through the cooler, known as tertiary air, into the calciner(Neuffer & Laney, 2007). Calcination is the most energy-demanding reaction in cement production; it typically occurs in a cement calciner. This reaction (1.1) can be expressed as below (Jensen,1999):

$$CaCO_3(s) \rightarrow CaO(s) + CO_2(g), \Delta H = +1782 \frac{kJ}{kgCaCO_3} \qquad (1.1)$$

The calcination process is a strong endothermic reaction in which limestone ($CaCO_3$) thermally decomposes into lime (CaO) and carbon dioxide (CO_2). As the meal is heated between 100°C and 500°C, moisture evaporates, and the temperature at which this reaction takes place is in the range of 700-900°C. The calcination reaction is highly endothermic and it can be used as a temperature-controlling tool in calciners (Fidaros et al., 2006). Calciners are divided into two main types: in-line calciners (ILCs) and separate-line calciners (SLCs) (Rahman et al., 2013a). In an ILC, tertiary air and kiln exhaust gases pass through the combustion zone of the calciner and are suitable for the combustion of high-volatility fuels. The temperature is kept approximately 800°C-850°C and the oxygen content is low, but

low-volatility fuels (e.g., petcoke) may have difficulty in combustion in an ILC. The calciner in an SLC does not pass through the kiln gases, and it burns low-volatility fuels using air containing 21% oxygen. SLCs are more suitable for low-volatility fuels such as petcoke due to their gas retention times and temperatures are higher. Modern systems offer a more flexible use with different options in SLCs (Gasser, 2000). FLS design of ILC single and SLC with dual type pre-heater is demonstrated in Figure 2.2.

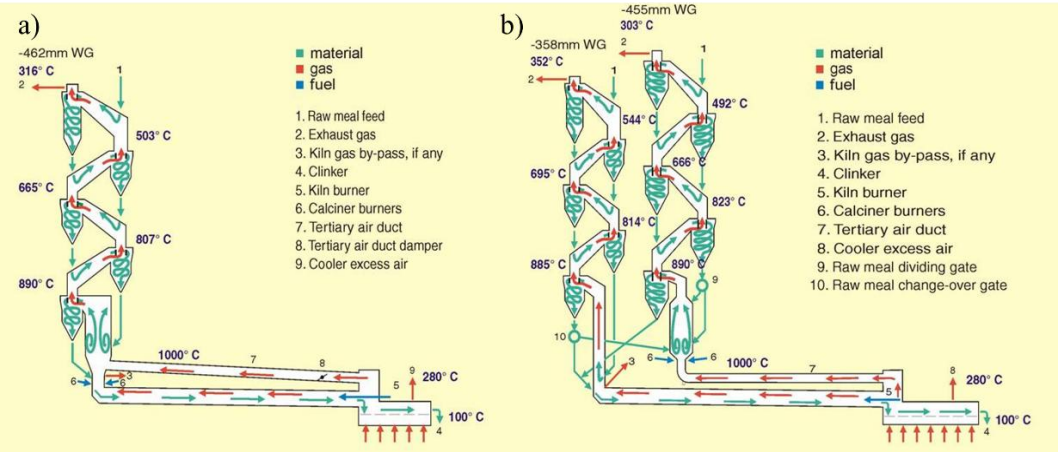


Figure 2.2 Typical schematic representation of a modern large kiln system of FLS design a)ILC single preheater, b)SLC with dual-string preheater (FLS In Line Calciner)

2.1.4 Rotary Kiln

The bottom cyclone feeds the calcined meal into the rotary kiln after it output the calciner. The rotary kiln, a slightly inclined metal cylinder tube, rotates at 2 rpm for sintering. Made of alumina and mangasia, refractory bricks line the inside of the kiln, protecting it from high heat and thermal losses (Polat & Tari, 2023). The burner in the kiln creates a high-temperature flame by burning the fuel. The calcined meal enters the kiln around 900°C, whereas the gas temperature is roughly 1,100°C. The kiln inclines and rotation allow the material to advance, and the temperature increases. The kiln first removes CO_2, and then reactions between calcium, silicon, aluminum, and iron oxides produce clinker.

The transfer section of the rotary kiln receives the raw material from the preheater tower at the top, while the flame tube at the other end meets the primary fuels such as petroleum coke, coal, fuel oil, natural gas, and secondary fuels. The inlet section of the kiln breaks down the carbonates into their oxides at temperatures of 800-900

°C. At temperatures of 1,000–1,200°C, solid-solid reactions begin, leading to the formation of dicalcium silicates. These conditions lead to the formation of the solid phases belite, aluminate, and ferrite. In addition, these temperatures trigger the release of inorganic volatiles, such as alkalis, sulfates, and chlorine, present in raw materials and fuels. The kiln experiences ring formation, which reduces the cross-sectional area due to the release of these volatiles. The material then reaches the sintering zone, where the aluminate and ferrite phases melt at temperatures between 1,300 and 1,450°C. This leads to the formation of the belite phase, which allows the solid particles to stick together, granulates them, and ultimately leads to the formation of clinker. After rapid cooling, the formed clinker exits the kiln system. The purpose of rapid cooling is to ensure that the alumina (C_3A) phase, which has an important effect on the hardening of the cement and provides slow and controllable hydration, remains stable. At temperatures of 1,250°C and above, the aluminate phase remains stable; at lower temperatures, it undergoes a reversible reaction, converting into belite and calcium oxide compounds. Depending on the content of the raw materials and fuels, the clinker's main components distribute over a wide range. Belite (C_2S) is a compound that slowly reacts with water, releasing a small amount of heat, and its binding properties become apparent in the following years. Secondary belite (C_3S) releases a moderate amount of heat during its reaction with water and has high binding properties. Ferrite (C_4AF) does not react with water and has very low binding properties. C_3S is a compound that reacts rapidly with water and releases a large amount of heat during its reaction. In addition to its binding properties, it is a compound that reduces the resistance of cement to sulfates. Clinker mixes with gypsum during grinding, causing the cement to harden immediately. While the transition section brings the calcined meal to the kiln, a flame pipe from the head section provides the fuels, allowing the flame to reach 2,000°C. Specialized burners provide fuel and hot air through the bottom end of clinker cooler, while the counterflow configuration feeds calcined meal through the upper end of calciner. Upon the introduction of the raw meal into the rotary kiln, the subsequent chemical reactions.Clinker processes predominantly occur at temperatures ranging from 700°C to 1450°C within the rotary kiln, where calcium oxide (CaO) reacts with quartz (SiO_2) nd the byproducts of clay mineral decomposition, including Al_2O_3 and Fe_2O_3 (Nakhaei, 2018). From an approximate

temperature of 700°C, belite (C_2S) will be formed from calcium oxide and quartz according to the following reaction (2.3) (Jensen, 1999),

$$2CaO + SiO_2 \rightarrow 2CaO \cdot SiO_2, \Delta H = -734 \frac{kj}{kg_{C_2S}} \quad (2.3)$$

As this reaction proceeds further, the amount of quartz in the system decreases are shown in Figure 2.3. At higher temperatures, i.e. around 900°C, aluminate (C_3A) and ferrite (C_4AF) are formed from clay (Fe_2O_3 and Al_2O_3) is following reaction (2.4) and (2.5) (Jensen, 1999),

$$3CaO + Al_2O_3 \rightarrow 3CaO.Al_2O_3, \Delta H = 27 \frac{kj}{kg_{C_3A}} \quad (2.4)$$

$$4CaO + Al_2O_3 + Fe_2O_3 \rightarrow 4CaO.Al_2O_3.Fe_2O_3, \Delta H = -105 \frac{kj}{kg_{C_4AF}} \quad (2.5)$$

Finally, at temperatures above 1300°C, a melt is formed which is primarily composed of aluminate (C_3A) and ferrite (C_4AF) phases. Then the formation of alite (C_3S) from calcium oxide and belite (C_2S) is accelerated according to the following endothermic reaction (2.6) (Jensen, 1999),

$$C_2S + CaO \rightarrow 3CaO.SiO_2, \Delta H = = +59 \frac{kj}{kg_{C_3S}} \quad (2.6)$$

The final clinker production step is a rapid cooling process when the maximum temperature has been reached (Steuch, 2004). If the cooling process takes place at a low rate, secondary belite (C_3S) and free calcium oxide may be formed as alite dissolves into the liquid phase. This may result in poor quality of the cement clinker especially the cement strength and the rate of strength development (Larsen, 2007).

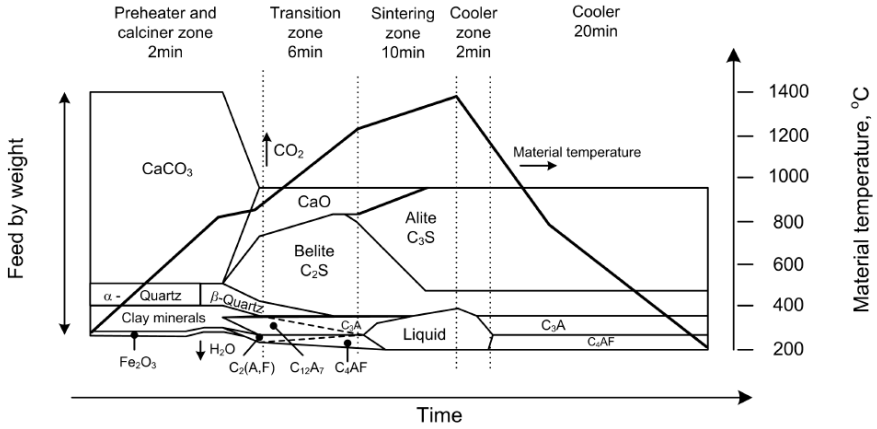


Figure 2.3 The illustration of the species present at various temperatures during the clinker production process in ILC cement plant with reaction times (Wolter, 1985)

Efforts to combust solid alternative fuels in rotary kilns required the installation of an auxiliary tube above the pre-existing main burner. This injection approach was ineffective as it transported the fuel above the flame and dropped it into the clinker bed without converting, providing only minimal degrees of substitution (Vaccaro, 2006; Emberger & Hoenig, 2011). In contrast to the overfiring site, other studies have also demonstrated that the middle of the main burner is the ideal location for alternative fuel injection (Nørskov, 2012). Figure 2.4 illustrates the Jetflex® burner from FLSmidth, a multi-channel burner designed to accommodate various fuels. It is utilized for gaseous, liquid, solid fossil fuels, alternative fuels, or a combination thereof. The design accepts oil, gas, powdered solid fuels, and alternative fuels, with a capacity of up to 250 MW. The burner output can be adjusted according to the fuel type. The Jetflex burner features a straight channel that allows powdered or solid fuels to flow easily. Rectangular nozzles and a vortex replace the traditional fuel channel, ensuring good fuel mixing. 20 axial air nozzles provide control over the flame shape at the burner tip. This reduces fuel velocity during ignition, increases fuel residence time in the flame, and enables early ignition of lower-quality fuels. These features facilitate the use of higher alternative fuel ratios (FLSmidth JetFlex Burner brochure, 2024).

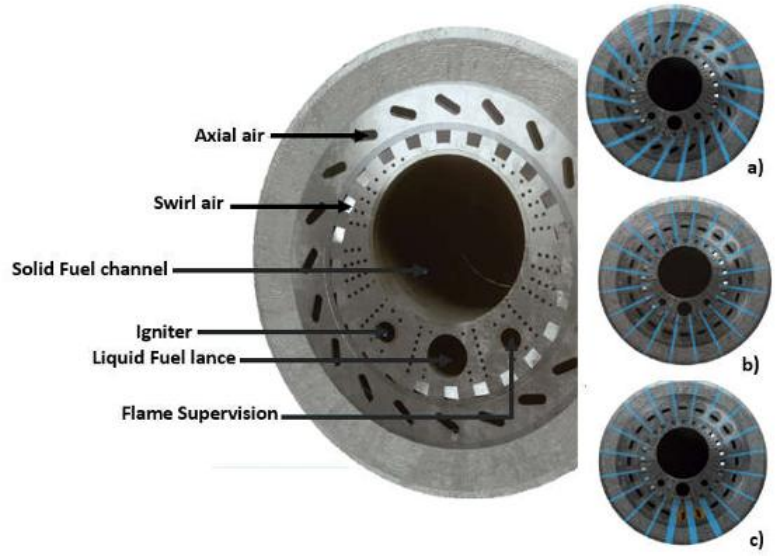


Figure 2.4 The Jetflex® burner from FLSmidth (FLSmidth JetFlex Burner brochure, 2024)

2.1.5 Clinker Cooling

The clinker passing through the kiln is transferred to the clinker cooler at a temperature of roughly 1,250°C and where the cooler layer forces ambient air to flow through, decreasing the clinker temperature to around 100°C. The heated air gathered by a cooler can be used for second air. Cooler has retention time is around 15 to 30 minutes.The cooler's purpose is to remove heat from the hot clinker, allowing for its storage or transportation for cement production. The clinker leaving the cooler is stored or directly ground to produce cement. Modern cement plants utilize closed-design grate coolers for their superior heat transfer properties. These coolers blow air into the clinker bed from the bottom (Atmaca, 2014). These coolers introduce air into the clinker bed from below. Various hoods capture air at distinct temperature levels. Secondary air is introduced into the rotary kiln, tertiary air is directed to the calciner, and the residual air is utilized in waste heat recovery systems. The oscillatory movement of the grate bars featuring a sawtooth design displaces the clinker. The forward force propels the clinker, and the reverse force changes the grate bars towards the bed. Significant advancements in cooler design include the effective distribution of cooling air with little pressure loss, optimized clinker movement inside the cooler, and reutilization of secondary air, tertiary air, and waste heat recovery systems. (Polat&Tari, 2023). The illustrated grate cooler unit is shown in Figure 2.5.

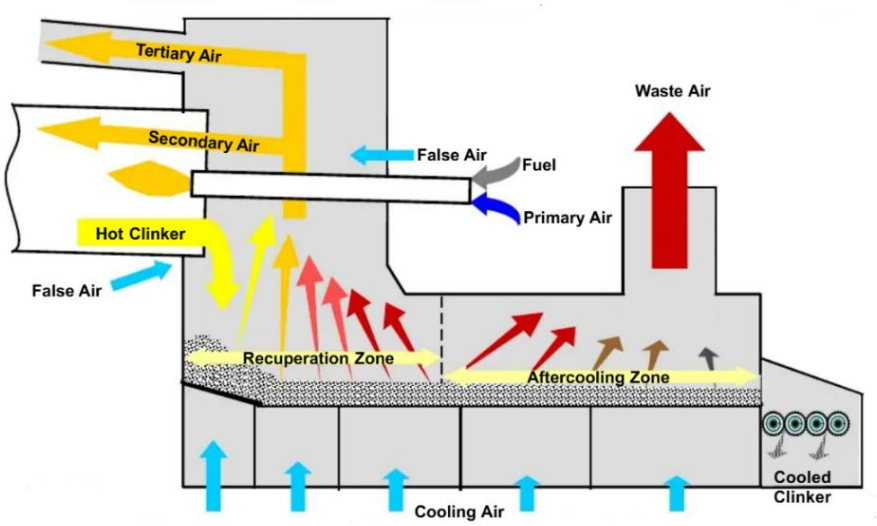


Figure 2.5 Typical Grate Clinker Cooler (Holcim Group Clinker Cooler, Retrieved November 4, 2024)

2.1.6 Alkali Bypass

Some PH/PC clay types have alkaline bypass unit at end of the kiln feed. The unit removes roughly up to 30% of the combustion gases from clay and cooled gas, and prevents the formation of deposits in the preheater(Sutou et al., 1999). The bypass system prevents volatile inorganic compounds, especially alkaline substances, from condensing inside the clay's preheater. Alkali accumulation can lead to a decrease in the quality of the cement, so it's crucial to reduce its amount. The bypass system reduces the alkali content in the clinker by removing the alkali, thus contributing to the production of quality cement (Neuffer & Laney, 2007). The calciner riser duct typically supplies this. The bypass system reduces the cement plant's thermal efficiency by removing hot gases from the process system. However, the reduction in thermal efficiency is less pronounced compared to a cement plant without a calciner (Bech&Mishulovich, 2004).

2.2 The Fuels in Cement Production Plant

The convenient fuel selection for calciner and rotary kiln in a cement plant is determined by the equilibrium among three primary factors: costs, product quality, and environmental impacts. One of the primary considerations for fuel selection is the cost, which encompasses the expenses associated with the purchase, transportation, and handling of the fuel, as well as the operational costs of its

combustion. Fuel cost is an important factor that cement manufacturers take into account. The second factor pertains to product quality. The chemical properties of the fuel and its transformation behavior in the calciner and rotary kiln can directly affect product quality. Therefore, the properties of the fuel should be carefully examined to maintain product quality. Environmental impacts, which include prompt emissions such as NO_x, CO, SO_2, and CO_2 released by cement plants, are important criteria. An evaluation of environmental impacts in fuel selection is necessary for both the sustainability of plant operations and environmental protection (Nakhaei, 2018). Here is a brief explanation of some crucial fuel parameters that could influence fuel selection:

Sulfur Content: The sulfur content of the fuel can cause SO_2 formation, especially at high temperatures in the rotary kiln (Bech & Mishulovich, 2004). However, the preheater system typically absorbs the released SO_2 from the fuel, except cement production lines without a bypass system (Hansen, 2003). Furthermore, the combustion within the rotary kiln may facilitate the circulation of sulfur between the kiln and the preheater system.

Nitrogen Content: Chemically bound nitrogen in the fuel typically oxidizes to form NO_x emissions. However, char reactions can reduce NO_x emissions; these reactions interact with NO_x formation and reduction.

Ash Content: The ash content of the fuel significantly affects the operation and maintenance processes of the cement calcination furnace and rotary kiln. Fuel with a high ash content has a lower gross calorific value, which increases transportation costs. Since the raw material composition also contains elements like calcium, silicon, and alumina found in the fuel ash, it should be optimized the raw material composition based on the fuel ash content to maintain clinker quality(Nørskov, 2012).

Volatile Elements: The circulation of alkali, sulfur, and chlorine compounds in the rotary kiln, calciner, and preheater system can be controlled by bypassing some gases from the calciner riser duct. If the calciner or rotary kiln fuel contains these volatile elements, it is necessary to increase the amount of bypass gases to maintain clinker quality and operational stability. This may reduce the thermal efficiency of

the pyro-system and limit the use of alternative fuels with high levels of these elements(Nakhaei, 2018).

2.2.1 Fossil Fuels Using in Cement Production Plant

The conventional (fossil) fuels used in the European cement industry are mostly coal, petcoke (a product of crude oil refining), and heavy oil. Natural gas is rarely used due to its higher cost (European Cement Industry, 1999). Coal primarily consists of carbon, oxygen, and oxygen due to its organic origin. The ASTM classifies coal into four categories: anthracite, bituminous, sub-bituminous, and lignite (brown coal), ranging from high to low. Cement nuclear power plants widely use bituminous and sub-bituminous coals among the mentioned coal types. According to ash content, coal can be classified as low, medium, and high ash coal, corresponding to 3-8%, 8-15%, and more than 15% ash, respectively. Medium-ash coal is the predominant type utilized in cement emissions. Cement calciners or rotary kilns typically grind solid conventional fuels to a fineness comparable to that of raw meals prior to combustion. The particle size of solid fuels is crucial, particularly for the conversion of fuels with low volatile content. Pulverizing coal usually takes place in coal mills. The size distribution of pulverized coal particles may vary depending on the operation of the coal mill. In the cement industry, a general rule for the size of pulverized coal particles is that the residue should be smaller than half the volatile content in the fuel at a 90-μm sieve (Nakhaei, 2018). Petcoke is a carbon-rich solid fuel that is a byproduct of the petroleum refining process and a by-product of a larger chemical process. The price of this fuel is relatively cheap, and, compared to coal, petroleum coke can be 50–70% cheaper. As a result, the production of petcoke has increased steadily in recent years, and cement plants are one of the largest consumers of petroleum coke. One of the main differences between petcoke and coal is that petcoke has a lower overall reactivity during combustion due to its lower volatile matter content, while coal has a lower reactivity to oxidation (Nakhaei, 2018). This can lead to lower fuel burn at the calciner outlet. For different calciner designs, replacing (high-volatile) coal with petcoke in the calciner increases stack NOx emissions by a factor in the range of 1.1–3.1 (Shenk &Jensen, 2009). The same criterion of a maximum of half of the

volatiles in the 90 μm residue is generally used for the size distribution of petcoke fuel particles, but it cannot be applied without reservations (Nakhaei, 2018).

2.2.2 Alternative Fuels Using in Cement Production Plant

Cement manufacturers worldwide use AF to control their costs and reduce their environmental impact. Cement manufacturers utilize a variety of fuels, including petroleum coke, TDF, and RDF, among others. Additionally, the country will benefit economically from the anticipated oil savings. The use of AF may lead to an increase in current costs and a decrease in the net cash flows of cement companies (Rahman et al., 2013b). The primary advantages of utilizing AF in kiln and calciner reduced the dependency on non-renewable fossil fuels, include petcoke and coal etc.The research has demonstrated that substituting conventional fossil fuels with AF can significantly contribute to reducing global emissions of greenhouse gases such as CO_2 and thereby mitigating the global climate change Kyoto target. The AF in cement kilns increase energy recovery from waste. The kiln uses all the energy directly for cement productionFurthermore, the combustion of alternative fuels in cement kilns facilitates the recovery of all waste materials by integrating the inorganic components into the crystalline structure of the clinker. Unlike specialized waste incinerators, the kiln recycles all solid waste without producing any liquid waste, eliminating the need for separate ash and slag disposal. AF are primarily wastes of various industrial or agricultural operations and present a significant solid waste management concern in numerous countries because to their substantial volume and potential toxicity. These waste materials were either dumped in landfills or incinerated in specialized incinerators. By utilizing pre-existing kiln infrastructure and energy demand, cement kilns offer an environmentally safe and secure alternative to traditional waste disposal in dedicated incinerators or landfills (Ariyaratne, 2009). The cement kiln's temperature exceeding 1500°C, along with its long residence times and turbulence, ensures the complete decomposition of organic components in the waste (Nirskov, 2012). However, the difficulties of alternative fuel (AF) combustion in rotary kiln and calciner firing should be evaluated. In this context, system optimization is important for the use of AF instead of fossil fuels. Understanding the energy efficiency response to AF is crucial for system optimization. Due to the complexity

of alkali-sulfur ratios and physical and chemical processes, each case should be examined individually (Chinyama, 2009). In order to replace fossil fuel with AF, it is first necessary to reduce moisture and particle size. This increases the calorific value during firing. An efficient pretreatment enhances the process of coprocessing. Since there is continuous heat exchange between the hot gases and the raw material during the clinker production process, heat transfer can be balanced. It is observed that AF shows a similar relationship in pretreatment and coprocessing. For optimum combustion, the starting temperature in coprocessing with AF should be above 850 °C and should last at least two seconds. Therefore, the injection point should be located in the calcination zone (Grosso et al., 2010). The process also determines the optimum particle size of the AF. The calciner design and residence time may allow for coarser materials than the main burner requirements. Larger particles work better in the calciner burner, while smaller particles work better in the main burner. Depending on the gas velocity and the surface of the AF, AF particles rise in the calciner, while larger particles move with the gas (Chatziaras, 2014). Fossil fuels are typically used with a residue of approximately 5% on a 90 μm sieve residue, whereas alternative fuels can be fed with millimeter-sized particles. Large fuel particles may lack sufficient time for complete combustion, resulting in unburned fuel dropping into the clinker bed and continuing in combustion. This may result in the establishment of local reducing conditions, adversely affecting both the quality of the clinker and the stability of the process. Certain alternative fuels can contain elevated ash concentration, with ash chemistry comprising elements such as oxides of aluminum, silicon, calcium, iron, and phosphorus. Moreover, volatile elements including S, Cl, Na, K, and Hg can be present in significant quantities. Ash will integrate with the clinker load and form a component of the clinker product. Volatile substances, including chlorine compounds, can evaporate at elevated temperatures and subsequently recondense in cooler regions, resulting in material loops and blockages. The volatile matter content in alternative fuels typically exceeds that of solid fossil fuels. This can influence the temperature and profile of the flame, which in turn can impact the transfer of heat to the clinker bed . The calorific value of certain alternative fuels can be much inferior than that of petcoke and lignite etc., owing to their chemical composition(ash, moisture, volatility etc.,). A lower calorific value requires a higher fuel flow rate to provide

the same thermal input. A higher fuel flow rate may cause handling and feeding problems due to larger volumes. Since the chemical composition and structure of alternative fuels are different, the kinetics of volatile matter release and coal oxidation may also be various. However, the dominance of mass and heat transfer due to high temperatures and large particle sizes limits the effect of chemical kinetics (Nørskov, 2012). The adverse impact of AF replacement on clinker production typically increases with increasing moisture content in the AF. A water vapor volume (ID) fan and preheater are indispensable. The capacity of the ID fan frequently constitutes a limitation. Elevated moisture levels can extend combustion duration and reduce peak flame temperature, adversely impacting the process. For fuel with high moisture content, the amount of flue gas can increase, which can limit production capacity and negatively affect process efficiency (Bäckström et al., 2015). Another major challenge of AF substitution is that fuel properties vary greatly, even from the same vendor, and the material is heterogeneous. This can impact emissions, process stability, and clinker quality. Fluctuations in heat input can cause temporary over- or under-combustion, which can increase sulfur volatilization and lead to unstable clinker formation. The physical structure of some alternative fuels can cause problems in storage, handling, and feeding. For example, sticky, low-density, or bulky fuels can cause problems such as equipment blockage or wear. This can affect both process stability and efficiency (Nørskov, 2012).

2.2.3 Refuse Derived Fuel (RDF)

Municipal solid waste (MSW) consists of discarded daily household items. It is also one of the most widely available alternative fuels. However, owing to its very heterogeneous composition and diverse characteristics, raw municipal solid waste requires pre-treatment. In order to solve the challenges posed by disparate heating values, moisture content, and irregular particle sizes, municipal solid waste (MSW) must undergo pre-treatment through methods including separation, sorting, screening, mixing, drying, and pelletizing.

The cement production plant can perform pre-treatment on-site, while the municipality can do it off-site. Fuel dosage After pre-treatment, the rotary kiln directly feeds MSW, now known as refuse-derived fuel (RDF), into the combustion zone, making it more suitable for use in clinker production. Depending on the waste

composition, the kiln introduces fuels at a pre-defined rate. Typically, an injection apparatus rotates with the kiln to inject RDFs. When the injector reaches the vertical position, the fuel falls into the center of the kiln (Hasanbeigi et al., 2012). Frauke et al., (2013) recommends a pneumatic conveying system for the transport of RDF to prevent damage to the rotating parts of the conveyor system. Industrial hangers usually store RDF due to its moisture content and odor. Substitution rates for MSW vary greatly depending on the composition and level of pretreatment. Substitution rates ranging from 2% for MSW subjected to only minimal mechanical treatment to 30% of the total thermal demand for MSW subjected to mechanical and biological pretreatment have been reported in the literature (Frauke et al., 2013). RDF combustion in the main burner is harder than in the calciner. The kiln burner requires alternative fuel quality, such as high heat value, particle size, and moisture content, for effective combustion; otherwise, it could lead to coating issues and negatively impact clinker quality. To ensure complete combustion in the kiln, reduce the RDF size below 25 mm. High thermal lower limits (TSR) further reduce this size to less than 3 mm(Baier &Menzel, 2011). Modern multi-channel burners, which offer better flame shape control, high flame momentum, and flexibility to use different types of AF, are required for the use of various types (Bapat, 2016). The fundamental characteristics of burners, including primary air pressure, flow rate, flame momentum, coal velocity, and solid alternative fuel velocity, fluctuate to enhance fuel combustion efficiency. A growing trend involves the utilization of a satellite burner alongside a main burner, potentially increasing the RDF input by as much as 50% (Sharma, 2023). Irish Cement Ltd. (ICL) in Limerick, Ireland, implemented a high-thrust low primary air modification, which increased petcoke combustion from 70% to 100% and sulfur uptake from 4% to 4.5% without causing coating problems. Such solutions apply to all high-sulfur alternative fuels. Considering the environmental impact, the use of RDF in kiln burners does not require special technology, but the maximum usage is limited to 30%. It is always difficult to predict the internal conditions of a kiln, so kiln burner modeling is required to determine fuel combustion behavior, such as coating formation, emissions, etc. (Sharma, 2023). In general, SO_2 and NO_x emissions may increase or decrease depending on the composition of the municipal waste. However,

substitution of fossil fuels with MSW always results in some reduction of CO_2 and CO emissions (Rahman et al., 2015).

2.2.4 Tire Derived Fuel (TDF)

In the cement process, tires serve as the oldest secondary solid waste fuel. The composition of tires varies depending on the amount of supporting material in them. In general, TDF (tire-derived fuel) is a high-quality fuel at around 30-35 MJ/kg and is approximately equivalent to high-quality coal. The nitrogen content of TDF is lower than coal, while the chloride content is higher (Barlaz, Eleazer & Whittle, 1993). TDF usually contains 0.5-2.0% sulfur, which is equal to or lower than most coals and coke. Metals such as lead, cadmium, and zinc may be present in TDF (Constans and Gossman, 1997). The cement industry limits the use of tires for co-processing due to the presence of zinc and sulfur. Zinc promt in the scrap tires can impact the hydration and hardening of the cement. Overheating the kiln results in a reducing atmosphere that is conducive to volatile sulfur formation. According to Nakomcic et al., (2016), the maximum substitution rates of scrap tires for a cement plant are less than 20% of the total fuel demand. The degree of preparation, particle size, and calorific value of solid fuels determine the feed point. The main burner in the rotary kiln with a preheater administers the primary fuel dosage, while the transition between the preheater and rotary kiln handles the secondary dosage. The convectional fossil fuels use the primary dosage, while alternative fuels like tires use the secondary dosage. Tire dosing takes place in the flue gas chamber at 1000°C and material temperature at about 800°C (Nakomcic et al., 2016). The organic components in the tires then burn at the higher temperature calcination zone (i.e., 1100°C to 1200°C). The transition and sinter zones oxidize inorganic compounds. The rate of tire feeding is crucial since it influences the CO formation in the kiln. The feeding system for tires controls the feeding rate through a vacuum chamber with a gate. Injecting the entire tires into the feed chute at the rotary kiln's transition chamber decreases the likelihood of complete tire combustion, lowers thermal efficiency, and produces more flue gases (Pedersen, 2018). On the other hand, shredding tires necessitates an additional investment and energy demand for the shredding equipment (Murray and Price, 2008). Long and short kilns may supply 5% and 20% of the overall energy demand through tire combustion, respectively

(Barlaz, Eleazer, and Whittle, 1993). The sulfur emitted during the combustion of tire-derived fuel, substituted for coal, is anticipated to react with limestone to produce gypsum, a primary material for cement.The substitution of TDF is anticipated to result in a reduction of nitrogen oxide emissions.Nonetheless, the location and duration of TDF combustion can result in variations in SO_x and NO_x concentrations, along with fluctuations in O_2 levels for certain facilities.

Tokheim (1999) conducted trials where they fed whole car tires to the kiln inlet at a maximum rate 1 ton/hour, achieving a 25% NO_x reduction and increasing the sulfur concentration in the precalcined material from 4% to 6%. The same study observed a 30–50% decrease in NO_x emissions and an increase in sulfur accumulation in the precalcined material upon adding crushed car tires to the kiln inlet.

2.2.5 Waste Oil (WO)

Waste oil originates from the automotive, railway, and marine industries. Cement kilns can use waste oils and solvents at a very low cost due to their high calorific value. The use of waste solvents is particularly cost-effective for cement plants located near other industrial establishments producing waste solvents. Replacing fossil fuels with waste oil and solvents results in reduced CO_2 emissions, NO_x emissions, mercury, and heavy metal emissions. However, SO_2 emissions may increase as a result of waste oil and solvent combustion. Fuel dosage the feed point for liquid fuels depends on their atomization capacity. Generally, there is no pretreatment for waste oils and solvents. The fuel oil firing system allows for their feeding from both the primary burner and the calciner (Rahman et al., 2015). Substitution ratio We cannot provide a generalized substitution ratio due to the variable properties of chemical and hazardous wastes. However, Karstensen et al. (2006), reported substitution rates of up to 57% for old pesticides. Waste oils and solvents possess a lower mineral content than conventional fossil fuels like coal and pet coke (Lemarchand et al., 2017). Sulfur, halogens, phosphorus, and heavy metals are more prevalent in waste oils, which present a technical challenge for storage due to potential environmental hazards. Giannopoulos et al. (2006) conducted a comprehensive kinetic PSR modeling investigation on cutting oil emulsions. It was determined that NO_x emissions from the pre-calciner are often significantly lower

than those from the cement kiln. Introducing reducing oil emulsion to the cement kiln appears advantageous, since it can reduce NO levels by as much as 50%. Conversely, introducing a nitrogen-rich cutting oil emulsion into the precalciner can raise NO levels when the fuel supply is insufficient. Burning untreated waste oil has significant environmental impacts, making it unrecommended for cement kilns (Murray & Price, 2008).

2.3 Literature Survey of Modelling Calciner

The literature provides a technical evaluation of previous research on the analysis of combustion gas products using several modeling methods, including ANSYS FLUENT, CHEMKIN-PRO, NASA-CEA, COMSOL, OPENFOAM, and GASEQ. This review examines the experimental and modeling research conducted on alternative fuels and fossil fuel combustion, specifically on their application in cement plant calciners. It also emphasizes identifying research gaps in the integration of software tools for the calcination process in cement manufacturing facilities. Additionally, the our simulation results are validated by our measurements and literature. In this study by Zajemska et al. (2014), they utilized the CHEMKIN-PRO program for numerical calculations of the chemical composition of flue gas produced by burning natural gas in an industrial heating device. The COMSOL Multiphysics program modeled the gas dynamics of the flue gas. Temperature and velocity profiles in the combustion chamber were determined using the COMSOL program and implemented in the CHEMKIN-Program. The results obtained from numerical simulations carried out in the experimental chamber showed a high level of agreement with the measurement results. Kayadelen (2017) examined the impact of varied quantities of natural gas diluent components, including ethane (C_2H_6), isobutane (C_4H_{10}), propane (C_3H_8), carbon dioxide (CO_2), and nitrogen (N_2) on methane-air combustion at different pressures, unburned mixture temperatures, and equivalence ratios. The results were compared with the results of the CEA code, a chemical balance application developed by NASA, and also with GASEQ. GASEQ-specific heat results were different from CEA. GASEQ could not separate the product species occurring at temperatures higher than 1000 K. Neglecting the effects of separations led the model to find the same specific heat values as GASEQ. The specific heat values of the model coincide

with the values of NASA CEA. The equilibrium products, enthalpy, and entropy values gave consistent results in both cases. The validation proved that the results presented in this study are reliable and also in excellent agreement with the famous codes of CEA and GASEQ. Sieradzka et al. (2020) conducted a study using Ansys Chemkin-Pro software to model the chemical implementation of gaseous pyrolysis products. This is important for understanding how different RDF fuels are. They investigated the mole fractions of emissions (H_2, H_2O, CH_4, C_2H_2, C_2H_4, C_3H_6, C_3H_8, CO, CO_2, HCl, and H_2S) generated from the pyrolysis of fuel at five distinct temperatures (700, 750, 800, 850, and 900°C), in addition to the chemical pathways for the chosen material. The obtained results revealed that, in contrast to temperature, the residence time had no effect on the product concentration. Chemkin-Pro was used to figure out what each product would look like at different temperatures and to come up with ideas about the reaction pathways that might be involved in the pyrolysis process. Furthermore, the obtained results validated the potential use of pyrolysis gas from RDF as a natural gas substitute in energy consumption sectors. Yilmaz et al. (2021) developed two models based on Gibbs energy minimization and equilibrium constant methods to predict gas emissions from combustion in a domestic boiler. They selected G20, G25, and NG as fuels and used CHEMKIN commercial software to predict gas emissions (NO, CO, N_2, O_2, CO_2, and H_2O) and adiabatic flame temperatures to verify the results. Under efficient boiler operating conditions, they observed small deviations compared to CHEMKIN results. The proposed models demonstrated their applicability to boilers and other combustion processes. Nakhaei et al. (2021) investigated NO emissions from two sequential cement calciners fired with petcoke and coal by using the commercial software Barracuda Virtual Reactor® 17.4.1. This paper implements the modeled solid phase in the Eulerian-Lagrangian approach using the Multiphase Particle-in-Cell (MP-PIC) method. The chemistry of gas phase combustion and NO formation/reduction were modeled using a global set of reaction kinetics. For both calciners, the total anticipated NO generation exceeds NO reduction, resulting in an increase in net NO production. The net production of NO in the coal fired calciner is over fifty percent of that in the petcoke-fired calciner. Marzouk (2023) obtained the AFTs for oxy-methane/hydrogen, air-methane/hydrogen for stoichiometric

conditions. The reaction temperature was 298.15 K , and the pressure was kept constant at 1 atm in study. Global one-step irreversible reaction for complete combustion and the GRI-Mech 3.0 basic mechanism for chemical equilibrium with associated thermodynamic data are used in the study. NASA CEARUN is implemented as the primary modeling tool. Excel and the Cantera-Python implementation of GRI-Mech 3.0 are implemented for comparison of results. The results revealed that the AFTs for oxy-methane had a complete combustion temperature of 5,166.47 K and a chemical equilibrium temperature of 3,050.12 K. For air-methane, this temperature decreased to 2,326.35 K and 2,224.25 K, respectively. For oxy-hydrogen, the complete combustion temperature of the AFTs was 4,930.56 K, and the chemical equilibrium temperature was 3,074.51 K. For air-hydrogen, this temperature decreased to 2,520.33 K and 2,378.62 K, respectively. For the eight combustion modeling cases, the relative deviation between the AFTs predicted by CEARUN and GRI-Mech 3.0 ranged from 0.064% to 3.503%. Hercog et al. (2023) report results of pilot-scale experiments performed at a 1 MW combustion facility at the Institute of Power Engineering, combined with CFD simulations of both pilot-scale and full-scale burners for a cement rotary kiln. They conducted numerical modeling by combusting petcoke with alternative fuels, such as municipal solid waste, biomass, and hydrogen, in a pilot-scale burner and subsequently validating the results. The researchers examined the combustion processes in a 75 MW industrial-scale cement rotary kiln burner to understand the internal circumstances of the reference cement plant and suggested possible alternatives for substituting fossil fuels with RDF. The results showed that the rotary kiln can integrate substantial quantities of alternative fuels. Alternative fuels such as RDF or biomass may substitute petcoke, and including hydrogen in the fuel mixture could improve combustion properties. Yang et al. (2024) adjusted the design and characteristics of a 4500 tons/day precalciner to mitigate nitrogen oxide (NO_x) emissions during combustion. The precalciner model is simulated by ANSYS FLUENT software. The effect of tertiary air duct (TAD) velocity and temperature on NO concentration was investigated. The results showed that the total NO concentration at the outlet was 526 ppm, and the error was within the allowable limit (496 ppm). The TAD velocity increased from 22 m/s to 38 m/s, and the NO concentration increased from 124 ppm to 220 ppm. At the temperature of

1123 K, the NO concentration peaked at 211 ppm. The relationship between the third air velocity and temperature is insignificant. The best conditions for low NOx combustion are 26 m/s air velocity and 1280 K temperature. Sánchez et al. (2024) reported models of the combustion chamber of a Ward-Cimpa furnace, 2.68 m wide and 3.32 m high, using OpenFOAM. They validated this model by comparing simulated CO and temperature values at the furnace output with literature data, observing differences of 13.72% and 12.23%, respectively. The results indicated that the increase of air flow led to an elevation in combustion activity, concluding in elevated temperatures and CO_2 emissions. The study revealed that the furnace was operating under inadequate air conditions, and employing higher air flow rates could enhance its performance. Li et al. (2024) studied the effects of oxygen-fuel combustion conditions on air flow, temperature distribution, and NO_x dispersion in the rotary kiln. Under oxygen-fuel conditions, the ignition point of pulverized coal was pushed back by 0.2 m, and the maximum temperature decreased from 2306 K to 2052 K. As the oxygen content increased, temperatures increased, but the flame length shortened. Under oxygen-fuel conditions, the oxidation rate of coal decreased, the gasification rate increased, and the combustion distance shortened. In addition, with an increase in primary air oxygen concentration, NO_x output decreased from 451 ppm to 406 ppm.

The novelty is that our study aims to determine the emission reduction by comprehensively modeling the thermodynamic and chemical processes of a calciner operating with alternative fuels. Our goal is to reduce the use of fossil fuels in the cement calciner and to analyze the behavior of these fuels. In addition, we verified the results obtained from thermodynamic analysis software such as NASA CEA and CHEMKIN-Pro with the measurement data taken from the factory and compared them with the literature to ensure reliability. To reduce energy and cost in the cement process, we aim to validate the emission and temperature data obtained by adjusting the fuel ratios in the simulations using Chemkin-Pro and NASA CEA calculations.

2.4 Material and Methods

2.4.1 Geometrical Model

Figure 2.6 illustrates the geometry and input/output boundary conditions of the examined existing calciners at the provided cement plant. Colorful arrows illustrate the flow directions of gas, air, and material from the supply from the rotary kiln and calciner. The blue one is a calcined meal, the green one is a non-calcined meal, the purple one is air, the black one is kiln inlet gas coming from the main burner and the red arrow is calciner fuel admission.

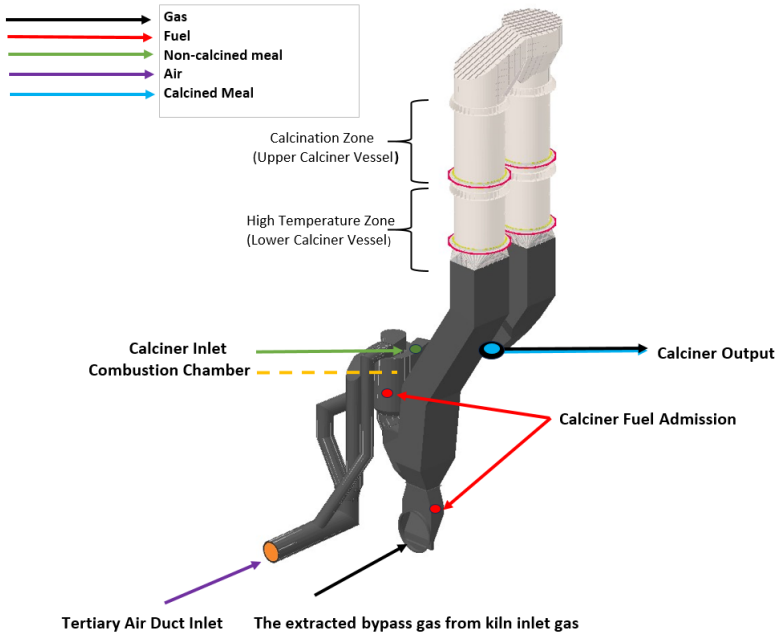


Figure 2.6 Geometry and boundary conditions of the existing calciners

2.4.2 Boundary Conditions

According to the data obtained from the control room of a cement factory with a clinker production capacity of 1647 ton/day, a total of 78 tons of petcoke and lignite mixture is fed into the system, with 9 ton/day coming from the existing calciner and 69 ton/day from the existing main burner. Of the petcoke and lignite mixture used, 65% is petcoke and 35% is lignite. TDF is not provided to the main burner. The waste fed into the main burner is listed as follows: 69 tons/day of a mixture of petcoke and lignite, 50 tons/ day of RDF, and 5 tons of waste oil. The waste fed into the calciner includes 9 tons/ day of a mixture of petcoke and lignite, 170

tons/day of RDF, 64 tons/day of TDF, and 5 tons /day of waste oil. The amount of alternative fuel fed into the calciner and the main burner is given in Table 2.1.

Table 2.1 The amounts of fossil and alternative fuels fed from existing calciner and main burner

Fuels Type	**Existing Calciner (tons/day)**	**%**	**Existing Main Burner (tons/day)**	**%**
Fossil Fuels (65% Petcoke+ 35% Lignite)	9 (5.85 + 3.15)	3.63 (2.36 + 1.27)	69 (44.85 + 24.15)	55.7 (36.2 + 19.5)
RDF	170.00	68.55	50.00	40.32
TDF	64.00	25.81	0.00	0.00
Waste Oil	5.00	2.02	5.00	4.03
Total	248.00	-	124.00	-

2.4.3 Fuel Properties and Characterization

The ultimate analysis (C, H, O, N, S) of proximate analysis (moisture, volatile matter, ash, fixed carbon, calorific value) alternative fuels provided by Türk Çimento Sanayicileri Birliği are presented in Appendix A, in Table A.1. Several variables need to be considered when fuels are selected. The quality of the product, emission values, and the operating process can be affected by these variables.

2.4.4 Combustion Gas Compositions

According to these data, the Amin (minimum air) and Vmin (minimum combustion gas) formula is calculated and the kiln gas composition comes from the main burner. In the calciner of a cement plant, "minimum air" refers to the minimum amount of air required to achieve complete combustion of the fuels used. This value is essential for ensuring that all the combustible components in the fuel are fully oxidized, which helps optimize fuel efficiency and minimize unburned residues. "Minimum combustion gas" refers to the least quantity of combustion gases required to sustain the optimal temperature and reaction parameters within the calciner. This guarantees excellent management of the heat and chemical processes within the calciner, resulting in optimal performance and minimized emissions. Both factors are essential to the functioning of the calciner. Maintaining acceptable minimum amounts of air and combustion gas is essential for optimizing combustion efficiency, minimizing emissions, and enhancing overall energy efficiency (Gasser, 2000). The kiln and calciner combustion gas composition calculation steps are demonstrated by the following equations. Where C, H, S, N, O, H_2O are the weight fractions (kg/kg fuel) of carbon, hydrogen, sulfur, nitrogen, and water in the fuel.

The minimum air Amin (Nm^3/kg fuel) can be calculated by given following equation (2.7):

$$Amin = 8.89\,x\,C + 26.5\,x\,H + 3.3\,x\,S - 3.3\,x\,O \quad (2.7)$$

The combustion gas emissions released can be given by the following equation (2.8),(2.9),(2.10) and (2.11):

$$0.79\,xA_{min} + 0.8\,x\,N \rightarrow N_2 \quad (2.8)$$

$$1.87\,x\,C \rightarrow CO_2 \quad (2.9)$$

$$0.7\,x\,S \rightarrow SO_2 \quad (2.10)$$

$$11.2\,x\,H + 1.24\,x\,H_2O + A_{min}\,x\,H_2O_{air} \rightarrow H_2O \quad (2.11)$$

Then, V_{min} can be obtained by the following equation (2.12):

$$V_{min} = (0.79\,x\,A_{min} + 0.8\,x\,N) + (1.87\,x\,C) + (0.7\,x\,S) + (11.2\,x\,H) + 1.24\,x\,H_2O + A_{min}xH_2O_{air} \quad (2.12)$$

The volume percent of each gas can be calculated as a proportion of volume (vol.%) divided by V_{min}. Kiln and calciner gas composition of volume (vol.%) is presented in Table 2.2. These data were converted to proportion of weight (wt%) and utilized for the NASA-CEA and Chemkin-Pro boundary conditions. In existing model, the percentage distribution of gas components is calculated at 1473.15 Kelvin for calciner and main burner. Average gas composition is follows: 67.56% N_2, 22.67% CO_2, 9.45% H_2O, and 0.33% SO_2. The results align with the existing literature. Zhang et al. (2024) reported the kiln gas composition as (wt%) 80.87% N_2, 15% CO_2, 2% H_2O, and 0.12% NO.

Table 2.2 Kiln and calciner combustion gas composition

Kiln Combustion Gas (vol.%)				
Main Burner Inlet (5.17 tons/hour)	H_2O	CO_2	SO_2	N_2
	8.3	31.7	0.76	72.22
Calciner Combustion Gas (vol.%)				
Calciner Inlet (10.33 tons/hour)	H_2O	CO_2	SO_2	N_2
	13.01	27.84	0.247	68.53

2.4.5 Raw Meal Properties

The non-calcined meal primarily comprises finely ground calcium carbonate and silicon dioxide. When the raw meal is introduced into the calciner, it undergoes a separation process. The hot meal (now calcined) is then transferred to the rotary kiln inlet. As the meal is heated between 100 °C and 500 °C, moisture evaporates, and when the temperature reaches 850 to 890 °C, the endothermic calcination reaction begins, converting $CaCO_3$ into CaO and CO_2. The activation energy required for this calcination process is supplied by the heat generated from fuel combustion (Fidaros et al., 2007). The chemical composition of raw meal and hot meal analysis results supplied by the cement factory are presented in Appendix A,

in Table A.2. The chemical composition of raw meal and hot meal analysis results (SiO_2, CaO, MgO, and Loss on Ignition (LOI)) supplied in wt% by the cement factory; the raw meal is 12.93%, 41.66%, 0.64%, and 33.42 % while the hot meal is 20.82%, 55.2%, 1.16 %, and 2.5 %. The analysis results are consistent with the literature (Abd El-Hafiz et al.,2015).

2.4.6 Temperature and Gas Species Measurements

The temperature data and outlet gas composition was collected by MRU-S type thermocouples and Optima MRU type exhaust gas analyzer in three different points. We sampled the data at three different points at the calciner's outlet. We maintained the same operating parameters of the cement calciner during the measurement to ensure the accuracy and stability of the test data. We took the average value every 10 and 15 minutes to ensure precision, and we observed no significant fluctuation in the measurement data. The measured gas concentration and temperature average values are as follows: 2.45% O_2, 0.17% CO, 17.9% CO_2, 240 PPM NO, 252 PPM NOx, and 300 PPM SO_2.The measurement temperature was averagely of 1173.15 Kelvin. Our measurements are consistent with the literature. Li et al. (2024) obtained the measurement data at the end of the rotary kiln. The observed values were as follows: O_2 at 3.25%, CO_2 at 15.88%, and NOx concentration at 1095 PPM. The temperature was measured at 1332 Kelvin. Wang et al. (2024) reported the variation in average sectional area concentrations of three principal gaseous components (CO_2, O_2, and NO) along the height of the calciner. The measurement data indicated 392 PPM NO, 5.8% O_2, and 25% CO_2 at 1170 KelvinBased on the measured data and results, the ratio of gases released from the fuel will be determined using computer tools such as NASA CEA and Chemkin-Pro software.

2.4.7 Adiabatic Flame Temperature of Fuels

The air-lignite/RDF/TDF/waste oil of AFT value is determined. The results indicate adiabatic flame temperatures related to fuel characteristics including volatile matter, ash content, and moisture content. The moisture content of RDF and waste oil is a key indicator of its performance as a fuel because moisture is not flammable. Excessive moisture in RDF and waste oil can inhibit ignition, reduce flame temperature, slow down the rate of combustion, extend the burn time,

lengthen the flame envelope, and increase the risk of flame instability. Ash content affects fuel reactivity, diminishing calorific value and postponing ignition. Lignite possesses the highest ash content, whereas petcoke exhibits a low ash concentration, rendering petcoke more combustible than lignite and RDF. The ignition and combustion of volatiles are essential phases in the combustion process; TDF, possessing the largest volatile content among fuels, exhibits superior flammability, whereas the little volatile content of petcoke renders it challenging to ignite (Sharma, 2023). The complete combustion of air-petcoke can be represented by a modeled reaction: The modeled simplified single-step reaction calculations (Khadka, 2021), (Felder&Rousseau, 1986) for air-petcoke/lignite/RDF/TDF/Waste oil complete combustion are shown in Appendix A in Table A.3, A.4, A.5, A.6, and A.7.

The bar chart in Figure 2.7 shown AFT for air-petcoke/lignite/RDF/TDF/Waste oil as 2355,8, 2407,62, 2269,35, 2419 and 2303,71 Kelvin, respectively.

The complete combustion of air-petcoke can be represented by a modeled reaction (2.13):

$$CH_{0.514}N_{0.014}S_{0.028}O_{1.09x10^{-3}}+1.14(O_2+3.78N_2)\rightarrow$$
$$CO_2+0.257H_2O+0.028SO_2+4.316N_2 \quad (2.13)$$

The complete combustion of air-lignite can be represented by a modeled reaction (2.14):

$$CH_{0.77}N_{0.023}S_{2.11\ x\ 10^{-3}}O_{0.086}+1.173(O_2+3.78N2)\rightarrow$$
$$CO_2+ 0.385H_2O+2.11\ x\ 10^{-3}SO_2+4.45N_2 \quad (2.14)$$

The complete combustion of air-RDF can be represented by a modeled reaction (2.15):

$$CH_{3.41}N_{0.031}S_{2.76\ x\ 10^{-3}}O_{1.03}+1.368(O_2+3.78N_2)\rightarrow$$
$$CO_2+ 0.325H_2O+2.76\ x\ 10^{-3}SO_2+5.18N_2 \quad (2.15)$$

The complete combustion of air-TDF can be represented by a modeled reaction (2.16):

$$CH_{1.138}N_{3.4x\ 10^{-3}}S_{8.07\ x\ 10^{-3}}O_{0.08}+1.268(O_2+3.78N_2)\rightarrow$$

$$CO_2 + 0.007H_2O + 8.07 \times 10^{-3}SO_2 + 4.72N_2 \quad (2.16)$$

The complete combustion of air-waste oil can be represented by a modeled reaction (2.17):

$$CH_{3.37}N_{0.041}S_{0.018}O_{0.69} + 1.538(O_2 + 3.78N_2) \rightarrow$$

$$CO_2 + 0.27H_2O + 0.018\,SO_2 + 5.83N_2 \quad (2.17)$$

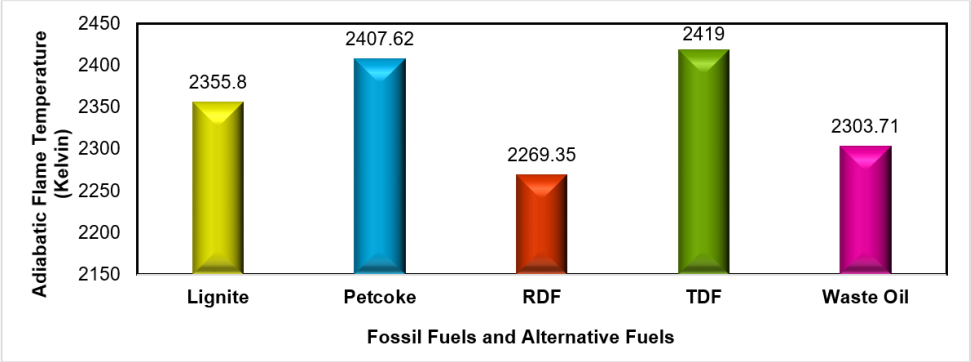


Figure 2.7 Adiabatic flame temperature of fuels

2.5 Numerical Calculations

The combustion gases from the calciner and primary burner were evaluated utilizing equilibrium models created with NASA CEA (Chemical Equilibrium with Applications) and Chemkin-Pro software. However, it is essential to acknowledge that equilibrium models lack the precision of kinetic models. To fully understand the impact of parameters such as time on the system, kinetic model studies are necessary. The CEA assumes that all gases behave ideally and that phase interactions can be disregarded. The equation of state for the mixture is represented by equation (2.18);

$$Pv = nRT \quad (2.18)$$

For a mixture with the number of species, the Gibbs energy per kilogram of the mixture, denoted as g, is represented by equation (2.19);

$$g = \sum_{j}^{j=NS} (n_j \mu_j) \quad (2.19)$$

where nj and μj are the number of moles and chemical potential of species j, respectively. The chemical potential per kilogram-mole of species j is defined to be (2.20);

$$\mu_i = \frac{\partial_g}{\partial_{n_i}}_{T,P,n_{i\neq j}} \quad (2.20)$$

The condition for chemical equilibrium is achieved by minimizing free energy, which is typically constrained by mass-balance equations. Helmholtz free energy is minimized when the volume (or density) is held constant as a thermodynamic state. The Lagrange multipliers method is utilized to minimize Gibbs free energy because of its better efficacy relative to alternative techniques. Due to the non-linear nature of the equations required to ascertain the composition variables, an iterative method is typically essential. In this iterative procedure, treating n as an independent variable is advantageous. The Newton-Raphson method is used to adjust the initial estimates of composition n_j Lagrange multipliers λj and moles of gaseous species (Yucel & Aydin, 2023). In Chemkin-Pro software, the combustion process of various fuels is simulated by first inputting the chemical compositions of the selected fuels. Essential process parameters, such as temperature, pressure, kiln gas flow rate, and tertiary air duct mass flow rate, are subsequently established to configure the simulation. Following configuration of these inputs, Chemkin-Pro performs calculations and produces results predicting the distribution and concentration of gaseous products arising from fuel combustion. This facilitates a comprehensive examination of the combustion process, aiding in the optimization of fuel consumption and the reduction of pollutants. The summary of flow chart of reaction mechanism modeling through NASA CEA and Chemkin-Pro Solver in Figure 2.8.

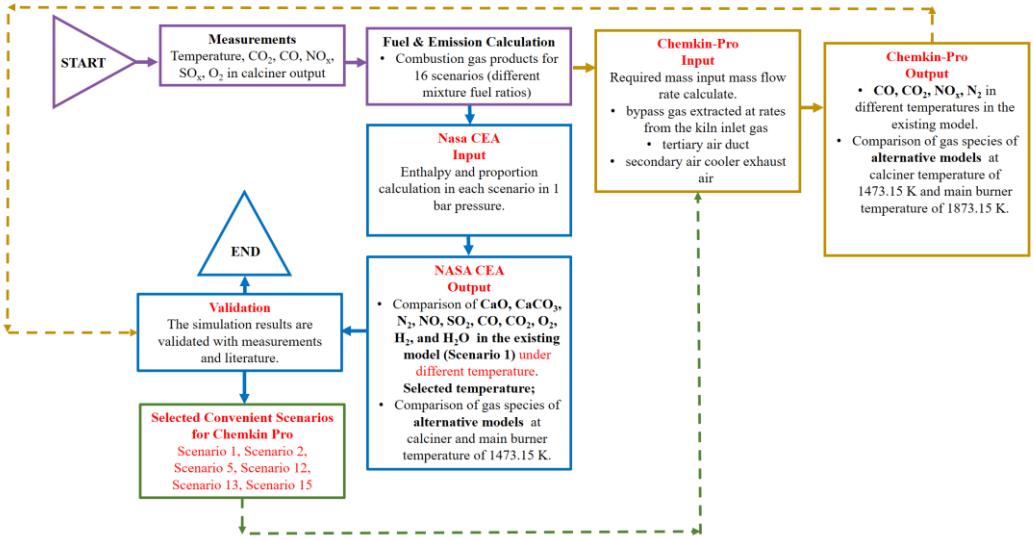


Figure 2.8 Flow chart of reaction mechanism modeling through NASA CEA and Chemkin-Pro Solver

2.5.1 NASA CEA Reaction Modelling

This study will utilize NASA's CEA computational tool to determine the gas emissions produced by the fuel. This software provides the computation of all requisite parameters pertinent to the analysis (NASA CEA, 2024).

The following is a comprehensive overview of the input selection procedure in CEA:

- Initially, it is essential to identify the sort of problem to be solved. The option "assigned temperature & pressure" is selected to define the reaction mechanism of the current model.
- The subsequent phase involves selecting the working conditions for the current model, based on literature data, which include a temperature range of 973.15 to 1473.15 Kelvin and a constant pressure of 1 bar. These settings are selected because the calciner functions within this temperature range and pressure.
- Subsequent to selecting this data, the following stage is to determine the type of fuel. Emissions produced from the fuel (N_2, CO_2, H_2O, SO_2) are classified as fuel, whilst the raw material limestone (CaCO3) is categorized as the oxidizer. Emissions' weight percentage and enthalpy values are input into the system

based on proximate and ultimate analysis results, as well as calciner output temperature.

- The oxidizer/fuel ratio is determined to be 0.15.
- Combustion is represented as a process with a constant enthalpy by assessing the total enthalpy of the air-fuel combination and keeping it invariant during the calculation of the chemical equilibrium composition. The total enthalpy calculation is crucial for the combustion model in the new code; hence, the relevant CEA studies are established using temperature (T) and pressure (P) utilizing the enthalpy data from the individual situation.
- Following completion of the simulation, CEA presents the results in various parts by examining the emissions produced within the temperature range of 973.15 to 1473.15 Kelvin, alongside other parameters.The species are included: calcium oxide (CaO), limestone ($CaCO_3$), nitrogen (N_2), nitrogen monoxide (NO), sulfur monoxide (SO), sulfur dioxide (SO_2), carbon monoxide (CO), carbon dioxide (CO_2), O_2 (oxygen), H_2 (hydrogen), and moisture (H_2O).

Based on the data, the emissions occurring in the temperature range of 973.15 to 1473.15 Kelvin were calculated by applying the existing model boundary conditions. The boundary conditions required for NASA CEA were calculated as % wt proportion of N_2,CO_2, H_2O, and SO_2 major combustion gases for 16 scenarios. The enthalpies (ΔH) of the gas components in these scenarios were calculated by NASA CEA. Feed points of fuel ratios for the existing model, alternative model 1, and alternative model 2 are presented in Appendix A in Table A.8. The required boundary conditions for the existing model, alternative models 1 and 2 are presented in Appendix A in Table A.9.

2.5.2 Chemkin-Pro Reaction Modelling

Numerical computations of combustion gas products for the cement calciner and main burner were conducted utilizing Chemkin-Pro. Chemkin-Pro, the most recent iteration of the commercial program, has grown from the Chemkin II code created at Scandia National Laboratories. This program models and simulates intricate chemical reactions, facilitating the assessment of chemical kinetics for diverse industrial processes and combustion systems in the conceptual design phase

(Sieradzka et al., 2020). The gaseous combustion products for both fossil and alternative fuels were computed using Chemkin-Pro, based on their chemical compositions. It is necessary to designate the raw materials as a system input for computations in Chemkin-Pro. In Figure 2.9 is demonstrated as simulation was conducted in the existing calciner (C1_R1) for bypass gas extracted from the kiln inlet gas at rates (C1_Inlet1) of 25.2 kg/sec and tertiary air duct (C1_Inlet2) of 14.01 kg/sec, respectively. In the main burner(C3_R1), simulation is performed for 9.84 kg/sec and 17.46 kg/sec for secondary air (C3_Inlet1) and cooler exhaust air (C3_Inlet2), respectively. The required boundary conditions of existing model calculation equations are demonstrated using mass balance is showed Appendix A in Figure A.1, A.2 and A.3. Calculations for the existing model materials in the calciner were conducted at five distinct temperatures: 973.15, 1073.15, 1173.15, 1273.15, 1373.15, and 1473.15 Kelvin. The main burner was consistently maintained at 1873.15 Kelvin. Ultimately, varying quantities of fossil fuels and alternative fuel compositions were utilized to create various models, with the results at 1473.15 Kelvin in the calciner emphasized as they offered the most favorable contrast for these models. The boundary conditions required for Chemkin-Pro were calculated as % wt and the major gas (CO_2,CO, N_2 and NO_x) is focussed.

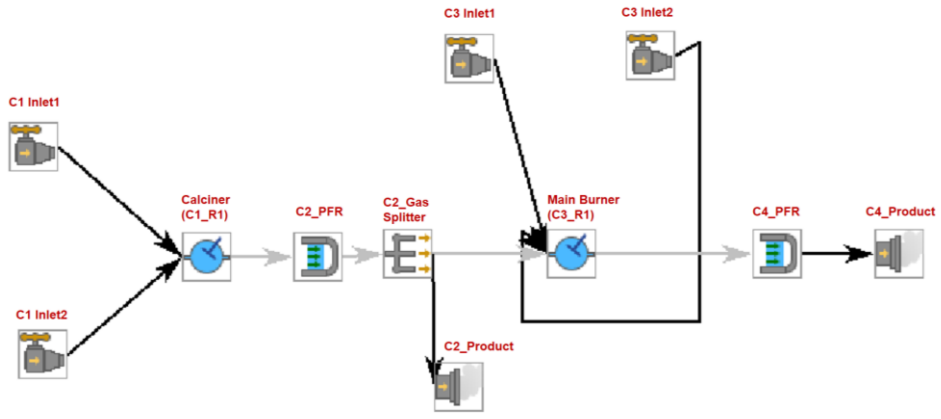


Figure 2.9 Diagram of calciner and main burner for calculation combustion gas composition with chemkin-pro

2.6 Result and Discussion

2.6.1 Validation of the Accuracy of the Model

Concentrations of combustion gases were quantified and corroborated by juxtaposing them with simulation outcomes derived from NASA-CEA and Chemkin-Pro at temperatures of 973.15 K, 1073.15 K, 1173.15 K, 1273.15 K, 1373.15 K, and 1473.15 K, respectively. At 1173.15 K, the recorded values were 2.45% O_2, 0.17% CO, 17.9% CO_2, 252 PPM NOx, and 300 PPM SO_2. NASA-CEA simulation results at 1173.15 K yield gas concentrations of 0.055% CO, 17.57% CO_2, and 980 PPM SO_2 in given bar chart Figure 2.10a. The CO_2 concentration indicates strong correlation with our results, suggesting that the simulation's CO_2 values closely match our experimental data. However, the concentrations of CO and SO_2 from NASA-CEA exhibit considerable discrepancies compared to the measurements. While our measurement shows 0.17% CO and 300 PPM SO_2, the NASA-CEA simulation predicts only 0.055% CO and 980 PPM SO_2, which indicates an estimation of these gas components. Chemkin-Pro simulation results at 1173.15 K for the major gas compounds are as follows: 17.05% CO_2, 0.029% CO, 2.80% O_2 and 463 PPM NO_x in given bar chart Figure 2.10c. The concentrations of CO_2 and O_2 align closely with our results, so confirming the validity of the CO2 simulation. However, the NO_x and CO measurements from Chemkin-Pro exhibit more deviation. Our observations indicate 240 PPM NO_x and 0.029% CO, while Chemkin-Pro simulates 463 PPM NOx and 0.029% CO, revealing a significant overestimation of CO and an underestimating of NO. In the literature, Li et al. (2024), simulated the following gas concentrations at the end of the rotary kiln: 3.20% O_2, 15.14% CO_2, 1096 PPM NO_x, and a temperature of 1320 Kelvin. Wang et al. (2024) reported simulation results of 5.8% O_2, 25% CO_2, 392 PPM NO, and a temperature of 1170 Kelvin in the calciner. Additionally, the verified NO concentration was 412.21 PPM, and the verified temperature was 1167.42 Kelvin. In a nutshell, the calculations directly determine the maximum possible emissions based on the elemental composition because NASA CEA and Chemkin software do not include a volatilization model. However, when considering mass transfer limitations, we may obtain different results from the actual emissions since not all elements are released. For validation, the closest data to the temperature and gas concentration measurements obtained from the calciner outlet points (NO=10PPM)

occurred at 1473.15 Kelvin (1200°C), therefore alternative models were simulated at 1473.15 Kelvin temperature. Nakhaei et al. (2021) reported a temperature range of 1150–1200°C for the existing calciner fuel inlet point in their study.

2.6.2 Comparison of NASA CEA and Chemkin-Pro

In the given bar chart in Figure 2.10b, the selected models are compared all models for NASA-CEA are illustrated in expanded Figures A.4 and Figure A.5 in Appendix A. The existing model and alternative models demonstrated gas species such as CO, H_2, NO, and O_2 gas in the almost same ratio of 80,30,10, and 50 PPM, respectively since this data is present in all the scenarios, not included in the comparison. The existing model indicates a concentration of SO_2 gas at 1360 PPM. In alternative model 1, where the petcoke rate was elevated by 40%, the maximum SO_2 gas concentration reached 1520 PPM in the 100/0 scenario. In alternative model 2, a 30% increase in the TDF rate in Scenario 15 (39/39) resulted in the highest SO_2 gas concentration of 1430 PPM. The closest SO_2 gas to the existing model was Scenario 10 (85/15) and Scenario 13 (0/78) as 1350 and 1290 PPM, respectively. In Scenario 13 (0/78) and Scenario 15 (39/39) where only alternative fuels (RDF and TDF) were supplied to the calciner, there was a potential for reducing CO_2 emissions because of the lower carbon percentage in RDF compared to coal and TDF. However, CO_2 emissions increased. This was attributed to an approximately 10% increase in the lignite and petcoke mixture rate, even though the RDF rate increased by 6% in the calciner, compared to Scenario 1 (65/35). Scenario 8 (65/35) had the same petcoke/lignite ratio as the Scenario 1(65/35). In alternative model 1, without TDF, CO_2 emissions can be reduced by increasing the RDF rate in the calciner by 30% compared to the existing system. In scenario 16 (0/0), using only alternative fuels (TDF and RDF) reduces CO_2 emissions, while scenario 15 (39/39) has the highest CO_2. The calorific value, influenced by the ash and moisture content in fuels, is essential for achieving full combustion. In scenario 1, it was 5402 kcal/kg, whereas in Alternative Model 1, it fluctuated between 4591 and 4982 kcal/kg. In Alternative Model 2, the scenario values from 13 to 16 were 5472, 4672, 5318, and 4173 kcal/kg, respectively. Elevating RDF decreased the calorific value due to elevated moisture content, whereas petcoke enhanced it. Luo et al. (2024) observed that utilizing RDF in cement manufacturers can decrease CO_2

emissions by 1.61 kg for every 1 kg of RDF utilized, in comparison to traditional fuels. This shows that RDF provides carbon dioxide reduction but at different rates depending on the material it is produced from, its carbon content, and its moisture content. It has been observed that when RDF is co-combusted in cement factories, more combustion air is required and using of RDF reduces kiln of the thermal efficiency. This situation is increasing of kiln specific heat consumption and potentially resulting in production loss.The RDF sourced from the calciner possesses lower caloric value and greater particle size, whereas the RDF from the flame pipe may exhibit smaller particle size and higher calofic content, since it is required to generate elevated temperatures in the sintering zone (Hasanbeigi & Bhadbhade, 2023). However, since waste feeding systems will differ, it has been reported in the literature that it would be beneficial to choose the RDF size according to the feeding. In scenarios 14 and 16 where RDF is fed from a 100% main burner, CO_2 gas decreases while the moisture rate increases. Considering that RDF has an adiabatic flame temperature of 2269.35 Kelvin; Due to RDF being a non-homogeneous fuel with high volatility, variable particle size distribution, and high moisture content, difficulties may be experienced in maintaining a stable flame and complete combustion cannot occur. The ignition of RDF in the main burner may lead to coating issues and affect clinker quality due to variations in heat value, particle size, and moisture content. It may lead to increased extra air relative to other scenarios. It may result in a reduction of calorific value (Hercog et al., 2023). In Alternative 1 scenarios and Scenarios 13 and 15; In the cases of co-firing of petcoke and RDF in the main burner, considering that the adiabatic flame temperature of petcoke is 2407 Kelvin; it can be expected to improve ignition and combustion in general, but in this case, attention should be paid to the larger particle size and moisture content of both fuels. According to the literature, the moisture content should be reduced to approximately 10–15% before feeding RDF to the main burner. In addition, a significant amount of pulverized coal should be fed from the main burner to maintain a sufficiently high temperature at rotary kiln's combustion zone and thus facilitate the necessary chemical reactions. In the Alternative 1 and Alternative 2 models, an increase in the RDF ratio within the fuel mixtures resulted in a decrease in SO_2 emissions, due to the reduced sulfur content in RDF relative to TDF and fossil fuels. Alternative 2 model scenarios, where RDF

substitutes fossil fuel, the sulfur concentration in the system decreased considerably (Hasanbeigi & Bhadbhade, 2023). The current investigation revealed that RDF-based production gas had a low calorific value of 2.67–4.34 MJ/Nm^3, rendering it the most appropriate source for gas firing from the calciner (Sharma, 2023).The alternative models demonstrate a larger quantity of RDF, indicating elevated moisture content. Conversely, studies involving TDF show a decrease in humidity. According to the literature, it has been stated that to offset carbon by substituting RDF instead of coal, the moisture content of RDF should be lower than 15%, and thus a 0.4 ton CO_2/ton coal emission reduction can be achieved (Chatziaras et al., 2014), SO_2 can be generated from sulfur compounds in the clinker (CaO) as well as from sulfur content in petcoke and TDF. Petcoke and TDF generate elevated SO_2 levels relative to RDF, while lignite yields reduced SO_2 emissions.The findings of the study were analogous to those of the research conducted by Hasanbeigi and Bhadbhade (2023). The utilization of TDF either diminishes or exerts a negligible effect on the emissions of diverse pollutants from cement kilns. Nevertheless, TDF may pose difficulties when directly introduced into the kiln because of the elevated zinc concentration in the ashes, which can substantially modify the cement composition. To reduce this issue, it is suggested to maintain replacement rates for kiln fuel below 20-30% (Hasanbeigi & Bhadbhade, 2023). Thus, introducing TDF into the calciner is regarded as a more suitable method. The chemical composition of combustion gas products was evaluated using Chemkin-Pro for the materials under investigation, with a detailed analysis presented for the principal combustion gas products at varying temperatures. Figure 2.10c illustrates the principal gases (CO_2, CO, N_2, and NO_x) and according to NASA-CEA result six scenarios (including existing scenario) are selected as Scenario 1(35/65), Scenario 2(0/100), Scenario5 (65/35), Scenario 12 (100/0), Scenario 13(0/78) and Scenario 15(39/39) ,respectively in Chemkin-Pro. As the temperature increased, the CO_2 and N_2 concentrations rose slightly, but the NO_x and CO concentrations dropped even slightly. In our study, the tertiary air inlet velocity was taken as 14.01 kg/s and the temperature as 780°C, and the kiln temperature was determined as 1400°C. The following explanation applies to this situation: The two primary types of NO_x emissions in the rotary kiln are fuel NO_x, which is formed from nitrogen in the fuel, and thermal NO_x, which is produced N_2 from airThe temperature in the precalciner

is lower than that in the rotary kiln, ranging from 850°C to 1200°C. Under these conditions, the majority of NO_x produced is NO. Therefore, we only consider fuel-derived NO in our study, ignoring thermal NO_x and instantaneous NO_x production. For example, volatile N and char N are present in coal. After being transformed into HCN and NH_3 intermediates, the volatile N is oxidized to NO. N_2 is generated when the unoxidized intermediates react with NO as reduction agents. The char N undergoes direct oxidation to NO. Because the char is reductive, some of the NO is converted to N_2. Volatile substances instantly oxidize in the pre-calciner under high temperatures and sufficient oxygen. The calciner system prompts the NO produced in the rotary kiln to enter the pre-calciner, where some of it is reduced by the powdered coal. The remaining NO is discharged from the system together with the NO produced in the pre-calciner. Yan et al. (2020) reported that NO formation in the precalciner related on the fuel nitrogen content and the oxygen level in the ignition zone. Sufficient oxygen ensures complete combustion of the fuel and increases NO production. The increase in tertiary air temperature reduces the amount of NO produced in the precalciner by reacting with intermediate products such as HCN and NH_3 with NO. This situation was also confirmed in our study: Most of the NO_x formed in the calciner is in the form of NO, and the decrease in the NO_x level with the increase in temperature is because the temperature promotes fuel combustion and more HCN and NH_3 react with NO. Therefore, the reduction in NO levels within the calciner can be attributed to these processes. Zhang et al. (2024) utilized ANSYS FLUENT software to analyze the structure and parameters of a pre-calciner with a capacity of 4500 t/day, aiming to mitigate NO_x emissions during combustion. This study investigated the effects of raw material angle, tertiary air velocity, and temperature on NO concentration. When the tertiary air velocity increased from 22 m/s to 38 m/s, the NO concentration at the precalciner outlet increased from 124 ppm to 220 ppm. When the temperature increased to 1123 K, the NO concentration reached 211 ppm. Our investigation, the insufficient oxygen, temperature, and tertiary air duct speed can be the causes of this behavior. Comparing gas concentrations in different scenarios by Chemkin-Pro is presented in the bar chart Figure 2.10d. In our existing system, in Scenario 1 (65/35), NO_x concentration was calculated as 331 PPM. However, in our modeling and calculations, it was determined that in scenarios where RDF and lignite were fed to

the calciner at the highest rate and volatility was high, NO_x concentrations increased to 596 PPM and 423 PPM for Scenario 2 (0/100) and Scenario 5 (35/65), respectively. In Scenario 12 (100/0), where RDF and petcoke were utilized at the maximum rate, the NO_x content diminished to 260 PPM, despite petcoke's lower volatility. Luo et al. (2024) documented that the utilization of alternative fuels (such as MBM, tires, RDF, and plastics) lowers NO_x emissions. The decline is elucidated by the conversion of nitrogen compounds emitted during the burning of alternative fuels or the pyrolysis process into N_2 gas via chemical processes. The significant volatility of alternative fuels facilitates the conversion of NO_x into N_2 gas. Furthermore, NO_x production is significantly influenced by the nitrogen content of fuels. Contrary to the literature, we obtained different results. Although petcoke has 1.4% N and RDF has 1.23% N content, in our analyses, RDF with high volatility has higher NO_x emissions despite its lower nitrogen content. The low volatility (9.64%) and low oxygen concentration (0.12%) of petcoke restrict NOx emissions, but the high oxygen content (17.08%) and volatility (53.7%) of RDF may have elevated NO_x generation by accelerating the combustion rate. The low volatility and high carbon content of petcoke may have diminished NO_x generation by stabilizing the combustion process. In scenario 13 (0/78), when only 72.65% RDF and 27.35% TDF were fed through the calciner, the NO_x concentration was calculated as 247 PPM at the lowest level with 0.3% N content, 60.3% volatility and 6.52% O_2 content of TDF. In scenario 15 (39/39), when the highest rate (36.29%) of TDF was fed through the calciner, the NO_x concentration was calculated as 416 PPM. In contrast to research, the criteria that determined emissions were not the amount of nitrogen in fuels but rather their volatility and oxygen content. Kinetic simulations and Chemkin-Pro complex system modeling were employed to explain these variations.

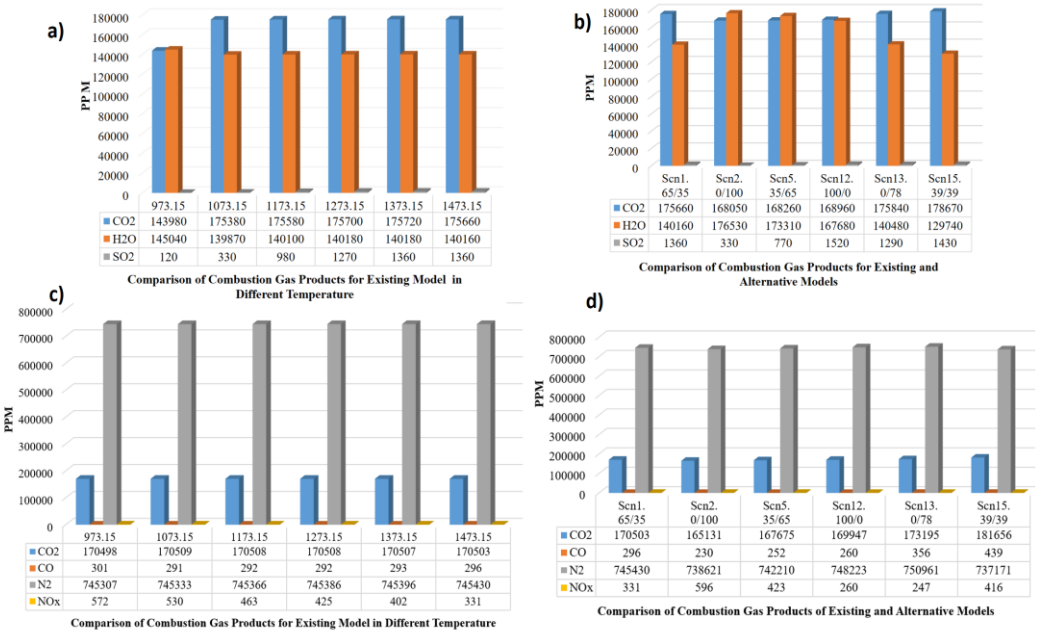


Figure 2.10 Combustion Gas Products of Prediction NASA CEA(a,b) and Chemkin-Pro (c,d) Software respectively. a;c) Comparison of combustion for existing model in different temperature b;d) Comparison of gas products for existing and alternative models

3
INTEGRATING SOLAR CALCINER TECHNOLOGY FOR REDUCTION EMISSION IN CEMENT PRODUCTION

3.1 Literature Survey of Implementing Solar Calciner in Cement Plant

Moumin et al. (2020) studied the potential of solar thermal shielding technology in the cement industry. DLR conducted a test and found that the CO_2 avoidance rate in solar cement plants ranged from 14 to 17%, resulting in a calculated CO_2 avoidance cost of 118 EUR/ton. A 15% increase in reactor efficiency reduced this cost by 26%. Solar shields reduced CO_2 emissions by 8–28% when used instead of fossil fuels in Spain.

Sahoo et al. (2023b) proposed a solar design model for cement industries in India. We used Mateo norm 8 software to obtain the DNI data available at each plant location. We included the annual thermal energy requirements for both the existing and proposed systems in the analysis, and also calculated and compared the CO_2 emission reduction potential with conventional data. The analysis estimated the annual process heating demand for the calcination process at each cement plant, based on the actual annual cement production. Solar radiation of each cement plant location was determined, and facilities with DNI > 1700 kWh/m^2/year found a total thermal energy saving of 133.36 PJ/year and a CO_2 reduction of 7413.73 thousand tons.

Nikolakopoulos et al. (2024) developed the conceptual design of the cement production process within the SolCement project. They carried out the calcination of limestone using concentrated solar energy instead of fossil fuels. They simulated and compared the two cases with and without a thermochemical energy storage reactor (TSR). The computational analysis contrasted two variants of the traditional SolCement method, one incorporating TSR and the other excluding it. The calculations indicated that the solar calciner functioning at 1000°C enhanced energy

efficiency, and that reallocating production capacity to daylight hours optimized overall performance. The suggested technique resulted in a 33% decrease in fossil fuel consumption; however, the overall emission reduction was limited to 9% because of emissions from limestone calcination. This corresponds to 493 kg CO_2/ ton clinker. Storing and reusing the CO_2-laden gas stream can reduce emissions by as much as 82%. TSR supplies 22% of the energy necessary for preheating during nocturnal operations, whereas basic Rankine cycles can recuperate 49% and 40% of the electrical energy needed to compress the CO_2 generated during the day and night, respectively. This provides a reduction of 33 kg CO_2/ton clinker or an additional 0.6% emissions reduction.

Wang et al. (2024) proposed a technology for the direct solar production of cement clinker using concentrated solar energy. The results demonstrated the production of cement clinker using concentrated solar energy.

In Chapter 2, we investigated the effect of integrating solar energy systems into conventional cement production processes on reducing CO_2 emissions. We developed a calciner system that operates solely on solar energy and evaluated its performance under various scenarios that combined the use of petcoke, lignite, RDF and TDF. In our study, we examined the effectiveness of solar calciners in regions with high solar radiation (DNI) values and revealed the potential of sustainable energy use in cement production under different geographical conditions. In addition, we obtained data for optimizing system performance by analyzing the effect of the number of heliostats on thermal efficiency and energy transfer. The innovative aspect of this study is the comparative analysis of the potential of solar energy systems integrated into conventional cement production processes to reduce CO_2 emissions with different geographical regions and fuel scenarios. In particular, we showed that solar calciners operate more efficiently in regions with high DNI values and increase the emission reduction potential. Additionally, we optimize the number of heliostats to provide a more efficient roadmap for sustainable cement production.

3.2 Modelling of the Hybrid Solar Cement Process

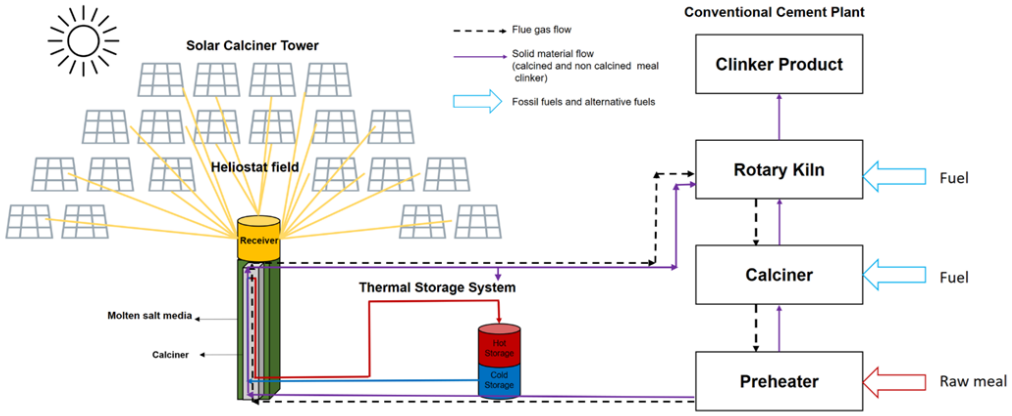


Figure 3.1 Solar cement plant schematic diagram

The proposed plant operates in hybrid mode, as shown in Figure 3.1. The conventional cement production process includes preheating, calcination, and firing stages. A solar power plant includes a solar calciner in a concentrated solar power plant to support the calcination process. The receiver collects solar energy to provide the required heat for calcination and then transmits this energy directly to a rotary kiln or thermal storage unit. The solar calciner maintains the raw materials at the outlet temperature, whereas heliostats direct sun radiation acroos extensive region and concentrate the solar energy by focusing it on a heat exchanger (receiver). Principle working of receiver is converted into heat, the sunlight is reflected by the heliostats to the central receiver at the top of the tower in the receiver. The receiver heat is transferred and stored in a heat transfer fluid (HTF).TES material, which is molten salt, can produce electricity through a traditional steam Rankine power cycle (Ding & Bauer, 2021). The collection of tubes in the receiver absorbs solar energy volumetrically via liquid components such as molten nitrate salt, water/steam, air, or liquid metals. Protecting the intermediate fluids and devices increases the overall energy efficiency. Considering the energy loss, the gas flow utilized HTF is raised to a certain temperature in the solar receiver so that sufficient energy can be provided for the calcination process

(Gonzalez & Flament, 2014). By storing solar heat inexpensively in the TES material and distributing it when sunlight is unavailable, CSPs can generate low-cost renewable electricity. Molten chloride some molten chloride salts, like $MgCl_2$/NaCl/KCl, have great thermophysical properties. They are very low in vapor pressure (~1 kPa at 800 °C) and have high thermal stability (>800 °C) compared to other salts (Ding et al., 2018). most promising TES/HTF materials in the next-generation molten salt technology due to its low costs (< 0.35 USD kg^{-1}) (Turschi et al., 2018). However, compared to the commercial molten nitrate salt technology, a significant additional challenge is the high corrosivity of molten chlorides to metallic building materials at high temperatures (Fernández et al., 2019). Therefore, effective, efficient, and affordable corrosion control technologies are required for this advanced technology.

3.2.1 CO_2 Emission Reduction Potential

CO_2 emission reduction potential for conventional cement plants belongs to existing and alternative scenarios. If solar energy replaces the calcination process, the solarization rate increases. In this case, the CO_2 reduction equation (3.1) is shown (Sahoo et al., 2023a):

$$\dot{m}_{CO_{2,red,max}} = \dot{m}_{CO_{2,conv}} - \dot{m}_{CO_{2,sol,min}} \tag{3.1}$$

CO_2 content in the raw material and the amount of fossil fuel and alternative fuel burned in the sintering rotary kiln determine the CO_2 emissions from the solar cement $\dot{m}_{mixture,kiln}$, as shown in equation (3.2):

$$\dot{m}_{CO_{2,sol,min}} = Y_{rm,CO_2}\dot{m}_{\mathrm{rm}} + \dot{m}_{mixture,kiln}LHV_{mixture,kiln}C_{CO_2,kiln} \tag{3.2}$$

CO_2 emissions from the conventional process $\dot{m}_{CO_{2,conv}}$ calculated based on the CO_2 concentration in the raw meal and the mixture of fossil and alternative fuels combusted in the main burner and cement calciner $\dot{m}_{mixture,calciner}$, as shown in equation (3.3):

$$\dot{m}_{CO_{2,conv}} = Y_{rm,CO_2}\dot{m}_{\mathrm{rm}} + \dot{m}_{mixture,kiln}LHV_{mixture,kiln}C_{CO_2,kiln} + \dot{m}_{mixture,calciner}LHV_{mixture,calciner}C_{CO_2,calciner} \tag{3.3}$$

Consequently, a reduction of CO_2 emissions when using a solar calciner in place of a conventional fuel-fired reactor is determined based on the fuel savings in the equation (3.4):

$$\dot{m}_{CO_{2,red,max}} = \dot{m}_{mixture,calciner} LHV_{mixture,calciner} C_{CO_2,calciner} \quad (3.4)$$

The mass balance of input data calculated for CO_2 reduction for all scenarios is in (Table 2.1), The clinker capacity is 1647 tons/day.

CO_2 mass fraction in the raw meal Y_{rm,CO_2} is determined where the weight of percent $CaCO_3 Wt\%_{\,raw\ meal}$ and then multiplied 1ton carbon emissions corresponding 1 ton 3.67 tonnes CO_2 emissions (Alsop, 2001) in equation (3.5):

$$Y_{rm,CO_2} = Wt\%_{\,CaCO_3} \frac{44\ g\ CO_2}{12 g\ C} = \frac{Wt\%_{hot\ meal,CaO} - Wt\%_{raw\ meal,CaO}}{Calcination\ degree(\%)} x3.67 \quad (3.5)$$

The raw meal mass flow is calculated using the clinker factor equation (3.6):

$$Clinker\ Factor = \frac{\dot{m}_{rm}}{\dot{m}_{clinker}} \quad (3.6)$$

Where $\dot{m}_{rm}$ is the mass flow rate of raw meal and $\dot{m}_{clinker}$ is the mass flow rate of clinker.

Spesific CO_2 emissions of fuel mixtures into kiln $C_{CO_{2,kiln}}$,and calciner $C_{CO_{2,calciner}}$ is calculated based on the fuel of carbon wt% respectively in equation (3.7):

$$C_{CO_{2,\frac{kiln}{calciner}}} = \frac{(\dot{m}_{mixture,\frac{kiln}{calciner}} . wt\% Carbon. \frac{44\ g\ CO_2}{12 g\ C})}{LHV_{\frac{kiln}{calciner}}} \quad (3.7)$$

Required input value of CO_2 reduction calculation for all scenarios are presented in Appendix B in Table B.1.

3.2.2 Heliostat field layout

The model setup begins by calculating the heat flux that the heliostat's solar field delivers to the reactor's top receiver. Subsequently, we computed the heat flux by utilizing the HTF in the jacket on the outside of the cement calciner. Appendix B in Table B.2 provides various parameters related to the heat flow and the parameters used to determine the solar field.

3.2.3 Heliostat system

The heliostats surround the solar tower, creating a solar field and reflecting sunlight to the receiver system at the top of it. Equation (3.8) calculates the amount of direct incident radiation (DII):

$$DII = DNI \times cos(\theta) \tag{3.8}$$

Here, cos(θ) represents the angle of incidence of light, and DNI represents the direct solar radiation. Equation (3.9) can estimate the amount of solar energy on the total surface of the mirrors:

$$q_{inc} = DII \times A_{hel} \tag{3.9}$$

Here, A_{hel} is defines aperture area of the heliostat.

Equation (3.10) defines to the solar heat source reflected onto the solar receiver (q_{ref}).

$$q_{ref} = q_{inc} \times \eta_{hel} \tag{3.10}$$

Here, η_{hel} is defines heliostat efficiency.

3.2.4 System for central receiving

The reflecting sun by heliostats is directed to HTF at solar receiver solar tower's top. The following equation (3.11) calculates the transfer of solar energy:

$$q_{rec} = q_{ref} - q_{trans.loss} \tag{3.11}$$

Here, ($q_{rec.loss}$) the heat loss solar energy in the solar receiver, which is a sum of the receiver's convection loss ($q_{conv.loss}$) and radiation loss ($q_{rad.loss}$) and the heat loss reflected from the receiver ($q_{ref.loss}$). The total solar heat loss in the receiver can be calculated in equation (3.12),(3.13),(3.14),(3.15):

$$q_{rec.loss} = q_{conv.loss} + q_{rad.loss} + q_{ref.loss} \tag{3.12}$$

$$q_{conv.loss} = \sum f_{mix} A_{r(T_{wall} - T_{amb})} \tag{3.13}$$

$$q_{rad.loss} = \sum \epsilon \sigma A_{r(T^4{}_{wall} - T^4{}_{amb})} \tag{3.14}$$

$$q_{ref.loss} = (1 - \delta) q_{ref} \tag{3.15}$$

Here, $A_r$is surface area of the solar receiver, f_{mix} is the convection coefficient of mixing, is the T_{amb} ambient temperature, T_{wall} is the wall temperature, σ is the

Stefan-Boltzmann coefficient, ϵ is the emissivity, and δ is the solar absorptance of the receiver surface. The thermal efficency of the receiver system can be calculated in equation (3.16):

$$\eta_{rec} = \frac{q_{rec}}{q_{ref}} = 1 - \frac{q_{trans.loss}}{q_{ref}} \tag{3.16}$$

The heat transferred from solar receiver to HTF can be calculated im equation (3.17):

$$q_{trans} = q_{rec}\eta_{rec} = \dot{m}_{HTF}\left(H_{HTF}^{out} - H_{HTF}^{in}\right) \tag{3.17}$$

Here, H_{HTF}^{out} andH_{HTF}^{in} are specific heat enthalpy and $\dot{m}_{HTF}$ is the mass flow rate of HTF at the outlet and inlet of the solar receiver,respectively. The calculation steps are performed using the Matlab program, and the corresponding results are provided in the Appendix B.

3.2.5 DNI and investigated plant location

This paper draws its focus from data collected from a real cement factory, calculating the required heat source values for scenarios that alter the ratios of fossil fuels and alternative fuels, as well as the required performance values when concentrated solar calciners replace conventional calciners in seven Turkish provinces. We determined the performance values for the implementation of concentrated solar calciners instead of conventional calciners in seven provinces in Turkey by referencing the Global Solar Atlas in Table 3.1 and solar source data in Figure 3.2.

Table 3.1 Climate data of Turkey province (Global Solar Atlas, 2024)

Province	**Annual total of DNI (kWh/m^2)**	**Daily DNI (kWh/m^2)**	**The design value of DNI (kW/m^2)**	**Average temperature (^oC)**
Samsun	1294	3.57	0.8	13.1

Table 3.1 Climate data of Turkey province (continue)

Istanbul	1305	3.67	0.8	15.1
Izmir	1834	5.06	1	17.6
Konya	1896	5.23	1	12.6
Erzurum	1813	5.00	1	5.9
Mersin	1918	5.29	1.2	18.4
Şanlıurfa	2225	6.14	1.4	17.8

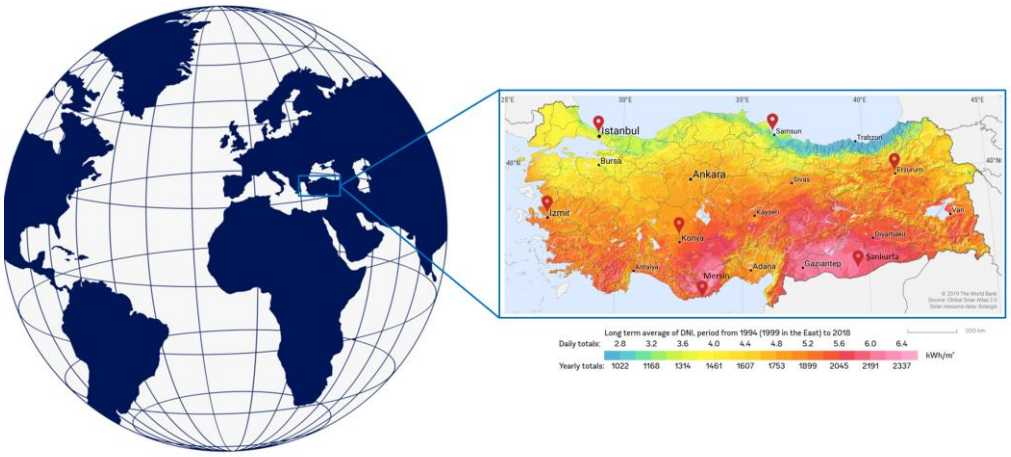


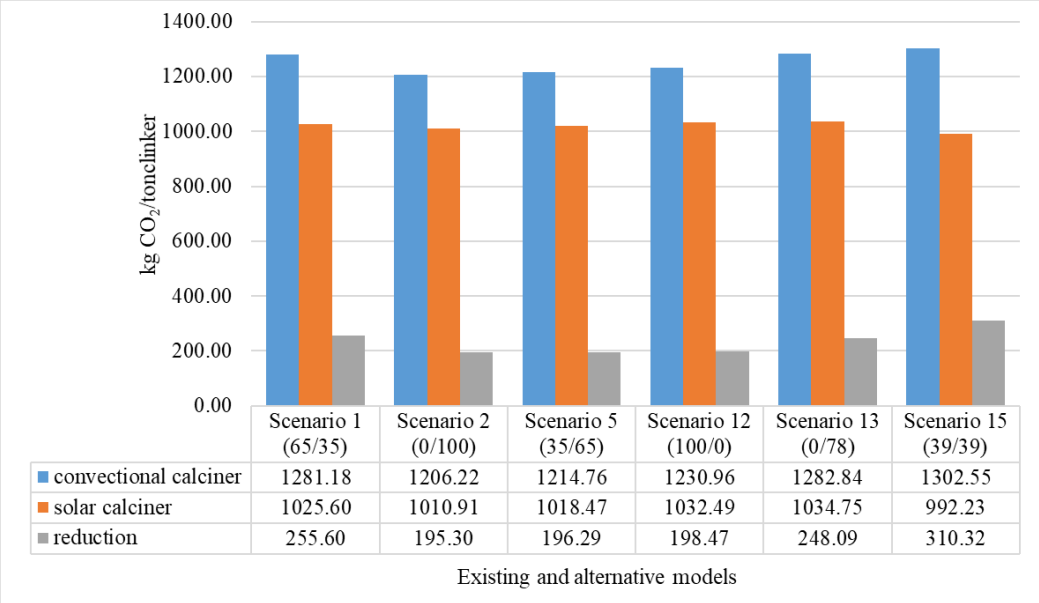
Figure 3.2 The annual DNI resource of the province in Turkey

3.3 Result and Discussion

3.3.1 Comparison CO_2 Emission Reductions in Conventional and Solar Calciner Systems

Where C_{CO_2} is the specific CO_2 emission factor per unit of heat content of the fuel. For all scenarios details on the used data see Table B.1. In the given bar chart in

(Figure 3.3), the CO_2 emissions in the conventional cement plant using these equations, considering various ratios of fossil fuel and alternative fuel scenarios, are calculated. In the existing scenario1 $\frac{\dot{m}_{CO_{2,conv}}}{\dot{m}_{clinker}}$ =1281.18 $\frac{kg_{CO_2}}{ton_{clinker}}$whereas the minimum emissions by utilizing the solar calciner equal $\frac{\dot{m}_{CO_{2,sol,min}}}{\dot{m}_{clinker}}$ = 1025.6 $\frac{kg_{CO_2}}{ton_{clinker}}$. Therefore, when a 100% solarized calciner was used instead of the calciner in the conventional existing system, the maximum CO_2 reduction was equal to 20%. In alternative scenarios, where we reduced fossil fuels from the calciner and kiln and increased alternative fuels, the maximum CO_2 reduction was approximately 16% for scenarios 2, 5, and 12, 19% for scenario 13, and 24% for scenario 15. Our calculations are close to align with the literature. They proposed a hybrid solar and coal co-driven clinker production process using a solar calciner for raw material calcination. However, their proposed configuration can reduce CO_2 emissions related to coal combustion in the conventional pre-calciner, which is estimated to be around 21% of the total (González &Flamant, 2014), (Moumin et al., 2020), (Sahoo et al., 2023b). Out of the remaining 34% of emissions, 13% is due to the fuel used in the clinker and 21% is due to the fuel used in the conventional calciner(Gardarsdottir et al., 2019), (Voldsund et al., 2019). Nikolakopoulos et al. (2024), reported the fossil fuel requirements and carbon footprint of the SolCement process in their study. Accordingly, the total CO_2 emission was 611 kg/ton clinker. This consisted of 118 kg CO_2/ton clinker in the flue gas and 493 kg CO_2/ton clinker from calcination. They found that reducing the total CO_2 emissions from calcination and combustion by 9.6% is possible, given that the amount of CO_2 released during the calcination of raw meal remains constant in all cases. Nikolakopoulos et al. (2023) In terms of CO_2 emissions, the conventional process produces 0.67 kg CO_2/kg clinker compared to 0.61 kg CO_2/kg clinker for the SOLCEMENT process. The SOLCEMENT process estimates a 32% energy reduction per clinker and an 8.6% reduction in kg CO_2/kg clinker.



	Scenario 1 (65/35)	Scenario 2 (0/100)	Scenario 5 (35/65)	Scenario 12 (100/0)	Scenario 13 (0/78)	Scenario 15 (39/39)
convectional calciner	1281.18	1206.22	1214.76	1230.96	1282.84	1302.55
solar calciner	1025.60	1010.91	1018.47	1032.49	1034.75	992.23
reduction	255.60	195.30	196.29	198.47	248.09	310.32

Figure 3.3 Comparison kg CO_2 /ton clinker of existing and alternative scenarios in the convectional calciner and solar calciner

3.3.2 The Operational Efficiency of Conventional Calciner Utilizing Solarization

Table 3.2 demonstrates the required heat source value of the convectional calciner ($Q_{conv.\ calciner}$) for each scenario. Different DNI values for the province of Turkey according to the $Q_{conv.\ calciner}$ for each scenario is calculated between 0.8 and 1.4 kW/m^2, which is the amount of heat transferred from the central receiver to the kiln at 1000 K. In the existing model (Scenario 1), when the petcoke and lignite ratios used in the entire system are taken into account, 9 tons of petcoke and lignite mixture is used in the calciner and 69 tons of petcoke and lignite mixture is used in the main burner. In Scenario 1 (fuel ratio 65% petcoke and 35% lignite), the fuel distribution in the calciner is 2.36% petcoke, 1.27% lignite, 68.55% RDF, 25.8% TDF and 2.02% waste oil, while 36.17% petcoke, 19.48% lignite, 40.32% RDF and 4.03% waste oil is used in the main burner. In Scenario 2-5-12, the RDF ratio is determined at around 96% in the calciner and about 44.4% in the main burner. In scenario 2, with a fuel ratio of 0% petcoke and 100% lignite, petcoke is excluded from the calciner, and the lignite ratio stands at 3.63%. Petcoke is not utilized in the main burner, whereas the lignite proportion stands at 44.34%. In scenario 5 (fuel ratio 35% petcoke and 65% lignite), 1.27% petcoke and 2.36% lignite are used in the calciner, and 19.45% petcoke and 36.18% lignite are used in the main burner. In scenario 12 (fuel ratio 100% petcoke and 0% lignite), 3.63% petcoke and 0%

lignite are used in the calciner, and 55.6% petcoke and 0% lignite are used in the main burner. In Scenario 13, no petcoke and lignite mixture is used in the calciner, while 78 tons of mixture is used in the main burner. In this case, the RDF ratio is 72.65% and the TDF ratio is 27.35% in the calciner, while the main burner contains 40.83% petcoke, 22.02% lignite, and 37.10% RDF. In scenario 15, a daily mix of 39 tons of petcoke and lignite is utilized in the calciner and main burner. The calciner comprises 10.22% petcoke, 5.50% lignite, 47.98% RDF, and 36.29% TDF, whereas the main burner utilizes 20.45% petcoke, 11.0% lignite, and 68.54% RDF.

Table 3.2 Requirement heat source value of convectional calciner

Existing and Alternative Scenarios	**$Q_{conv.calciner}$ (MW)**
Scenario 1 (65/35)	57.3
Scenario 2 (0/100)	44.2
Scenario 5 (35/65)	44.4
Scenario 12 (100/0)	44.8
Scenario 13 (0/78)	55.9
Scenario 15 (39/39)	68.4

Applied solarization to each scenario and the bar chart in Figure 3.4 shows the amount of heat transferred from the central receiver to the kiln. The calculated heat source values based on the number of heliostats changing, which corresponded to the heat value calculated for each scenario of the convectional calciner. We selected these values to be close to the values in Table 3.2. We evaluate the close heat value of each scenario, which includes scenarios 1-13, scenarios 2-5-12, and scenario 15. Figure 3.5 demonstrates the effect of DNI on the operation performance of CSP for existing and alternative scenarios in provinces of Turkey, the solar heat required. Figure 3.6 illustrate the relationship between different DNI values, the thermal

efficiency of the receiver, and the corresponding number of heliostats required to generate. The corresponding results are shown in the Appendix B.

The selected heliostat number is 2000. In scenario 1 and scenario 13, the required heat source value is 57.3 MW and 55.9 MW, respectively. These values correspond to applied solarization, with a DNI value of 1.2 and a thermal efficiency of 85.9% in Mersin province. 61.7 MW of solar energy transferred to the kiln as (q_{trans}) and 73.1 MW of heat transferred from the central receiver to the calciner as (q_{rec}) in both scenarios. For scenarios 2, 5, and 12, there is an average required heat source of 44.5 MW in the convectional calciner. In these cases, the DNI value is 1, and thermal efficiency is 82.3% in Izmir, Konya, and Erzurum provinces, resulting in q_{trans} of 49 MW and qrec of 59.4 MW. In scenario 15, the DNI value is 1.4, and thermal efficiency is 86% in Şanlıurfa provinces, leading to qtrans of 74.6 MW and qrec of 86.8 MW. The results suggested that DNI is influencing the overall performance of the solar energy system. Elevated DNI circumstances enhance the energy transfer from the solar receiver to the calciner while concurrently increasing thermal losses.The selected heliostat number is 2400. In scenarios 1 and 13, the DNI value is 1 and the thermal efficiency is 84.4%, while qtrans is 61.7 MW and qrec is 73.1 MW. In scenarios 2, 5, and 12, the shown DNI value is 0.8, and thermal efficiency is 81.8%, while qtrans is 46.4 MW and qrec is 56.6 MW. Assuming the DNI value remains constant, adding heliostats increases thermal efficiency, heat transfer from the central receiver to the calciner, and solar energy transfer to the kiln. However, we observe a decrease in both the DNI value and thermal efficiency in the same scenarios when we solely increase the number of heliostats. In lower DNI values, an increased number of heliostats is necessary to achieve the required design temperature because of reduced solar heat and heat transfer to the kiln.

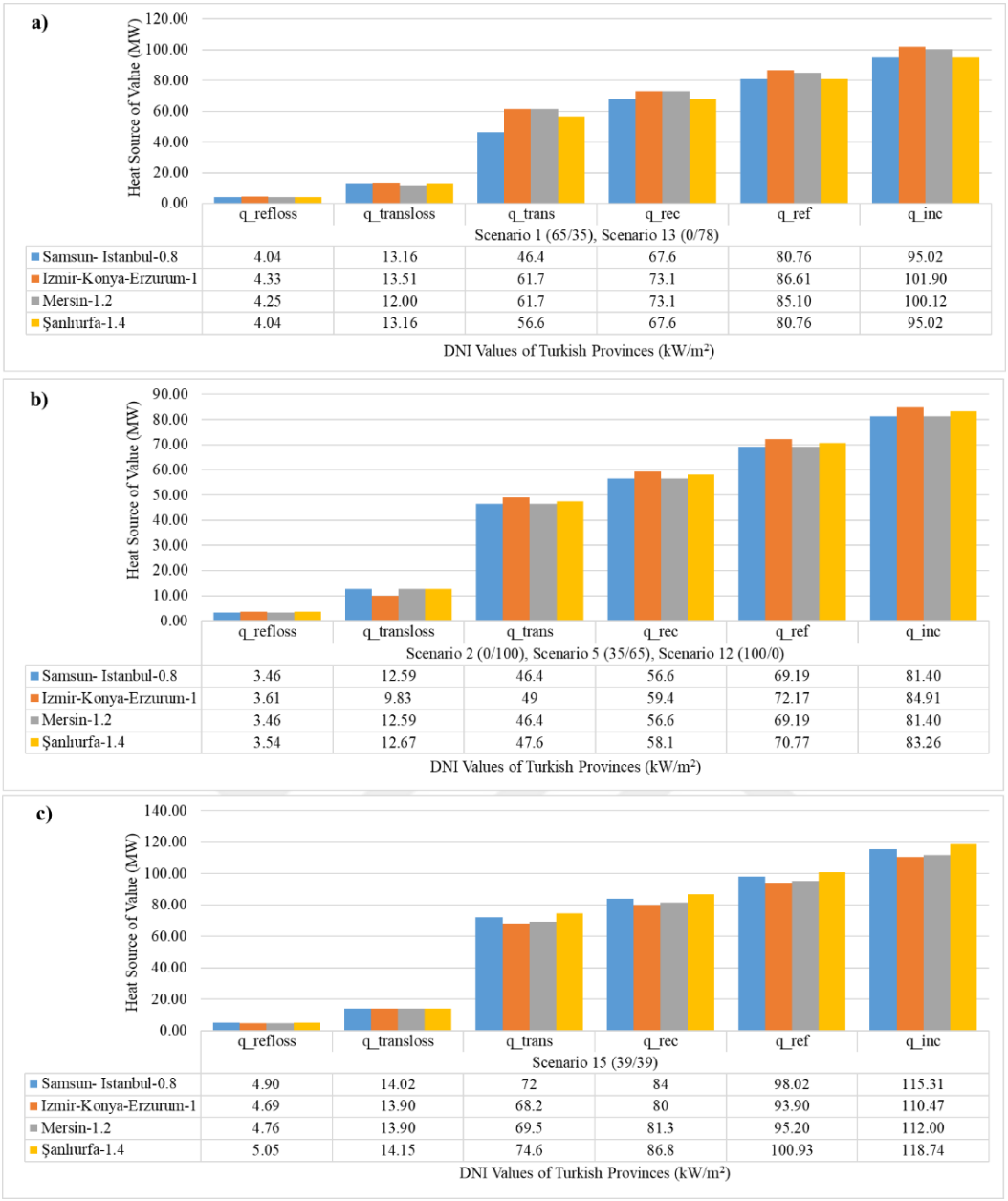


Figure 3.4 Impact of DNI on CSP performance for existing and alternative scenarios in Turkey's provinces: a) Scenario 1, Scenario 13; b) Scenario 2, Scenario 5, Scenario 12; c) Scenario 15

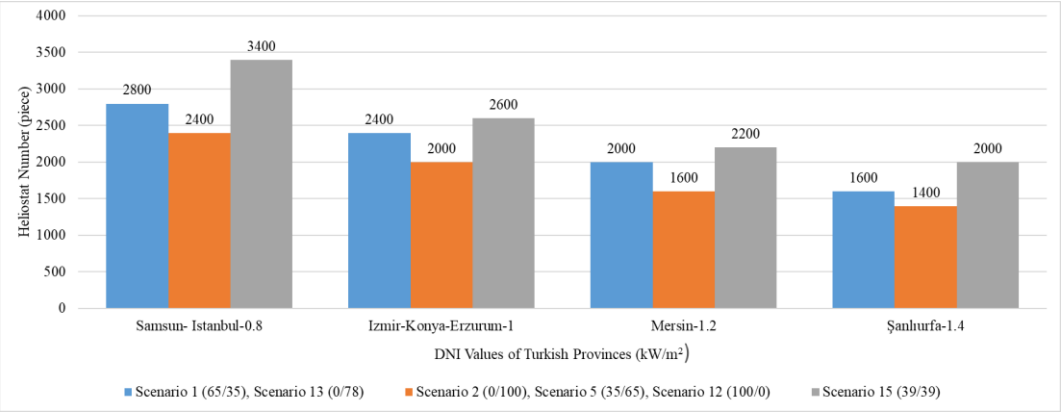


Figure 3.5 Impact of heliostat number of the solar receiver on CSP performance for existing and alternative scenarios in Turkey's provinces

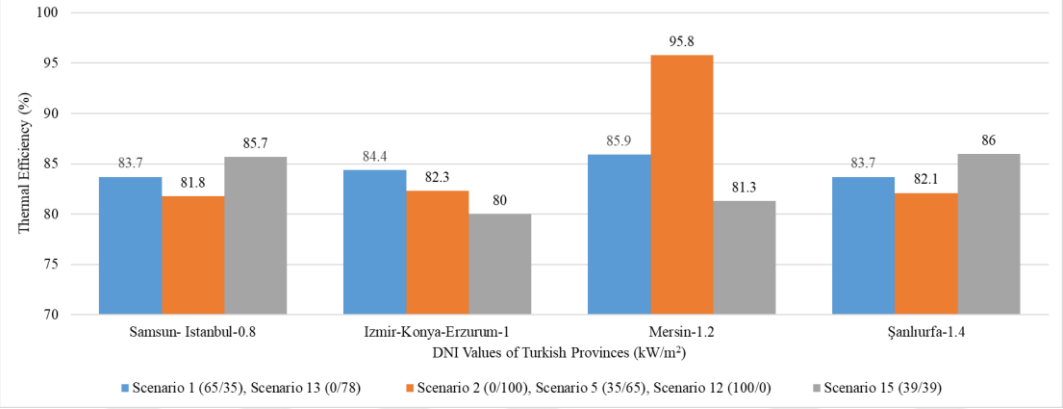


Figure 3.6 Impact of thermal efficiency of the solar receiver on CSP performance for existing and alternative scenarios in Turkey's provinces

4
CONCLUSION

In Chapter 1, the research concluded that CO_2 emissions in cement kiln operations might be significantly decreased by including RDF and TDF as alternative fuels. RDF, owing to its reduced sulfur concentration, decreases SO_2 emissions; yet, it requires meticulous management due to its elevated moisture level. Scenario 2 (0/100), featuring the highest lignite use, exhibited elevated NOx emissions, whereas Scenario 12 (100/0), characterized by increased petcoke and RDF content, demonstrated reduced CO_2 emissions but heightened SO_2 emissions. Scenario 13 (0/78) is distinguished for optimal emission control, utilizing RDF and TDF in the calciner, and achieved the greatest reduction in SO_2 and NO_x emissions. Nonetheless, the divergent calculation methodologies employed by NASA CEA, emphasizing chemical equilibrium, and Chemkin, advocating kinetic analysis, may result in discrepancies in emission forecasts. Therefore, additional research is necessary to standardize these methodologies and enhance the accuracy of emission predictions in the complex processes of cement manufacturing.

Future Work: Incorporating CFD modeling in future study could produce more accurate predictions of emission dynamics and heat distributions, especially in intricate industrial environments such as cement kilns. Although NASA CEA and Chemkin-Pro offer accessible and dependable tools for preliminary assessment, integrating them with CFD simulations could enhance the precision of assessments, including temperature distributions and flow dynamics. Additional investigation into hybrid modeling methodologies will enhance the efficacy of emission control techniques and process optimization in cement manufacturing facilities.

In Chapter 2, the conclusions of this study show that the solar energy system integrated into traditional cement production processes provides a significant effect in reducing CO_2 emissions. The analyses showed that using a calciner with 100% solar energy reduced CO_2 emissions by approximately 20%, bringing the traditional emission level of 1281.18 kg CO_2/ton clinker down to 1025.6 kg CO_2/ton clinker. The use of alternative fuels resulted in emission reductions ranging from 16% to

24% in other scenarios. In scenario 15, a CO_2 reduction of 24% was achieved, reaching an emission value of 973 kg CO_2/ton clinker. This shows that the combined use of solar energy and alternative fuels offers an effective solution in terms of emission reduction. In terms of heat requirement, in proviences with high DNI values (1.2 kW/m²) such as Mersin, 61.7 MW of heat was transferred from the calciner to the kiln with 85.9% thermal efficiency and 73.1 MW from the central receiver to the calciner. In regions with lower DNI values (1 kW/m²) such as İzmir, Konya and Erzurum, 49 MW of heat was transferred to the calciner with 82.3% thermal efficiency and 59.4 MW from the central receiver to the kiln. In Şanlıurfa, which has the highest DNI value (1.4 kW/m²), 74.6 MW of heat was transferred with 86% thermal efficiency.

Which cities and scenarios is the use of solar calciners more effective? According to the data examined in the study, Mersin and Şanlıurfa stand out as the regions where solar calciners are most efficient and have the highest CO_2 reduction potential. These regions achieve both thermal efficiency increases and optimized energy transfer due to their high DNI values. Especially in scenarios such as scenario 15, where 24% emission reduction is achieved, the use of solar calciners in high DNI regions such as Şanlıurfa and Mersin provides more effective results. We have also observed a significant effect on system efficiency when we increase the number of heliostats. We achieved 61.7 MW of heat transfer with 84.4% thermal efficiency when we used 2400 heliostats. These results indicate that careful optimization of the number of heliostats is necessary to enhance system performance. These data demonstrate that solar energy-integrated cement production processes can significantly reduce CO_2 emissions and reduce reliance on fossil fuels. The numerical results obtained based on various scenarios and geographical regions provide a comprehensive roadmap for the transition to sustainable energy use in cement production.

REFERENCES

Abd El-Hafiz, N. A., Abd El-Moghny, M. W., El-Desoky, H. M., & Afifi, A. A. (2015). Characterization and technological behavior of basalt raw materials for Portland cement clinker production. International Journal of Innovative Science, Engineering & Technology, 2(7).

Alsop, P. A. (2001). The Cement Plant Operations Handbook (Cilt 3). International Cement Review.

Ariyaratne, W. (2009). *Alternative fuels in cement kilns - Characterization and experiments* [Master Thesis]. Telemark University College, Faculty of Technology.

Atmaca, A. (2014). Increasıng Efficıency and Reducıng Pollutants in Cement Industry by Thermodynamıc And Exergoeconomıc Methods [PhD Thesis]. Mechanical Engineering, University of Gaziantep.

Bäckström, D., Johansson, R., Andersson, K., Wiinikka, H., & Fredriksson, C. (2015). On the use of alternative fuels in rotary kiln burners — An experimental and modelling study of the effect on the radiative heat transfer conditions. *Fuel Processing Technology, 138, 210–220.* *https://doi.org/10.1016/j.fuproc.2015.05.021*

Baier, H., & Menzel, K. (2011). Potentials of AFR co-processing. *IEEE*, *63*, 1–8. https://doi.org/10.1109/citcon.2011.5934550

Bapat, J. (Ed.). (2016). Advanced Fuel Burnıng Technologıes in Cement Productıon. *Indian Cement Review*, *30*, No 6, 44–46.

Barlaz, M.A., Eleazer, W.E., Whittle, D.J. (1993), *Potential to use waste tires as supplemental fuel in pulp and paper mill boilers, cement kilns and in road pavement*, Waste Management & Research, 11, 463-480. https://doi.org/10.1006/wmre.1993.1050

Bech, C., & Mishulovich, A. (2004). Preheaters and precalciners. In *Innovations in Portland Cement Manufacturing*, pages 269–286. Portland Cement Association, Skokie, Illinoins, USA. ISBN 0-89312-234-3.

Cansiz, O. F., Bankir, M. B., & Unsalan, K. (2023). Post-fire behaviour estimation of eco friendly cement-based composites. *International Journal of Global Warming*, 30(2), 193. https://doi.org/10.1504/ijgw.2023.10056072

Carotenuto, A., Simona Di Fraia, M., Uddin, R., & Vanoli, L. (2022). Comparison of combustion and gasification for energy recovery from residual woody biomass. International Journal of Heat and Technology, 40(4), 888–894. https://doi.org/10.18280/ijht.400404

Chatziaras, N., Psomopoulos, C. S., & Themelis, N. J. (Eds.). (2012). *Use of alternative fuels in cement industry*. Vol. 1, pp 521–529. 12th International Conference on Protection and Restoration of the Environment.

Chinyama, M.P. (2011). Alternative Fuels in Cement Manufacturing. In *InTech eBooks*. https://doi.org/10.5772/22319

Constans, D., & Gossman, D. (1997), *Tyre derived fuel use in cement kilns, GCI tech notes.* Gossman Consulting, Inc., Volume 3, No.9

Ding, W., & Bauer, T. (2021). Progress in research and development of molten chloride salt technology for next generation concentrated solar power plants. *Engineering*, *7*(3), 334–347. https://doi.org/10.1016/j.eng.2020.06.027

Ding, W., Shi, H., Xiu, Y., Bonk, A., Weisenburger, A., Jianu, A., & Bauer, T. (2018). Hot corrosion behavior of commercial alloys in thermal energy storage material of molten MgCl2/KCl/NaCl under inert atmosphere. *Solar Energy Materials and Solar Cells*, *184*, 22–30. https://doi.org/10.1016/j.solmat.2018.04.025

Emberger, B., and Hoenig, V. "Rotary kiln burner technology for alternative fuel co-firing," *Cement International*, vol. 9, no. 5, pp. 48–60, 2011.

European Cement Industry. (1999). *Best Available Techniques for The Cement Industry*. CEMBUREAU, Brussels. Retrieved November 8, 2024, from http://files.gamta.lt/aaa/Tipk/tipk/4_kiti%20GPGB/40.pdf

Felder, R., & Rousseau, R. (1986). Elementary principles of chemical processes (2nd ed.). https://www.osti.gov/scitech/biblio/6084376

Fernández, A. G., Gomez-Vidal, J., Oró, E., Kruizenga, A., Solé, A., & Cabeza, L. F. (2019). Mainstreaming commercial CSP systems: A technology review. *Renewable Energy*, *140*, 152–176. https://doi.org/10.1016/j.renene.2019.03.049

Fidaros, D., Baxevanou, C., Dritselis, C., & Vlachos, N. (2006). Numerical modelling of flow and transport processes in a calciner for cement production. Powder Technology, 171(2), 81–95. https://doi.org/10.1016/j.powtec.2006.09.011

FLS In Line Calciner. (n.d.). Infinity for Cement Equipment. Retrieved November 9, 2024, from https://www.cementequipment.org/home/kiln-system-process/

*FLSmidth JetFlex Burner brochure***.** Retrieved November 4, 2024, from https://www.scribd.com/document/740924862/JETFLEX-burner-brochure

Frauke, S., Ioanna, K., Maria, S. B., Serge, R., & Luis, D. S. (2013). Best Available Techniques (BAT) Reference document for the production of cement, lime and magnesium oxide. *IndustrialEmissions Directive*. https://doi.org/10.2788/12850

Gardarsdottir, S., De Lena, E., Romano, M., Roussanaly, S., Voldsund, M., Pérez-Calvo, J., Berstad, D., Fu, C., Anantharaman, R., Sutter, D., Gazzani, M., Mazzotti, M., & Cinti, G. (2019). Comparison of Technologies for CO2 Capture from Cement Production—Part 2: Cost Analysis. *Energies*, *12*(3), 542. https://doi.org/10.3390/en12030542

Gasser, U. (2000). Holderbank cement seminar, Process Technology, combustion, gas flows, and gas composition. *Holderbank management and consulting*. https://archive.org/details/HolderbankCementEngineeringBook/

Giannopoulos, D., Kolaitis, D., Togkalidou, A., Skevis, G., & Founti, M. (2006). Quantification of emissions from the co-incineration of cutting oil emulsions in cement plants – Part I: NOx, CO and VOC. *Fuel*, *86*(7–8), 1144–1152. https://doi.org/10.1016/j.fuel.2006.10.025

González, R. S., & Flamant, G. (2014). Technical and Economic Feasibility Analysis of using concentrated solar thermal technology in the cement Production Process: Hybrid Approach—A Case Study. *Journal of Solar Energy Engineering*, *136*(2). https://doi.org/10.1115/1.4026573

Grosso, M., Motta, A., & Rigamonti, L. (2010). Efficiency of energy recovery from waste incineration, in the light of the new Waste Framework Directive. *Waste Management*, *30*(7), 1238–1243. https://doi.org/10.1016/j.wasman.2010.02.036

Hansen, J. P. (2003). *SO2 emissions from cement production* [PhD Thesis, Technical University of Denmark]. https://orbit.dtu.dk/en/publications/so2-emissions-from-cement-production

Hasanbeigi, A., & Bhadbhade, N. (2023). Emissions impacts of alternative fuels combustion in the cement industry. *Global Efficiency Intelligence*. Florida, United States. https://www.globalefficiencyintel.com/emissions-impacts-of-alternative-fuels-combustion-in-the-cement-industry.(Accessed 14 September 2024)

Hasanbeigi, A., Lu, H., Williams, C., Price, L. (2012). International Best Practices for Pre- Processing and Co-Processing Municipal Solid Waste and Sewage Sludge in the Cement Industry. *Lawrence Berkley National Laboratory*.

Hercog, J., Lewtak, R., Glot, B., Jóźwiak, P., Nehring, G., Tavares, V. D., Nunes, A. M., & Gaspar, D. (2023). Pilot testing and numerical simulations of the multifuel burner for the cement kiln. *Fuel*, 342, 127801. https://doi.org/10.1016/j.fuel.2023.127801

Holcim Group Clinker Cooler. (n.d.). Retrieved November 4, 2024, from https://www.scribd.com/presentation/320000792/Clinker-Coolers

Jensen, L. S. (1999). NOx from cement production - reduction by primary measures [PhD Thesis], Denmark Technical University, Department of Chemical and BiochemicalEngineering]. https://orbit.dtu.dk/en/publications/id(f1b315a7-d898-4cbc-8a9e-c6a9273648ab).html

Karstensen, K. H., Kinh, N. K., Thang, L. B., Viet, P. H., Tuan, N. D., Toi, D. T., Hung, N. H., Quan, T. M., Hanh, L. D., & Thang, D. H. (2006). Environmentally sound destruction of obsolete pesticides in developing countries using cement kilns. *Environmental Science & Policy*, *9*(6), 577–586. https://doi.org/10.1016/j.envsci.2006.05.005

Kayadelen, H. K. (2017). Effect of natural gas components on its flame temperature, equilibrium combustion products and thermodynamic

properties. Journal of Natural Gas Science and Engineering, 45, 456–473. https://doi.org/10.1016/j.jngse.2017.05.023

Khadka, D. (2021). Calcination applying H2 combustion in O2 in a CO2-rich atmosphere [Master's thesis]. University of South Eastern Norway.

Khurana, S., Banerjee, R., Gaitonde, U., 2002. Energy balance and cogeneration for a cement plant. Applied Thermal Engineering 22, 485-494.

Larsen, M. B. (2007). *Alternative fuels in cement production* [PhD Thesis, Technical University of Denmark]. https://orbit.dtu.dk/files/154611641/Thesis_Morten_Boberg_Larsen_2007.pdf

Lemarchand, D., Thevenet, C., Bernard, D., Tetreault, N., & De Souance, A. (2017). Increasing the use of alternative fuels at cement plants : international best practice. In *International Finance Corporation (IFC)* (pp. 1–90). https://documents.worldbank.org/curated/en/563771502949993280/Increasing-the-use-of-alternative-fuels-at-cement-plants-international-best-practice

Li, Q., He, F., Mei, S., Xie, J., Zhang, C., & Deng, Y. (2024). Effect of oxy-fuel combustion with different O2/CO2 fractions on the pulverized coal combustion mechanism and heat transfer characteristics in rotary kilns: A numerical simulation study. Chemical Engineering Journal, 494, 153181. https://doi.org/10.1016/j.cej.2024.153181

Luo, Z., Song, H., Huang, Y., & Jin, B. (2024). Recent Advances on the Uses of biomass Alternative Fuels in cement manufacturing Process: A review. *Energy&Fuels*, 38(9). https://doi.org/10.1021/acs.energyfuels.3c04535

Maldonado, F. C. (2021). *Pilot testing, simulation, and scaling of an oxyfuel burner for cement kilns* [PhD Thesis]. Institut für Feuerungs- und Kraftwerkstechnik (IFK) der Universität Stuttgart.

Marzouk, O. A. (2023). Adiabatic Flame Temperatures for Oxy-Methane, Oxy-Hydrogen, Air-Methane, and Air-Hydrogen Stoichiometric Combustion using the NASA CEARUN Tool, GRI-Mech 3.0 Reaction Mechanism, and Cantera Python Package. Engineering Technology & Applied Science Research, 13(4), 11437–11444. https://doi.org/10.48084/etasr.6132

Meier, A., Bonaldi, E., Cella, G. M., Lipinski, W., & Wuillemin, D. (2005). Solar chemical reactor technology for industrial production of lime. *Solar Energy*, *80*(10), 1355–1362. https://doi.org/10.1016/j.solener.2005.05.017

Meier, A., Gremaud, N., & Steinfeld, A. (2004). Economic evaluation of the industrial solar production of lime. *Energy Conversion and Management*, *46*(6), 905–926. https://doi.org/10.1016/j.enconman.2004.06.005

Moumin, G., Ryssel, M., Zhao, L., Markewitz, P., Sattler, C., Robinius, M., & Stolten, D. (2020). CO2 emission reduction in the cement industry by using a solar calciner. Renewable Energy, 145, 1578–1596. https://doi.org/10.1016/j.renene.2019.07.045

Murray, A., & Price, L. (2008). Use of Alternative Fuels in Cement Manufacture: Analysis of Fuel Characteristics and Feasibility for Use in the Chinese Cement Sector. *Ernest Orlando Lawrence Berkeley National Laboratory*. https://escholarship.org/content/qt8sf9s522/qt8sf9s522.pdf?t=p0wse4

Nakhaei, M. (2018). Multi-phase flow and fuel conversion in cement calciner [PhD dissertation, Technical University of Denmark]. https://backend.orbit.dtu.dk/ws/files/192962989/Fil_fra_trykkeri_Mohammadhadi_Nakhaei.pdf

Nakhaei, M., Grévain, D., Jensen, L. S., Glarborg, P., Dam-Johansen, K., & Wu, H. (2021). NO emission from cement calciners firing coal and petcoke: A CPFD study. *Applications in Energy and Combustion Science*, 5, 100023. https://doi.org/10.1016/j.jaecs.2021.100023

Nakomcic-Smaragdakis, B., Cepic, Z., Senk, N., Doric, J., & Radovanovic, L. (2016). Use of scrap tires in cement production and their impact on nitrogen and sulfur oxides emissions. *Energy Sources Part a Recovery Utilization and Environmental Effects*, *38*(4), 485–493. https://doi.org/10.1080/15567036.2013.787473

NASA CEA application. Available online at: https://CEA.grc.NASA.gov/ (Accessed 14 September 2024)

Neuffer, B., & Laney, M. (2007). *Alternative Control Techniques Document Update - NOx emissions from new cement kilns*. U.S. Environmental Protection Agency Office of Air Quality Planning and Standards Sector Policies and Programs Division Research Triangle Park, North Carolina.

Nikolakopoulos, A., Steriotis, T., Charalambopoulou, G., Karagiannakis, G., Dimitrakis, D., Michalis, V., & Katsiotis, M. (2024). Reducing carbon emissions in cement production through solarization of the calcination process and thermochemical energy storage. *Computers & Chemical Engineering*, *180*, 108506. https://doi.org/10.1016/j.compchemeng.2023.108506

Nørskov, L. K. (2012). *Combustion of solid alternative fuels in the cement kiln burner* [Industrial PhD thesis, University of Denmark, Chemical Engineering]. https://backend.orbit.dtu.dk/ws/files/74227236/PhD._thesis_Linda_N_rskov_31072012..PDF

Pedersen, M. N. (2018). Co-firing of alternative fuels in cement kiln burners [PhD Thesis, Technical University of Denmark]. https://backend.orbit.dtu.dk/ws/files/161972551/808873_PhD_thesis_Morten_Nedergaard_Pedersen_fil_fra_trykkeri.pdf

Peng, Q., Ding, J., Wei, X., Yang, J., & Yang, X. (2009). The preparation and properties of multi-component molten salts. *Applied Energy*, *87*(9), 2812–2817. https://doi.org/10.1016/j.apenergy.2009.06.022

Peng, Q., Yang, X., Ding, J., Wei, X., & Yang, J. (2012). Design of new molten salt thermal energy storage material for solar thermal power plant. *Applied Energy*, *112*, 682–689. https://doi.org/10.1016/j.apenergy.2012.10.048

Polat, O., & Tari, I. (2023). Solar Hybridization Paths for Cement Production Processes. *Heat Transfer Engineering*, *45*(2), 165–175. https://doi.org/10.1080/01457632.2023.2178281

Rahman, A., Rasul, M., Khan, M. M. A., & Sharma, S. C. (2013a). Cement calciner model development for optimizing the usage of alternative fuels. CQUniversity. https://hdl.handle.net/10018/1015983

Rahman, A., Rasul, M., Khan, M., & Sharma, S. (2013b). Impact of Alternative Fuels on the Cement Manufacturing Plant Performance: An Overview. *Procedia Engineering*, *56*, 393–400. https://doi.org/10.1016/j.proeng.2013.03.138

Rahman, A., Rasul, M., Khan, M., & Sharma, S. (2015). Recent development on the uses of alternative fuels in cement manufacturing process. *Fuel*, *145*, 84–99. https://doi.org/10.1016/j.fuel.2014.12.029

Rende, K., Ercan, Ö., Hilmioğlu, B., Ergenekon, P., & Sadıkoğlu, H. (2018). Assessment of CO2 reduction techniques of cement production in Turkey. *International Journal of Global Warming*, *16*(1), 18–38. https://doi.org/10.1504/IJGW.2018.094308

Sahoo, N., Kumar, A., & Samsher, N. (2021). A Preliminary assessment of solar industrial process heating for cement industry. In Lecture notes in mechanical engineering (pp. 171–177). https://doi.org/10.1007/978-981-16-2794-1_15

Sahoo, N., Kumar, A., & Samsher, N. (2023a). Design of solar cement plant for supplying thermal energy in cement production. *Journal of Cleaner Production*, *426*, 139151. https://doi.org/10.1016/j.jclepro.2023.139151

Sahoo, N., Kumar, A., & Samsher, N. (2023b). Potential of solar thermal calciner technology for cement production in India and consequent carbon mitigation. *Process Safety and Environmental Protection*, *179*, 667–676. https://doi.org/10.1016/j.psep.2023.09.041

Sánchez, G. F. G., Velasco, J. L. C., & Díaz, D. a. F. (2024). Numerical investigation of combustion in a panela furnace using openfoam. Ingeniería Y Competitividad, 26(1). https://doi.org/10.25100/iyc.v26i1.13410

Savaş, A. F., & Kolip, A. (2015). Comparative energy and exergy analyses of a serial and parallel flow four-stage cyclone pre-calciner cement plant. *International Journal of Exergy*, *17*(4), 492. https://doi.org/10.1504/ijex.2015.071562

Sharma, P. (2023). Process Design and Integration of Refuse Derived Fuel (RDF) Gasification in Cement Manufacturing Process [PhD Thesis]. Bırla Instıtute Of Technology And Scıence Pılanı (Rajasthan) Indıa.

Shenk, R. E., & Jensen, L. S. (2009). Calciner burner design for alternative fuels. *IEEE Xplore*, 1–11. https://doi.org/10.1109/citcon.2009.5116166

Sieradzka, M., Rajca, P., Zajemska, M., Mlonka-Mędrala, A., & Magdziarz, A. (2020). Prediction of gaseous products from refuse derived fuel pyrolysis using chemical modelling software - Ansys Chemkin-Pro. *Journal of*

Cleaner Production, 248, 119277. https://doi.org/10.1016/j.jclepro.2019.119277

Solar resource of Turkey. *Global Solar Atlas*. The World Bank Group. Retrieved October 10, 2024, from https://globalsolaratlas.info/download/turkey

Steuch, H. E. (2004). Clinker coolers. *In Innovations in Portland Cement Manufacturing* (pp. 477–498). Portland Cement Association, Skokie, Illinoins, USA.

Sutou, K., Harada, H., & Ueno, N. (1999, April 23). Chlorine bypass system for stable kiln operation and the recycling of waste. In *IEEE/PCA CEMENT INDUS TRY TECHNICAL CONFERENCE*. https://doi.org/10.1109/citcon.1999.767038

Tokheim, L.A. The Impact of Staged Combustion on the Operation of a Precalciner Cement Kiln. Ph.D. Thesis, Telemark College, Porsgrunn, Norway, 1999.

Tomatis, M., Jeswani, H. K., Stamford, L., & Azapagic, A. (2020). Assessing the environmental sustainability of an emerging energy technology: Solar thermal calcination for cement production. *The Science of the Total Environment*, *742*, 140510. https://doi.org/10.1016/j.scitotenv.2020.140510

Turchi, C. S., Vidal, J., & Bauer, M. (2018). Molten salt power towers operating at 600–650 °C: Salt selection and cost benefits. *Solar Energy*, *164*, 38–46. https://doi.org/10.1016/j.solener.2018.01.063

Vaccaro, M. (2006). *Burning alternative fuels in rotary cement kilns* (Vol. 9). Cement Industry Technical Conference, IEEE. https://doi.org/10.1109/citcon.2006.1635711

Voldsund, M., Gardarsdottir, S., De Lena, E., Pérez-Calvo, J., Jamali, A., Berstad, D., Fu, C., Romano, M., Roussanaly, S., Anantharaman, R., Hoppe, H., Sutter, D., Mazzotti, M., Gazzani, M., Cinti, G., & Jordal, K. (2019). Comparison of Technologies for CO2 Capture from Cement Production—Part 1: Technical Evaluation. *Energies*, *12*(3), 559. https://doi.org/10.3390/en12030559

Wang, G., Shui, P., Yin, T., Cui, H., & Tian, Y. (2024). Optimizing Nitrogen Oxide Emissions in Industrial Calcination through Staged Combustion: A CFD-, MP-PIC-, and RSM-Based Approach for Enhanced Process Efficiency. *Industrial & Engineering Chemistry Research*, *63*(33), 14541–14553. https://doi.org/10.1021/acs.iecr.4c01329

Wang, Y., Wang, Z., Lei, D., Zang, C., & Guo, D. (2024). Technology verification of portland cement clinker production driven by concentrated solar energy directly. *Renewable Energy*, *232*, 121064. https://doi.org/10.1016/j.renene.2024.121064

Wolter, A. (1985). Influence of the kiln system on the clinker properties, Zement-Kalk-Gips, vol. 38(10), pp. 612–614.

Yang, Y., Zhang, Y., Li, S., Liu, R., & Duan, E. (2020). Numerical simulation of low nitrogen oxides emissions through cement precalciner structure and

parameter optimization. *Chemosphere*, 258, 127420. https://doi.org/10.1016/j.chemosphere.2020.127420

Yılmaz, S., Kumlutaş, D., Yücekaya, U. A., & Cumbul, A. Y. (2021). Prediction of the equilibrium compositions in the combustion products of a domestic boiler. Energy, 233, 121123. https://doi.org/10.1016/j.energy.2021.121123

Yucel, O., & Aydin, E. S. (2023). Modeling of biomass-based hydrogen production via catalytic sorption-enhanced reformer integrated with a gasifier. Journal of the Indian Chemical Society, 100(1), 100854. https://doi.org/10.1016/j.jics.2022.100854

Zajemska, M., Musiał, D., & Poskart, A. (2014). Application of CHEMKIN and COMSOL programs in the calculations of chemical composition of natural gas combustion products. Combustion Science and Technology, 186(2), 153–172. https://doi.org/10.1080/00102202.2013.854206

Zhang, X., Tian, J., Wang, X., Zhu, Y., Hu, T., & Hu, P. (2024). Multiphase flow simulation and industrial application of an in-line gasifier for NOx emissions control from cement kiln. *Journal of Industrial and Engineering Chemistry*. https://doi.org/10.1016/j.jiec.2024.08.019

Zhao, Y. (2020). *Molten chloride thermophysical properties, chemical optimization, and purification*. National Renewable Energy Laboratory. https://doi.org/10.2172/1734652

A

APPENDIX PROCESS OVERVIEW AND EMISSION MODELLING USING COMPUTATIONAL TOOLS IN CEMENT PRODUCTION

Table A.1 Proximate and ultimate analysis of fuels fed to the calciner and main burner

	Fossil Fuels		**Alternative Fuels**		
wt(%)	**Lignite**	**Petcoke**	**RDF**	**TDF**	**WO**
C	73.78	87.8	34	74.3	40.8
H	4.74	3.76	5.97	6.88	7.8
S	0.42	6.73	0.25	1.59	2
N	2.01	1.4	1.23	0.3	2
O	13.74	0.12	17.08	6.52	8
Moisture	0.01	0.01	33	1.61	33
Ash	10.61	0.18	6.4	8.8	6.4
Fixed Carbon	55.46	90.17	6.87	26.55	-
Volatile	33.93	9.64	53.7	60.3	-

TablE A.2 Average chemical composition of raw meal and hot meal

wt. (%)	Raw Meal	Hot Meal
SiO_2	12.93	20.82
CaO	41.66	55.2
MgO	0.64	1.16
LOI	33.42	2.5

Adiabatic Flame Temperature Calculation

Table 2.5-2.6-2.7-2.8-2.9 displays the chemical composition of fossil and alternative fuels, which Türk Çimento Sanayicileri Birliği has analyzed for cement production, and also the calculation of fuels is shown as a pseudo-chemical formula (Khadka, 2021).

- **Petcoke /Air Combustion**

Table A.3 Petcoke composition and its chemical formula

Element	Wt%	Mol/100 gm	Mol/mol C
C	87.80 ÷ 12	7.32	1
H	3.76 ÷ 1	3.76	0.514
O	0.12 ÷ 16	0.0075	1.02×10^{-3}
S	6.73 ÷ 32	0.21	0.028
N	1.40 ÷ 14	0.1	0.014
H_2O	0.01 ÷ 18	0.00055	7.51×10^{-5}

Ash	0.18	-	1.557 g/mol C

Therefore, the pseudo-chemical formula of petcoke is as follows:

$$CH_{0.514}N_{0.014}S_{0.028}O_{0.00102}(H_2O)_{7.51\times10^{-5}} = CH_{0.514}N_{0.014}S_{0.028}O_{1.09\times10^{-3}}$$

We define the stoichiometric combustion of the identified petcoke and air below:

$$CH_{0.514}N_{0.014}S_{0.028}O_{1.09\times10^{-3}} + \alpha(O_2 + 3.78N_2) \rightarrow CO_2 + \frac{0.514}{2}H_2O + 0.028SO_2 + (3.78\alpha + \frac{0.014}{2})N_2$$

Where,

$$\alpha = x + \frac{y}{4} + z -, (CxHyNzSO\alpha) \text{(Felder et al., 1986)}$$

$$= 1 + \frac{0.514}{4} + 0.014 - \frac{1.09\times10^{-3}}{2} = 1.14$$

Hence,

The combustion stoichiometry is;

$$CH_{0.514}N_{0.014}S_{0.028}O_{1.09\times10^{-3}} + 1.14(O_2 + 3.78N_2) \rightarrow O_2 + 0.257H_2O + 0.028SO_2 + 4.316N_2$$

Utilizing the average Cp approach, the subsequent equation was used to calculate the combustion product temperature (Tp).

$$Tp = Tr + \frac{\text{LHV} \cdot N_{fuel} \cdot M_{fuel}}{\Sigma N_{i,P} \cdot C_{Pi}} \text{where,}$$

Tr = 298.15 Kelvin

N_{fuel} = 1 mol

$M_{fuel,\text{petcoke}}$ = 13.26 gr/mol

The assumed of lower heating value of petcoke is 34.87 MJ/kg. When we assume average Cp (kj/mol.K) at 1500 K and ascertaining specific heat at a constant pressure of product species i.e. Cp,H_2O, Cp,CO_2, Cp,SO_2, & Cp,N_2 using physical property table, we get.

Cp,H_2O=0.0467; Cp,CO_2=0.0584 ; Cp,SO_2=0.0559; Cp,N_2=0.0350

The product temperature is calculated below:

$$Tp = Tr + \frac{\text{LHV} \cdot N_{fuel} \cdot M_{fuel}}{\Sigma N_{i,P} \cdot C_{Pi}}$$

$$=298.15+\frac{34.87x\ 10^{3}x13.26x10^{-3}}{(1\times0.0584)+(0.257\times0.0467)+(0.028\times0.0559)+(4.316\times0.0350)}=2371.3\ K$$

The reactans average temparature and products temperature is calculated below:

$$Tave=\frac{298.15+2371.3}{2}=1334.73\ K$$

This suggests the first assumption of $Tave$=1500 K was excessive. Consequently, assessing the specific heat and flame temperature utilizing the revised average temperature, $Tave$=1334.73 K.

Cp,H_2O=0.045; Cp,CO_2=0.0564; Cp,SO_2=0.0556; Cp,N_2=0.029

$$Tp = Tr+\frac{\text{LHV}\cdot N_{fuel}.M_{fuel}}{\Sigma\, N_{i,P}.C_{Pi}}$$

$$=298.15+\frac{34.87x\ 10^{3}x13.26x10^{-3}}{(1\times0.0564)+(0.257\times0.045)+(0.028\times0.0556)+(4.316\times0.029)}=2673.14\ K$$

The reactans average temparature and products temperature is calculated below:

$$Tave=\frac{298.15+2673.3}{2}=1485.64K$$

We are recalculating the specific heat and flame temperature using of the new average temperature, i.e. $Tave$=1485.6 K.

Cp,H_2O=0.046; Cp,CO_2=0.058; Cp,SO_2=0.056; Cp,N_2=0.035

$$Tp = Tr+\frac{\text{LHV}\cdot N_{fuel}.M_{fuel}}{\Sigma\, N_{i,P}.C_{Pi}}$$

$$=298.15+\frac{34.87x\ 10^{3}x13.26x10^{-3}}{(1\times0.058\ )+(0.257\times0.046)+(0.028\times0.056)+(4.316\times0.035)}=2376.71\ K$$

The reactans average temparature and products temperature is calculated below:

$$Tave=\frac{298.15+2376.71}{2}=1337.43K$$

We are recalculating the specific heat and flame temperature using of the new average temperature, $Tave$=1337.43K.

Cp,H_2O=0.054; Cp,CO_2=0.057; Cp,SO_2=0.056; Cp,N_2=0.034

$$Tp = Tr+\frac{\text{LHV}\cdot N_{fuel}.M_{fuel}}{\Sigma\, N_{i,P}.C_{Pi}}$$

$$=298.15+\frac{34.87x\ 10^{3}x13.26x10^{-3}}{(1\times0.057)+(0.257\times0.054)+(0.028\times0.056)+(4.316\times0.034)}=2407.62\ K$$

The reactans average temparature and products temperature is calculated below:

$$Tave=\frac{298.15+2407.62}{2}=1352.88K$$

The variation in average temperature is less than 20 K. The ultimate adiabatic flame temperature of the coal and air combustion reaction is approximately $\approx 2407.62\ K$.

- **Lignite /Air Combustion**

Table A.4 Lignite composition and its chemical formula

Element	Wt%	Mol/100 gm	Mol/mol C
C	73.78 ÷ 12	6.15	1
H	4.74 ÷ 1	4.74	0.77
O	8.43÷ 16	0.52	0.085
S	0.42÷ 32	0.013	2.11 x 10-3
N	2.01÷ 14	0.143	0.023
H_2O	0.01 ÷ 18	0.00055	8.94 x 10-5
Ash	10.61	-	1.856 g/mol C

Therefore, the pseudo-chemical formula of lignite is as follows:

$$CH_{0.77}N_{0.023}S_{2.11\ x\ 10^{-3}}O_{0.085}(H_2O)_{\ 8.94\ x\ 10\text{-}5}=CH_{0.77}N_{0.023}S_{2.11\ x\ 10^{-3}}O_{0.085}$$

We define the stoichiometric combustion of the identified lignite and air below:

$$CH_{0.77}N_{0.023}S_{2.11\ x\ 10^{-3}}O_{0.085}+\alpha(O2+3.78N_2)\rightarrow CO2+\frac{0.77}{2}H_2O+2.11\ x\ 10^{-3}$$

$$SO_2+(3.78\alpha+\frac{0.023}{2})N_2$$

Where,

$$\alpha = x + \frac{y}{4} + z - \frac{\alpha}{2}\ ,\ (CxHyNzSOa)$$

$$= 1 + \frac{0.77}{4} + 0.023 - \frac{0.085}{2} = 1.173$$

Hence,

The combustion stoichiometry is;

$$CH_{0.77}N_{0.023}S_{2.11 \times 10^{-3}}O_{0.086} + 1.173(O_2 + 3.78N2) \rightarrow CO_2 + 0.385H_2O + 2.11 \times 10^{-3}\ SO_2 + 4.45N_2$$

Utilizing the average Cp approach, the subsequent equation was used to calculate the combustion product temperature (Tp).

$$Tp = Tr + \frac{\text{LHV} \cdot N_{fuel} \cdot M_{fuel}}{\Sigma N_{i,P} \cdot C_{Pi}}$$

where,

Tr = 298.15 Kelvin

N_{fuel} = 1 mol

$M_{fuel,\text{lignite}}$ = 14.53 gr/mol

The assumed of lower heating value of lignite is 29.38 MJ/kg. When we assume average Cp (kJ/mol·K) at 1500 K and determining specific heat at a constant pressure of product species i.e. Cp,H_2O, Cp,CO_2, Cp,SO_2, & Cp,N_2 using physical property table, we get.

Cp,H_2O=0.0467; Cp,CO_2=0.0584; Cp,SO_2=0.0559; Cp,N_2=0.0350

The product temperature is calculated below:

$$Tp = Tr + \frac{\text{LHV} \cdot N_{fuel} \cdot M_{fuel}}{\Sigma N_{i,P} \cdot C_{Pi}}$$

$$= 298.15 + \frac{29.38x\ 10^3 x 14.53 x 10^{-3}}{(1 \times 0.0584) + (0.385 \times 0.0467) + (2.11 \times 10^{-3} \times 0.0559) + (4.48 \times 0.0350)} = 2127.96\ K$$

The reactans average temparature and products temperature is recalculated below:

$$Tave = \frac{298.15 + 2127.96}{2} = 1213.05\ K$$

This suggests the first assumption of $Tave$=1500 K was excessive. Consequently, assessing the specific heat and flame temperature utilizing the revised average temperature, i.e. $Tave$=1213.05 K.

Cp,H_2O= 0.0436; Cp,CO_2=0.0566; Cp,SO_2=0.0553; Cp,N_2=0.0337

$$Tp = Tr + \frac{\text{LHV} \cdot N_{fuel} \cdot M_{fuel}}{\Sigma N_{i,P} \cdot C_{Pi}}$$

$$=298.15 + \frac{34.87x\ 10^3 x 13.26x10^{-3}}{(1\times0.0566)+(0.385\times0.0436)+(2.11\ \text{x}\ 10^{-3}\times0.0553)+(4.45\times0.0337)} = 2367.25\ K$$

The reactans average temparature and products temperature is recalculated below:

$$Tave = \frac{298.15+2673.3}{2} = 1332.7K$$

We are recalculating the specific heat and flame temperature using of the new average temperature, $Tave$=1332.7K.

Cp,H_2O= 0.0450; Cp,CO_2=0.0574; Cp,SO_2=0.0556; Cp,N_2=0.0343

$$Tp = Tr + \frac{\text{LHV} \cdot N_{fuel} \cdot M_{fuel}}{\Sigma N_{i,P} \cdot C_{Pi}}$$

$$=298.15 + \frac{34.87x\ 10^3 x 13.26x10^{-3}}{(1\times0.0574)+(0.385\times0.0450)+(2.11\ \text{x}\ 10^{-3}\times0.0556)+(4.45\times0.0343)} = 2192.53\ K$$

The reactans average temparature and products temperature is recalculated below:

$$Tave = \frac{298.15+2192.53}{2} = 1245.34\ K$$

We are recalculating the specific heat and flame temperature using of the new average temperature, $Tave$=1245.37 K.

Cp,H_2O= 0.0440 ; Cp,CO_2=0.0568; Cp,SO_2=0.0554; Cp,N_2=0.0339

$$Tp = Tr + \frac{\text{LHV} \cdot N_{fuel} \cdot M_{fuel}}{\Sigma N_{i,P} \cdot C_{Pi}}$$

$$=298.15 + \frac{34.87x\ 10^3 x 13.26x10^{-3}}{(1\times0.0568)+(0.385\times0.0440)+(2.11\ \text{x}\ 10^{-3}\times0.0554)+(4.45\times0.0339)} = 2355.8\ K$$

The reactans average temparature and products temperature is recalculated below:

$$Tave = \frac{298.15+2355.8}{2} = 1326.97\ K$$

The variation in average temperature is less than 80 K. The ultimate adiabatic flame temperature of the coal and air combustion reaction is approximately $\approx 2355.8\,K$.

- **RDF /Air Combustion**

Table A.5 RDF composition and its chemical formula

Element	Wt%	Mol/100 gm	Mol/mol C
C	34 ÷ 12	2.83	1
H	5.97 ÷ 1	5.97	2.11
O	17.08÷ 16	1.067	0.38
S	0.25÷ 32	7.81×10^{-3}	2.76×10^{-3}
N	1.23÷ 14	0.087	0.031
H_2O	33÷ 18	1.83	0.65
Ash	6.4	-	4.173 g/mol C

Therefore, the pseudo-chemical formula of RDF is as follows:

$$CH_{2.11}N_{0.031}S_{2.76 \times 10^{-3}}O_{0.38}(H_2O)_{0.65} = CH_{3.41}N_{0.031}S_{2.76 \times 10^{-3}}O_{1.03}$$

We define the stoichiometric combustion of the identified RDF and air below:

$$CH_{3.41}N_{0.031}S_{2.76 \times 10^{-3}}O_{1.03} + \alpha(O_2 + 3.78N_2) \rightarrow CO_2 + \frac{0.65}{2}H_2O + 2.76 \times 10^{-3}SO_2 + (3.78\alpha + \frac{0.031}{2})N_2$$

Where,

$$\alpha = x + \frac{y}{4} + z - \frac{\alpha}{2}\,,\ (CxHyNzSOa)$$

$$= 1 + \frac{3.41}{4} + 0.031 - \frac{1.03}{2} = 1.368$$

Hence, The combustion stoichiometry is;

$$CH_{3.41}N_{0.031}S_{2.76\ x\ 10^{-3}}O_{1.03}+1.368(O_2+3.78N_2)\rightarrow CO_2+0.325H_2O+2.76\ x\ 10^{-3}SO_2+5.18N_2$$

Utilizing the average Cp approach, the subsequent equation was used to calculate the combustion product temperature (Tp).

$$Tp = Tr+\frac{\text{LHV}\cdot N_{fuel}.M_{fuel}}{\Sigma N_{i,P}.C_{Pi}}$$

where,

Tr = 298.15 Kelvin

N_{fuel} = 1 mol

$M_{fuel,\text{RDF}}$ = 32.41gr/mol

The assumed of lower heating value of RDF is 15.02 MJ/kg. When we assume average Cp (kJ/mol·K) at1500 K and determining specific heat at a constant pressure of product species i.e. Cp,H_2O, Cp,CO_2, Cp,SO_2, & Cp,N_2 using physical property table, we get.

Cp,H_2O=0.0467; Cp,CO_2=0.0584; Cp,SO_2=0.0559; Cp,N_2=0.0350

The product temperature is calculated below:

$$Tp = Tr+\frac{\text{LHV}\cdot N_{fuel}.M_{fuel}}{\Sigma N_{i,P}.C_{Pi}}$$

$$=298.15+\frac{15.02x\ 10^3 x32.41x10^{-3}}{(1\times0.0584)+(0.325\times0.0467)+(2.76\ x\ 10^{-3}\times0.0559)+(5.18\times0.0350)} = 2206.92\ K$$

The reactans average temparature and products temperature is recalculated below:

$$Tave=\frac{298.15+2206.92}{2} = 1252.54\ K$$

This suggests the first assumption of $Tave$=1500 K was excessive. Consequently, assessing the specific heat and flame temperature utilizing the revised average temperature, $Tave$=1252.54 K.

Cp,H_2O= 0.0441; Cp,CO_2=0.0569; Cp,SO_2=0.0554; Cp,N_2=0.0339

$$Tp = Tr+\frac{\text{LHV}\cdot N_{fuel}.M_{fuel}}{\Sigma N_{i,P}.C_{Pi}}$$

$$=298.15+\frac{15.02x\ 10^{3}x32.41x10^{-3}}{(1\times0.0569)+(0.325\times0.044)+(2.76\ \text{x}\ 10^{-3}\times0.0554)+(5.18\times0.0339)}=2269.35\ K$$

The reactans average temparature and products temperature is recalculated below:

$$Tave=\frac{298.15+2269.35}{2}=1283.75K$$

The variation in average temperature is less than 40 K. The ultimate adiabatic flame temperature of the coal and air combustion reaction is approximately ≈2269.35 K.

- **TDF /Air Combustion**

Table A.6 TDF composition and its chemical formula

Element	Wt%	Mol/100 gm	Mol/mol C
C	74.3÷ 12	6.19	1
H	6.88 ÷ 1	6.88	1.11
O	6.52÷ 16	0.41	0.066
S	1.59÷ 32	0.05	8.07 x 10^{-3}
N	0.3÷ 14	0.021	3.4 x 10^{-3}
H_2O	1.61÷ 18	0.089	0.014
Ash	8.8	-	2.201 g/mol C

Therefore, the pseudo-chemical formula of TDF is as follows:

$$CH_{1.11}N_{3.4x\ 10^{-3}}S_{8.07\ x\ 10^{-3}}O_{0.066}(H_2O)_{\ 0.014}=CH_{1.138}N_{3.4x\ 10^{-3}}S_{8.07\ x\ 10^{-3}}O_{0.08}$$

We define the stoichiometric combustion of the identified TDF and air below:

$$CH_{1.138}N_{3.4x\ 10^{-3}}S_{8.07\ x\ 10^{-3}}O_{0.08}+\alpha(\ O_2+3.78N_2)\rightarrow CO_2+\frac{0.014}{2}H_2O+8.07\ \text{x}\ 10^{-3}SO_2+(3.78\alpha+\frac{3.4x\ 10^{-3}}{2})N_2$$

Where,

$$\alpha=x+\frac{y}{4}+z-\frac{\alpha}{2}\ ,\ (CxHyNzSO\alpha)$$

$$=1+\frac{1.138}{4}+3.4 \text{ x } 10^{-3}-\frac{0.08}{2}=1.247$$

Hence, The combustion stoichiometry is;

$$CH_{1.138}N_{3.4\text{x }10^{-3}}S_{8.07\text{ x }10^{-3}}O_{0.08}+1.268(\ O_2+3.78N_2)\rightarrow CO_2+\ 0.007H_2O+8.07\text{ x }10^{-3}SO_2+\ 4.72N_2$$

Utilizing the average Cp approach, the subsequent equation was used to calculate the combustion product temperature (Tp).

$$Tp = Tr+\frac{\text{LHV}\cdot N_{fuel}.M_{fuel}}{\Sigma\, N_{i,P}.C_{Pi}}$$

where,

Tr = 298.15 K

N_{fuel} = 1 mol

$M_{fuel,\ TDF}$= 14.72 gr/mol

The assumed of lower heating value of TDF is 31.76 MJ/kg. When we assume average Cp (kJ/mol·K) at1500 K and determining specific heat at a constant pressure of product species i.e. Cp,H_2O, Cp,CO_2, Cp,SO_2, & Cp,N_2 using physical property table, we get.

Cp,H_2O=0.0467; Cp,CO_2=0.0584; Cp,SO_2=0.0559; Cp,N_2=0.0350

The product temperature is calculated below:

$$Tp = Tr+\frac{\text{LHV}\cdot N_{fuel}.M_{fuel}}{\Sigma\, N_{i,P}.C_{Pi}}$$

$$=298.15+\frac{31.76x\ 10^3x14.72x10^{-3}}{(1\times0.0584)+(0.007\times0.0467)+(8.07\text{ x }10^{-3}\times0.0559)+(4.72\times0.0350)}=2112.72\ K$$

The reactans average temparature and products temperature is recalculated below:

$$Tave=\frac{298.15+2112.72}{2}=1205.43K$$

This suggests the first assumption of $Tave$=1500 K was excessive. Consequently, assessing the specific heat and flame temperature utilizing the revised average temperature, $Tave$=1205.43 K.

Cp,H_2O= 0.0436; Cp,CO_2=0.0565; Cp,SO_2=0.0553; Cp,N_2=0.0337

$$Tp = Tr + \frac{\text{LHV} \cdot N_{fuel} \cdot M_{fuel}}{\Sigma N_{i,P} \cdot C_{Pi}}$$

$$=298.15+\frac{31.76x\ 10^{3}x14.72x10^{-3}}{(1\times0.0565)+(0.007\times0.0436)+(8.07\ \text{x}\ 10^{-3}\times0.0553)+(4.72\times0.0337)} = 2420\ K$$

The reactans average temparature and products temperature is recalculated below:

$$Tave=\frac{298.15+2420}{2} = 1359.07\ K$$

We are recalculating the specific heat and flame temperature using of the new average temperature, $Tave$=1359.07 K.

Cp,H_2O= 0.0453; Cp,CO_2=0.0573; Cp,SO_2=0.0557; Cp,N_2=0.0344

$$Tp = Tr + \frac{\text{LHV} \cdot N_{fuel} \cdot M_{fuel}}{\Sigma N_{i,P} \cdot C_{Pi}}$$

$$=298.15+\frac{31.76x\ 10^{3}x14.72x10^{-3}}{(1\times0.0573)+(0.007\times0.0453)+(8.07\ \text{x}\ 10^{-3}\times0.0557)+(4.72\times0.0344)} = 2419\ K$$

The reactans average temparature and products temperature is recalculated below:

$$Tave=\frac{298.15+2419}{2} = 1358.57K$$

The variation in average temperature is less than 20 K. The ultimate adiabatic flame temperature of the coal and air combustion reaction is approximately ≈2419 K.

- **Waste Oil /Air Combustion**

Table A.7 Waste oil composition and its chemical formula

Element	Wt%	Mol/100 gm	Mol/mol C
C	40.8÷ 12	3.4	1
H	7.8 ÷ 1	7.8	2.29
O	8÷ 16	0.5	0.15
S	2÷ 32	0.063	0.018
N	2÷ 14	0.14	0.041

H2O	33÷ 18	1.83	0.54
Ash	6.4	-	4.039 g/mol C

Therefore, the pseudo-chemical the formula of WO is as follows:

$$CH_{2.29}N_{0.041}S_{0.018}O_{0.15}(H_2O)_{0.54}=CH_{3.37}N_{0.041}S_{0.018}O_{0.69}$$

We define the stoichiometric combustion of the identified WO and air below:

$$CH_{3.37}N_{0.041}S_{0.018}O_{0.69}+\alpha(O_2+3.78N_2)\rightarrow CO_2+\frac{0.54}{2}H_2O+0.018\,SO_2+(3.78\alpha+\frac{0.041}{2})N_2$$

Where,

$$\alpha=x+\frac{y}{4}+z-\frac{\alpha}{2},\ (CxHyNzSOa)$$

$$=1+\frac{3.37}{4}+0.041-\frac{0.69}{2}=1.538$$

Hence, The combustion stoichiometry is;

$$CH_{3.37}N_{0.041}S_{0.018}O_{0.69}+1.538(O_2+3.78N_2)\rightarrow CO_2+0.27H_2O+0.018\,SO_2+5.83N_2$$

Utilizing the average Cp approach, the subsequent equation was used to calculate the combustion product temperature (Tp).

$$Tp = Tr+\frac{\text{LHV}\cdot N_{fuel}.M_{fuel}}{\Sigma N_{i,P}.C_{Pi}}$$

where,

Tr = 298.15 K

N_{fuel} = 1 mol

$M_{fuel,\text{waste oil}}$ = 27.56 gr/mol

The assumed of lower heating value of TDF is 20.17 MJ/kg. When we assume average Cp (kJ/mol·K) at 1500 K and determining specific heat at a constant pressure of product species i.e. Cp,H_2O, Cp,CO_2, Cp,SO_2, & Cp,N_2 using physical property table, we get.

Cp,H_2O=0.0467; Cp,CO_2=0.0584; Cp,SO_2=0.0559; Cp,N_2=0.0350

The product temperature is calculated below:

$$Tp = Tr + \frac{\text{LHV} \cdot N_{fuel} . M_{fuel}}{\Sigma N_{i,P} . C_{Pi}}$$

$$= 298.15 + \frac{20.17x\ 10^3 x 27.56x10^{-3}}{(1\times0.0584)+(0.27\times0.0467)+(0.018\times0.0559)+(5.83\times0.0350)} = 2247.8\ K$$

The reactans average temparature and products temperature is recalculated below:

$$Tave = \frac{298.15+2247.8}{2} = 1272.9\ K$$

This suggests the first assumption of $Tave$=1500 K was excessive. Consequently, assessing the specific heat and flame temperature utilizing the revised average temperature, $Tave$=1272.9 K.

Cp,H_2O= 0.0443; Cp,CO_2=0.0570; Cp,SO_2=0.0555; Cp,N_2=0.0340

$$Tp = Tr + \frac{\text{LHV} \cdot N_{fuel} . M_{fuel}}{\Sigma N_{i,P} . C_{Pi}}$$

$$= 298.15 + \frac{20.17x\ 10^3 x 27.56x10^{-3}}{(1\times0.0570)+(0.27\times0.0443)+(0.018\times0.0555)+(5.83\times0.0340)} = 2303.71\ K$$

The reactans average temparature and products temperature is recalculated below:

$$Tave = \frac{298.15+2399.41}{2} = 1300.93K$$

The variation in average temperature is less than 30 K. The ultimate adiabatic flame temperature of the coal and air combustion reaction is approximately ≈2303.71 K.

Existing Calciner, Alternative Model 1, and Alternative Model 2

Table A.8 Feed points of fuel ratios for the existing model, alternative 1 model, and alternative 2

Existing Model	
Petcoke/Lignite (%) in all system Calciner: 9 tons/day petcoke and lignite mixture Main Burner: 69 tons/day petcoke and lignite mixture	Feed Points of Fuel Ratios

Scenario 1 (65/35) (65% Petcoke+35% Lignite)	Calciner: 2.36% Petcoke, 1.27% Lignite, 68.55% RDF, 25.8% TDF, and 2.02% Waste Oil Main Burner: 36.17% Petcoke, %19.48 Lignite, 40.32% RDF, and 4.03% Waste Oil
Alternative Model 1	
Petcoke/Lignite ratio (%) in all system Calciner: 9 tons/day petcoke and lignite mixture Main Burner: 69 tons/day petcoke and lignite mixture	Feed Points of Fuel Ratios TDF and Waste Oil=0% Calciner: RDF~96%, Main Burner: RDF~44.4%
Scenario 2 (0/100) (0% Petcoke+100% Lignite)	Calciner: Petcoke 0% and Lignite3.63% Main Burner: Petcoke 0% and Lignite%44.34
Scenario 3 (15/85) (15% Petcoke+85% Lignite)	Calciner: Petcoke 0.54% and Lignite3.09% Main Burner: Petcoke 8.33% and Lignite42.22%
Scenario 4 (25/75) (25% Petcoke+75% Lignite)	Calciner: Petcoke 0.91% and Lignite2.72% Main Burner: Petcoke 13.92% and Lignite41.75%
Scenario 5 (35/65) (35% Petcoke+65% Lignite)	Calciner: Petcoke 1.27% and Lignite2.36%

	Main Burner: Petcoke 19.45% and Lignite 36.18%
Scenario 6 (45/55) (45% Petcoke+55% Lignite)	Calciner: Petcoke 1.63% and Lignite2% Main Burner: Petcoke 25.02% and Lignite 30.58%
Scenario 7 (55/45) (55% Petcoke+45% Lignite)	Calciner: Petcoke 2% and Lignite1.63% Main Burner: Petcoke 30.56% and Lignite25%
Scenario 8 (65/35) (65% Petcoke+35% Lignite)	Calciner: Petcoke 2.36% and Lignite1.27% Main Burner: Petcoke 36.18% and Lignite19.48%
Scenario 9 (75/25) (75% Petcoke+25% Lignite)	Calciner: Petcoke 2.72% and Lignite0.91% Main Burner: Petcoke 41.75% and Lignite13.92%
Scenario 10 (85/15) (85% Petcoke+15% Lignite)	Calciner: Petcoke 3.09% and Lignite0.54% Main Burner: Petcoke 47.26% and Lignite8.34%
Scenario 11 (95/5) (95% Petcoke+5% Lignite)	Calciner: Petcoke 3.45% and Lignite0.18% Main Burner: Petcoke 52.82% and Lignite2.78%

Scenario 12 (100/0) (100% Petcoke+0% Lignite)	Calciner: Petcoke 3.63% and Lignite0% Main Burner: Petcoke 55.6% and Lignite0%
Alternative Model 2	
Different weight feeding Petcoke/Lignite mixture (tons/day) in Calciner and Main Burner, respectively (65% Petcoke+35% Lignite)	Feed Points of Fuel Ratios Calciner and Main Burner: Waste Oil = 0%
Scenario 13 (0/78) Calciner: 0 tons/day petcoke and lignite mixture Main Burner: 78 tons/day petcoke and lignite mixture	Calciner: 72.65% RDF, 27.35% TDF Main Burner: Petcoke 40.83%, Lignite 22.02%, and RDF 37.10%
Scenario 14 (78/0) Calciner: 78 tons/day petcoke and lignite mixture Main Burner: 0 tons/day petcoke and lignite mixture	Calciner: %20.46 Petcoke, %11.02 Lignite, 47.74% RDF, and 20.78 % TDF Main Burner: RDF 100 %
Scenario 15 (39/39) Calciner: 39 tons/day petcoke and lignite mixture Main Burner: 39 tons/day petcoke and lignite mixture	Calciner: Petcoke 10.22%, Lignite 5.50%, 47.98% RDF, and 36.29% TDF Main Burner: Petcoke 20.45 %, Lignite11.0%, and RDF 68.54%

Scenario 16 (0/0) Calciner: 0 tons/day petcoke and lignite mixture Main Burner: 0 tons/day petcoke and lignite mixture	Calciner: 72.65% RDF, 27.35% TDF Main Burner: RDF 100%

Table A.9 Required boundary conditions of existing and alternative models for NASA CEA

	Fuel				**Oxidizer**	**Oxidizer/Fuel**
Scenario 1 (65/35)	N_2	CO_2	H_2O	SO_2	$CaCO_3$	0.15
	proportion (wt.%)					
	67.56	22.67	9.45	0.33	100.00	
	enthalpy (kj/mol)					
	61.18	-282.84	-134.03	-55.58	NASA CEA	
Scenario 2 (0/100)	**proportion (wt.%)**					
	65.92	21.88	12.12	0.08	100.00	
	enthalpy (KJ/mol)					
	55.51	-256.47	-136.44	-102.56	NASA CEA	
Scenario 3 (15/85)	**proportion (wt.%)**					
	65.97	21.89	12.01	0.13	100.00	

	enthalpy (kj/mol)				
	56.20	-257.64	-136.69	-59.76	NASA CEA
Scenario 4 (25/75)	**proportion (wt.%)**				
	66.01	21.89	11.94	0.16	100.00
	enthalpy (KJ/mol)				
	56.73	-258.51	-136.88	-48.88	NASA CEA
Scenario 5 (35/65)	**proportion (wt.%)**				
	66.04	21.90	11.87	0.19	100
	enthalpy (KJ/mol)				
	57.21	-259.33	-137.05	-43.38	NASA CEA
Scenario 6 (45/55)	**proportion (wt.%)**				
	66.07	21.90	11.81	0.22	100.00
	enthalpy (kj/mol)				
	57.70673	-260.167	-137.219	-38.941	NASA CEA
Scenario 7 (55/45)	**proportion (wt.%)**				
	66.07	21.90	11.81	0.22	100.00

	enthalpy (KJ/mol)				
	57.72	-260.19	-137.23	-38.79	NASA CEA
Scenario 8 (65/35)	**proportion (wt.%)**				
	66.13	21.91	11.68	0.27	100.00
	enthalpy (kj/mol)				
	58.72	-261.95	-137.59	-34.13	NASA CEA
Scenario 9 (75/25)	**proportion (wt.%)**				
	66.17	21.91	11.62	0.30	100.00
	enthalpy (KJ/mol)				
	59.23	-262.87	-137.77	-32.36	NASA CEA
Scenario 10 (85/15)	**proportion (wt.%)**				
	66.1979	21.91154	11.5628	0.327756	100.00
	enthalpy (KJ/mol)				
	59.71	-263.74	-138.00	-31.01	NASA CEA
Scenario 11 (95/5)	**proportion (wt.%)**				
	66.23	21.92	11.50	0.35	100.00

	enthalpy (KJ/mol)					
	60.21	-264.63	-138.14	-30.00	NASA CEA	
Scenario 12 (100/0)	**proportion (wt.%)**					
	66.25	21.93	11.45	0.37	100.00	
	enthalpy (KJ/mol)					
	60.51	-265.31	-138.24	-29.96	NASA CEA	
Scenario 13 (0/78)	**proportion (wt.%)**					
	67.52	22.70	9.47	0.31	100.00	
	enthalpy (KJ/mol)					
	62.36	-283.75	-136.59	-43.67	NASA CEA	
Scenario 14 (78/0)	**proportion (wt.%)**					
	67.11	22.44	10.15	0.30	100.00	
	enthalpy (KJ/mol)					
	50.25	-287.07	-117.56	-208.39	NASA CEA	
Scenario 15 (39/39)	**proportion (wt.%)**					
	67.94	23.01	8.70	0.34	100.00	

	enthalpy (KJ/mol)					
	56.85	-289.75	-124.28	-112.31	NASA CEA	
Scenario 16 (0/0)	**proportion (wt.%)**					
	73.63	16.94	9.31	0.12	100.00	
	enthalpy (KJ/mol)					
	111.39	-268.63	-128.20	-171.38	NASA CEA	

*The places shown as NASA CEA in the table are automatically calculated by the solver.

Mass Balance Calculation

- **Clinker Cooler Unit**

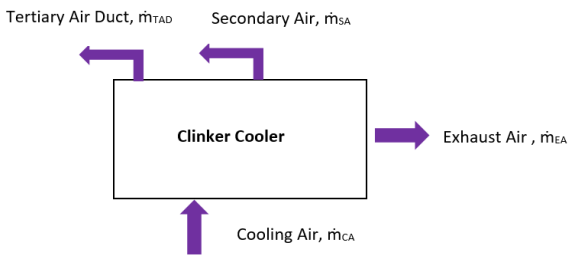


Figure A.1 Schematic view of the clinker cooler (Atmaca &Yumrutaş, 2015)

Specific air at the cooler ($\dot{m}_{CA}$) is measured in the cement factory as 1,68 Nm^3/kg clinker. Cooler exhaust flow rate ($\dot{m}_{EA}$) and total secondary air flow rate ($\dot{m}_{SA}$) are measured as 0,71 and 0.40 Nm^3/kg clinker respectively. With these data, we can calculate the air balance to determine the tertiary air duct mass flow rate ($\dot{m}_{TAD}$).

For the clinker cooler the following relations hold:

Clinker production capacity: $1647 \frac{ton\ clinker}{day} \times \frac{1\ day}{24\ hr} \times \frac{1\ hr}{3600\ s} \times \frac{1000\ kg\ clinker}{1\ ton\ clinker} = 19.06 \frac{kg\ clinker}{s}$

$$\rho air = 1.29\ \frac{kg\ air}{Nm^3}$$

$$\dot{m}_{input} = \dot{m}_{output}$$

$$\dot{m}_{TAD} + \dot{m}_{SA} + \dot{m}_{EA} = \dot{m}_{CA}$$

$$\dot{m}_{TAD} = [1.68\text{-}(0.71+0.4)]\frac{Nm^3}{kg\ clinker} \times 19.06\ \frac{kg\ clinker}{s} \times 1.29\ \frac{kg\ air}{Nm^3} = 14.01\ \frac{kg\ air}{s}$$

- **Calciner Unit**

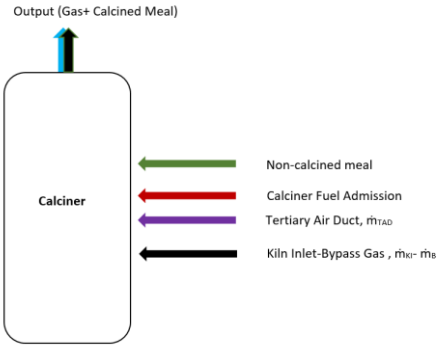


Figure A.2 Schematic view of the calciner (Kolip & Savaş, 2010)

Kiln inlet gas mass flow rate calculation:

The kiln inlet gas flow rate is measured in cement factory as 1.0394 Nm^3/kg clinker.

$$\rho_{kiln\ gas} = 1.354\ \frac{kg\ gas}{Nm^3}$$

$$(\dot{m}_{KI}) = 1.0394\ \frac{Nm^3}{kg\ clinker} \times 1.354\ \frac{kg\ gas}{Nm^3} \times 19.06\ \frac{kg\ clinker}{s} = 26.83\ \frac{kg\ gas}{s}$$

Bypass gas mass flow rate calculation:

Some of the gas and laden dust particles (around 6%) entering the simulation domain from the kiln inlet leave from a bypass placed upstream of the riser section. The main outlet of the domain is placed at the exit of the swanneck.

$$(\dot{m}_B) = (\dot{m}_{KI}) \times 6\% = 26.83\ \frac{kg\ gas}{s} \times 6\% = 1.6\ \frac{kg\ gas}{s}$$

The extracted bypass gas from kiln inlet gas mass flow rate calculation:

$$(\dot{m}_{KI})\text{- }(\dot{m}_{B})= (26.83\text{-}1.6)\ \frac{kg\ gas}{s}= 25.2\ \frac{kg\ gas}{s}$$

- **Raw Meal Properties**

According to the data, the calcination degree is calculated by the given equation (Alsop, 2001):

$$Calcination\ Degree\ \ (\%) = 100\ \text{x}\left[1 - \frac{((LOI\ hot\ meal\ (100 - LOI\ raw\ meal))}{LOI\ raw\ meal(100 - LOI\ hot\ meal)}\right]$$

$$Calcination\ Degree\ (\%) = 100\ \text{x}\ \left[1 - \frac{((2.5(100 - 33.42))}{33.42(100 - 2.5)}\right] = 95\%$$

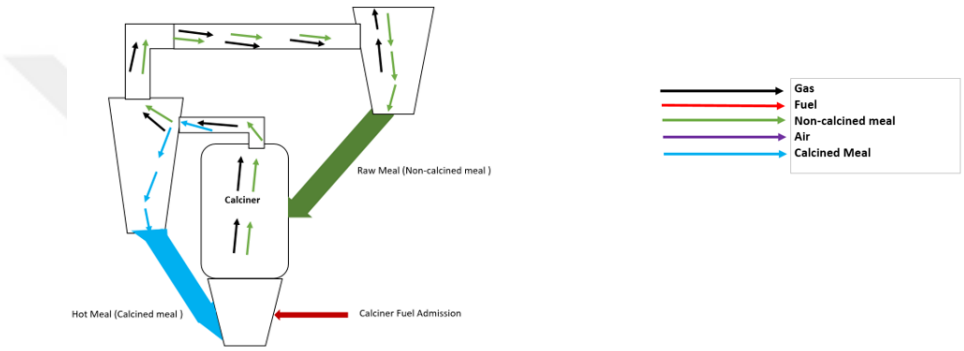


Figure A.3 Schematic view of raw meal and gas flow directions in calciner(Kolip &Savas, 2010)

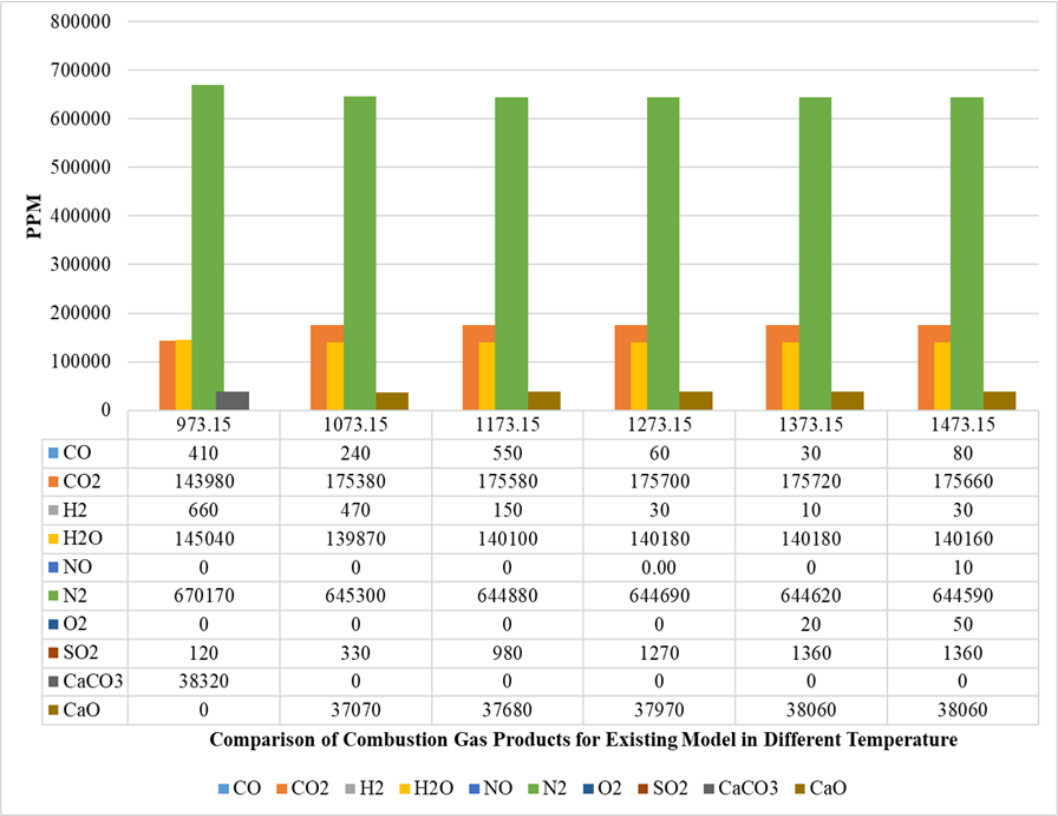
$CaCO_3$ wt.(%) calculation from calcination degree (Alsop, 2001):

$$\text{Wt.(\%)}_{CaCO3} = \frac{(55.2-41.66)}{95\%}= 14.25$$

Calciner inlet mass flowrate calculation:

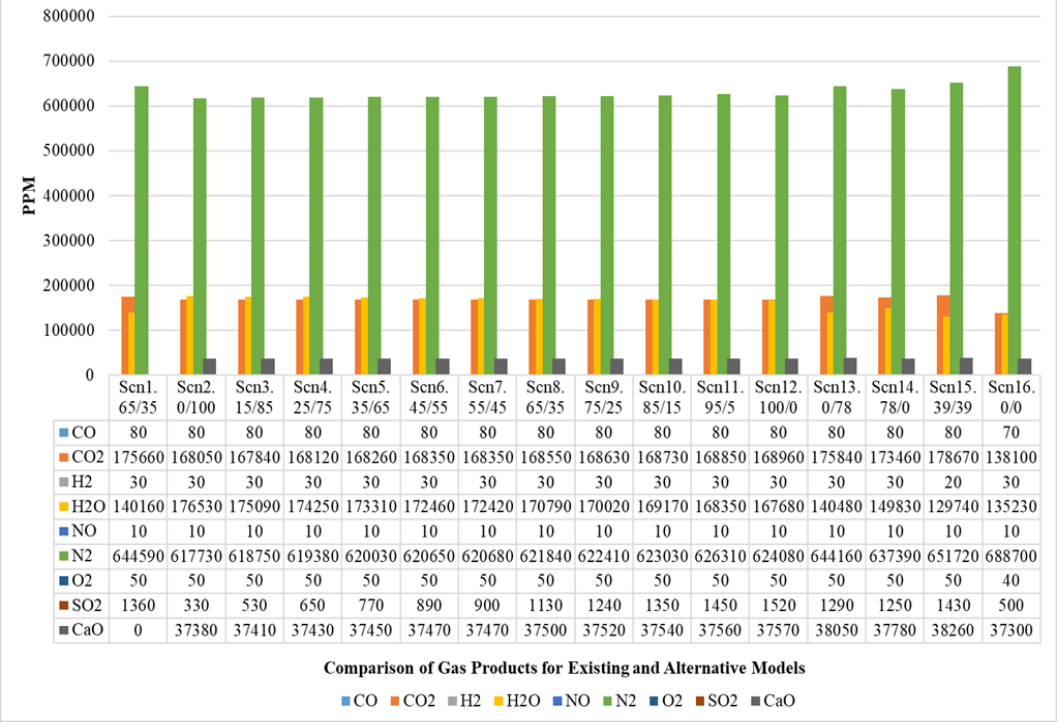
$$Clinker\ Factor = \frac{\text{Raw Meal (kg)}}{Clinker\ Output(kg)}$$

$$1.630 = \frac{\text{kg raw meal/s}}{19.06\ kg\ clinker\ /s}= 31.07\ \text{kg raw meal/s}$$



	973.15	1073.15	1173.15	1273.15	1373.15	1473.15
CO	410	240	550	60	30	80
CO2	143980	175380	175580	175700	175720	175660
H2	660	470	150	30	10	30
H2O	145040	139870	140100	140180	140180	140160
NO	0	0	0	0.00	0	10
N2	670170	645300	644880	644690	644620	644590
O2	0	0	0	0	20	50
SO2	120	330	980	1270	1360	1360
CaCO3	38320	0	0	0	0	0
CaO	0	37070	37680	37970	38060	38060

Figure A.4 Comparison of combustion gas products for existing model in different temperature by NASA-CEA simulation



	Scn1. 65/35	Scn2. 0/100	Scn3. 15/85	Scn4. 25/75	Scn5. 35/65	Scn6. 45/55	Scn7. 55/45	Scn8. 65/35	Scn9. 75/25	Scn10. 85/15	Scn11. 95/5	Scn12. 100/0	Scn13. 0/78	Scn14. 78/0	Scn15. 39/39	Scn16. 0/0
CO	80	80	80	80	80	80	80	80	80	80	80	80	80	80	80	70
CO2	175660	168050	167840	168120	168260	168350	168350	168550	168630	168730	168850	168960	175840	173460	178670	138100
H2	30	30	30	30	30	30	30	30	30	30	30	30	30	30	20	30
H2O	140160	176530	175090	174250	173310	172460	172420	170790	170020	169170	168350	167680	140480	149830	129740	135230
NO	10	10	10	10	10	10	10	10	10	10	10	10	10	10	10	10
N2	644590	617730	618750	619380	620030	620650	620680	621840	622410	623030	626310	624080	644160	637390	651720	688700
O2	50	50	50	50	50	50	50	50	50	50	50	50	50	50	50	40
SO2	1360	330	530	650	770	890	900	1130	1240	1350	1450	1520	1290	1250	1430	500
CaO	0	37380	37410	37430	37450	37470	37470	37500	37520	37540	37560	37570	38050	37780	38260	37300

Figure A.5 Comparison of combustion gas products for existing model and alternative models by NASA-CEA simulation

B

APPENDIX INTEGRATING SOLAR CALCINER TECHNOLOGY FOR REDUCTION EMISSION IN CEMENT PRODUCTION

Maximum CO_2 Reduction of Potential

Table B.1 Required input value of CO_2 reduction calculation for all scenarios

Parameter	Description	Value
$\dot{m}_{rm}$	Raw meal mass flow rate	31.07
$\dot{m}_{clinker}$	Clinker mass flow rate	19.06
Y_{rm,CO_2}	Mass fraction of CO_2 in the raw meal	0.525
ṁrm/ ṁclinker	Raw meal to clinker factor	1.63
ṁmixture, kiln	Mixture of fuels mass flow into kiln	1.44
ṁmixture, calciner	Mixture of fuels mass flow into calciner	2.87

Parameter	Scenario 1 (65/35)	Scenario 2 (0/100)	Scenario 5 (35/65)	Scenario12 (100/0)
LHVmixture, kiln	25,142.36	23,016	24,084	26,067.3
$C_{CO_{2,kiln}}$	$8.94433.10^{-5}$	$8.92738.10^{-5}$	$8.94666.10^{-5}$	$8.97826.10^{-5}$
LHVmixture,calciner	19,986.76	15,397	15,467	15,620.5
$C_{CO_{2,calciner}}$	$8.49408.10^{-5}$	$8.42505.10^{-5}$	$8.42927.10^{-5}$	$8.43917.10^{-5}$

Table B.2 Information on the solar field and parameters related to heat flux (Aydin &Yucel, 2023)

Solar power plant properties	Unit	Value
The aperture area of a single heliostat	m^2	60
Receiver aperture area	m^2	30
Effective aperture area of solar field	m^2	102,000
η_{hel}	%	85
f_{mix}	-	0.001
δ	%	95
ϵ	-	0.88
σ_0	kW/m^2K	$5.67x10^{-11}$
A_r	m^2	30
T_{wall}	Kelvin	1000
Cp_{HTF}	kJ/kgK	$0.9896 + 1.046e\text{-}^4(T_{wall}\text{-}703)$
$H_{HTF}(MgCl_2 - KCl)$	kJ/kg	207

Matlab Program

```
clc
clear
```

```
for i=1:6
for j=1:15


%% Solar thermal power refected towards a central receiver system
number_hel=800+j*200;
A_hel=60; % aperture area of the single heliostat m2
DNI=0.2+i*0.2; %direct normal irradiance kw/m2
teta=45*(pi/180); %incident angle
DII=DNI*cos(teta); %direct incident irradiance  %kw/m2
% DII=0.7854; %kw/m2
q_inc=DII*A_hel*number_hel; %solar power incident on the total area of heliostat mirror
n_hel=0.85; % the heliostat efficiency
q_refl=q_inc*n_hel;
%% Central receiver at the top of the solar tower is used to transfer the sunlight refected by heliostats to the HTF
sigma=0.95; %solar absorptance of the tube panels
q_ref_loss=(1-sigma)*q_refl; %power loss refected from the receiver
eps=0.88; %hemispherical emittance
sb=5.67e-11; %kW/m2K stefan boltzman constant
Ar=30; % m2 lateral surface of the tube
Twall=1000; %K
Tamb=298.15; %K
q_rad_loss=eps*sb*Ar*(Twall^4-Tamb^4);
fmix=0.3622;%the mixed convection coefficient
q_conv_loss=fmix*Ar*(Twall-Tamb);
q_rec_loss=q_ref_loss+q_rad_loss+q_conv_loss; %solar thermal power loss in the receiver
q_rec=q_refl-q_rec_loss; %reflected solar power from heliostats
%%
```

```
n_rec=1-(q_rec_loss./q_refl); %Thermal efficiency of receiver system
% m_HTF=1000/3600; %mass flow rate of heat transfer fluid kg/h
% h_out_HTF=-5300; %specific enthalpy of HTF kj/kg
% h_in_HTF=-6300; %specific enthalpy of HTF
q_trans=q_rec.*n_rec; %Transferred heat
% q_trans=m_HTF.*(h_out_HTF-h_in_HTF);
% h_out_HTF=(q_trans./m_HTF)+h_in_HTF;


hf_molten_salt=207; %kj/kg MgCl2 KCl 298K
cp_molten_salt=0.9896+1.046e-4*(Twall-703);
h_out_HTF=hf_molten_salt+cp_molten_salt*(Twall-Tamb);
m_HTF=q_trans/(h_out_HTF-hf_molten_salt); %MW
% h_out_HTF=(q_trans./m_HTF)+hf_molten_salt;
flux=q_trans/90


flux_table(j,i)=flux;
q_trans_table(j,i)=q_trans;
q_rec_table(j,i)=q_rec;
n_rec_table(j,i)=n_rec;


end


end
```

PUBLICATIONS FROM THE THESIS

Conference Papers

1. Cebeci, H.H., Yücel, Ö. and Sadikoglu, H. (2024). Reaction Mechanism Modelling for Cement Calciner, *7th International Conference Engineering Science*, Ankara Bilim University, 2024.

Papers

1. Cebeci, H.H., Yücel, Ö. and Sadikoglu, H. (xxxx) 'Evaluation of refuse-derived and tyre-derived fuels in cement industry: a study on emission characteristics', *Int. J. Global Warming*, Vol. X, No. Y, pp.xxx–xxx.

Projects

1. Cebeci, H. H., M.A., Insel, O., Yücel, and Sadikoglu, H. (2024). *Çimento fırınında ve kalsinatörde ikame edilen alternatif yakıt ve kömürün reaksiyon mekanizmalarının NASA CEA ve CHEMKIN-Pro ile modellenmesi* [Unpublished project report]. TUBİTAK 1002-A Hızlı Destek Modülü. Project Code: 224M035.